PULSEBACK CLEANING OF PANEL BED FILTER FOR TREATING A LIQUID

by

David Roberts Whitmire

Thesis submitted to the Graduate Faculty of the
Virginia Polytechnic Institute and State University
in partial fulfillment of the requirements for the degree of
MASTER OF SCIENCE
in
Chemical Engineering

APPROVED:

A.M. Squires, Chairman

G.B. Wills

J.H. Hunter

February, 1978

Blacksburg, Virginia

ACKNOWLEDGMENTS

The writer wishes to express appreciation to

for providing an opportunity to work on this project. Gratitude is also extended to and for advice and counsel on the project.

Appreciation is also extended to for financial and other support during the work of this writer.

Special appreciation is extended to and for technical support during the project.

TABLE OF CONTENTS

TABLE OF CONTENTS - continued.

LIST OF TABLES

LIST OF FIGURES

LIST OF FIGURES - continued.

LIST OF FIGURES - continued.

LIST OF FIGURES - continued.

INTRODUCTION

The gas-solid contact system, invented in 1876, which provided the reactor for the Deacon chlorine process made use of a transverse gas flow through a bed of granular solid. The panel was formed by placing the granular material between two upright columns of louvers, resembling venetian blinds. A filtration device of high efficiency and utilizing the panel bed concept has been developed by Lee et. al. (1). As the gas flows transversely through the panel, particulates in the gas strike the sand and are retained generally at or near the surface of the sand. As the amount of dust resting upon the sand increases, the pressure drop across the panel increases. When the pressure drop reaches a pre-selected value, the dust can be removed from the panel by a technique known as puffback.

The puffback procedure consists of the sudden opening of a valve which releases air from a relatively high pressure source connected to the clean side of the panel. This blast of air flows from the back or clean side of the panel to the front or dirty side in the opposite direction to the normal gas flow. The surge of air causes the removal of sand and dust from the dirty side of the panel. Removal of the dust causes a decrease of the pressure drop across the panel bed and allows for another filtration cycle. For further information on use of the panel bed for gas cleaning, refer to the work of Rodon (2).

The present research was undertaken to study the liquid analog of the earlier work on the panel bed gas filter. Figure 1 illustrates a panel bed for liquid filtration.

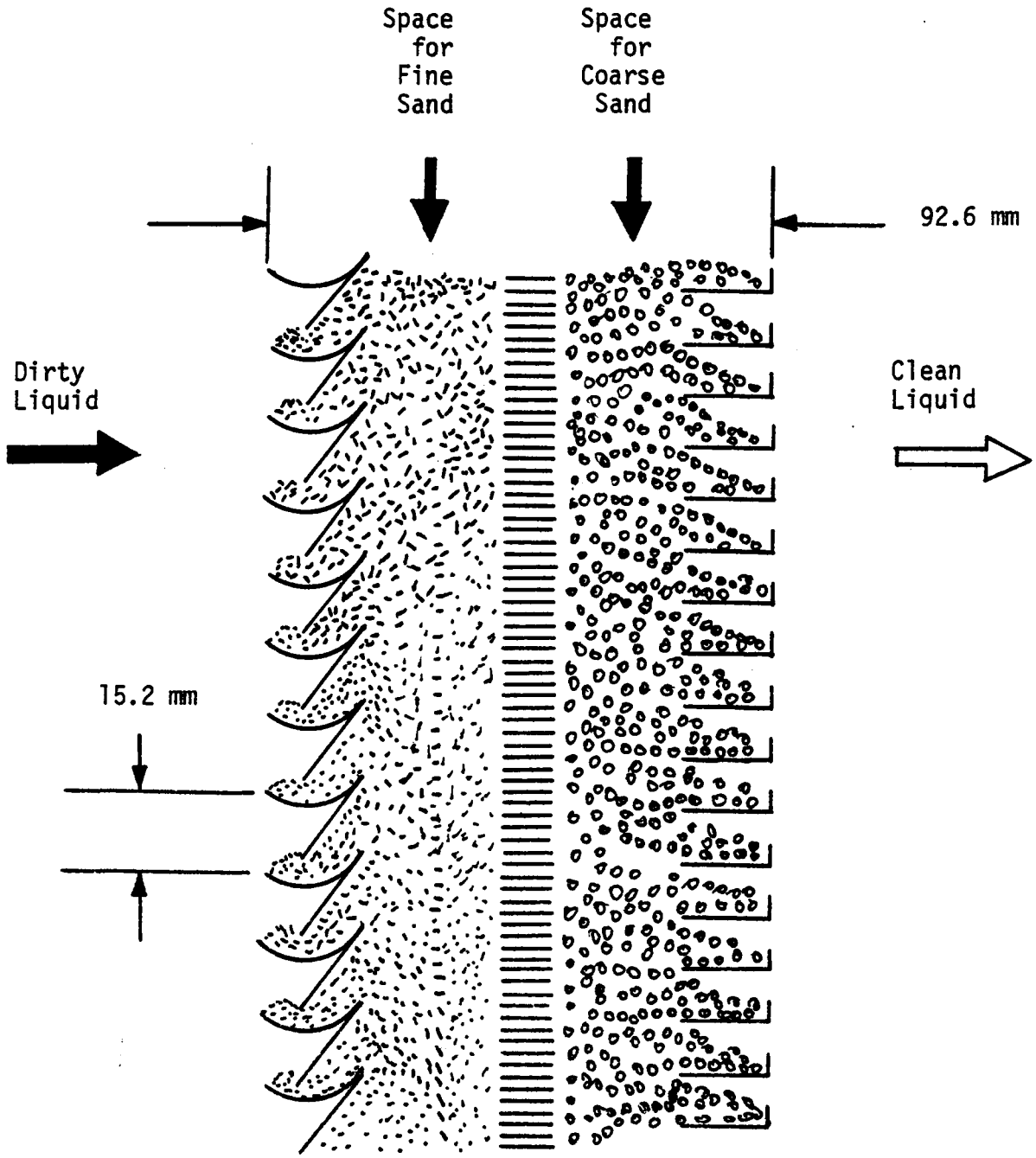

Figure 1. Arrangement of louvers for the pulseback experiments.

There are many opportunities for application of a high efficiency filter with liquid streams. These applications range from the filtration of water to the removal of ash particles from the liquid product of a coal liquefaction plant. Also, the panel could contain a catalyst, reactant, or adsorbant rather than, or as well as, a filter medium.

Exploratory work by Squires (3) showed that "pulseback" cleaning (i.e., a reverse surge flow of liquid) has the same general effect as puffback, that is to say, the reverse surge flow causes a mass movement of sand toward the liquid-entry surfaces of a panel bed fitted for treating a liquid. It is contemplated that high pressure air will be used to cause pulseback, as it is used in puffback.

The objectives of this research include:

1. To perform pulseback within a static liquid environment using panels of quartz sand.
2. To obtain time history data of the pressure drop across the panel bed along with the sand spill for each pulseback for several pulseback equipment configurations.
3. To correlate the pertinent variables involved in pulseback.

In summary, the purpose here is to obtain data shedding light upon the soil mechanics of pulseback. These experiments are needed before work can begin upon process applications of the liquid panel bed and its industrial scale-up.

LITERATURE REVIEW

The phenomenon termed pulseback is a soil failure caused by the application of fluid drag forces. This statement is underpinned considerably by Lambe and Whitman (4). To understand pulseback it is necessary to review studies of fluid drag forces in beds of granular solids and the failure of granular soils.

Fluid Flow

Drag Forces. The fundamental application of the forces due to a flowing fluid are illustrated in Figure 2. The total drag force consists of two components: (1) the fictional forces which act tangentially, and, (2) the "form drag" which acts in the direction of the velocity of the undisturbed fluid. Mechanistic theories have been suggested to explain the origin of these forces, but these phenomena are still not fully understood (5,6).

Muskat (7) has presented an orderly analysis of the situation by using the equations of continuity and motion. This analysis leads to the familiar Navier-Stokes equation. However, due to the complex geometry for a bed of granular solids with irregular particle shapes, the complete and exact solution of the equations derived by Muskat is impossible. Engineering problems involving flow through porous media can be solved, however, and these solutions generally involve empirical models.

Empirical Models. D'arcy's Law, presented below, is perhaps the most widely known empirical model which treats flow in porous media:

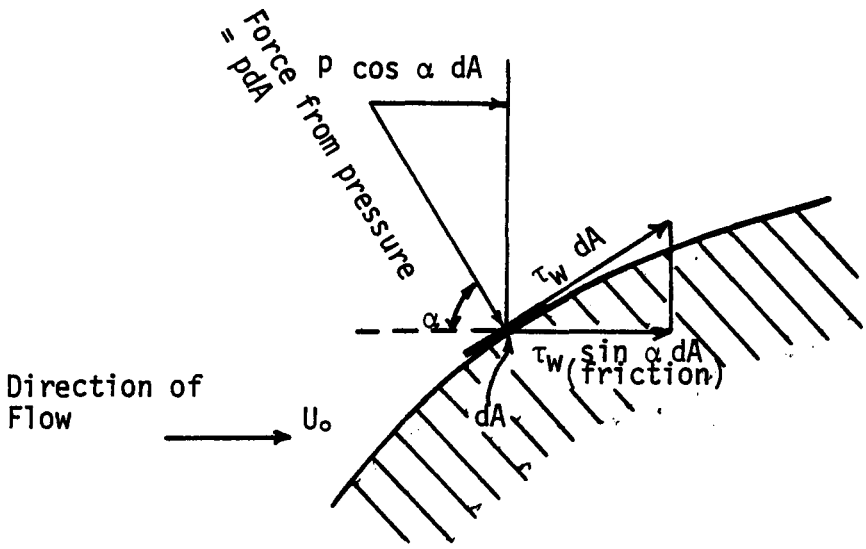

Figure 2. Schematic diagram illustrating the forces present due to the flow of a fluid over a submerged object.

$$U_o = \frac{-k}{\mu} \frac{dP}{dx} \tag{1}$$

where: U_o = velocity of the undisturbed fluid, L/θ

k = permeability (D'arcy), L^2

μ = fluid viscosity, $M/L^2 - \theta$

dP/dx = differential pressure drop, $(F/L^2)/L$

This relationship was developed experimentally by D'arcy in 1850 (8). Muskat (9) has discussed the utility of the permeability and presents typical values. D'arcy's Law can be obtained by integrating Stokes Law (10) over the area of the porous bed. Stokes Law has proved to be usefully accurate when the Reynolds Number based on the effective diameter is less than 0.1. This is not surprising since Stokes Law considers only the drag forces and ignores any inertial effects which occur during flow.

To account for the inertial effects, the following model has been suggested by Reynolds (11) and Muskat (12):

$$\frac{-dP}{dx} = \frac{\mu U_o}{R} + \frac{\rho}{G_c k^{\frac{1}{2}}} U_o^2 \tag{2}$$

where: $\frac{dP}{dx}$ = differential pressure drop

μ = fluid viscosity, $M/L^2 - \theta$

U_o = velocity of the undisturbed fluid, L/θ

k = permeability (D'arcy), L^2

G_c = gravitational constant, $M\text{-}L/F\text{-}\theta^2$

ρ = fluid density, M/L^3

Ward (13) has verified equation (2) for the flow of water through granular solids, which is the situation encountered in pulseback.

Other models have been developed, but they are of the same basic form as equation (2). For flow through a bed of granular solids, Leva (9) has developed the following correlation:

$$\Delta P = \frac{2 f_m G^2 L (1-\varepsilon)^{3-n}}{D_p G_c \phi_s^{3-n} \varepsilon^3} \tag{3}$$

where: ΔP = pressure drop, F/L^2

L = depth of bed, L

G_c = gravitational constant, $ML/F\theta^2$

D_p = average particle diameter, L

ε = porosity (void volume/total volume), dimensionless

n = constant (a function of the particle Reynolds Number), dimensionless

ϕ_s = shape factor

G = superficial mass velocity, $M/\theta L^2$

ρ = fluid density, M/L^3

f_m = friction factor (a function of the particle Reynolds Number), dimensionless

The particle Reynolds Number (NRE) is defined as:

$$NRE = \frac{D_p G}{\mu} \tag{4}$$

Values for n and f_m are given by Leva (10). A similar model has been developed by Ergun and is presented later.

Soil Mechanics

The information presented in this section is generally applicable to saturated sand. This is the type of soil useful in pulseback studies.

Soil Strain. When a soil failure occurs, a quantity of sand moves along a failure surface (16). This failure surface can be either curved or planar and can exist either at a soil boundary or at a section within the soil (17). The motion of the sand during a failure constitutes a straining of the soil. This strain results from the sliding, rolling, and deforming of the individual particles within the soil (18). The strain in soil is caused by stresses within the soil. Typically, when soil failure at a boundary is considered, the stresses responsible for the failure are referred to as shearing stresses.

Shear Strength. The ability of a soil to resist movement due to shear stress was studied by Coulomb (19). Coulomb's equation for shearing resistance is now commonly used and appears below:

$$S = (\sigma - U_w) \tan \phi \qquad (5)$$

where: S = shearing resistance, F/L^2

σ = stress normal to the failure surface, F/L^2

$U_w = \rho_w h_w$ = neutral stress due to water, F/L^2

h_w = total head of water, L

ρ_w = density of water, M/L^3

ϕ = angle of internal friction (this is a constant for a given soil in a given state), dimensionless.

The quantity ($\sigma - U_w$) is frequently referred to as the effective stress, σ_h (20). As Lambe (21) has pointed out, the effective stress is the most useful stress quantity to consider when dealing with sand saturated with water.

Obviously, the shearing resistance of a cohesionless soil like sand is unaffected by any hydrostatic head of water. During equilibrium, the shear stress on any horizontal section of submerged sand is zero (22). Any hydrodynamic head, such as occurs when water flows through sand, can alter the shearing resistance of the sand as illustrated by Terzaghi (23). For example, the hydrodynamic head resulting from the essentially vertical, upward flow of water can fluidize sand causing "quicksand" (24).

Time Effects. It has been observed that the rate of loading affects the way that wet sand responds to stress. If shearing stresses are applied relatively slowly, the ultimate shear of the sand may result in channeling and localized sand movement. However, during a relatively rapid loading, a uniform movement of the entire sand mass will occur.

Whitman and Healy (25) have studied these two effects. They found that the angle of internal friction is not a function of the rate of loading. They also found that the ability of the sand to dissipate the excess pore pressure caused by the loading is time dependent. It was discovered that the strength of the sand used by Whitman and Healy increased by 40 percent when the loading velocity was changed from 457.2 mm/sec to 2.03 mm/sec. These workers believe

that the stresses not carried by the water through the dissipation of excess pore pressure must be carried by the soil skeleton.

Note that the geostatic normal stresses on a soil vary with the depth of the failure in question. The shearing resistance of an isotropic, homogeneous sand will be relatively less toward the top of the sample than the bottom. It appears, therefore, that channeling will occur toward the top of a sample of sand.

Summary

The fact that sand is submerged has no effect on the shearing resistance of the sand. However, the hydrodynamic head caused by the flow of water may indeed increase or reduce the shearing resistance of the sand. Moreover, sand can be strained and moved by the application of shearing stresses. It appears that these stresses can be produced by the drag and inertial forces which result from the flow of a fluid across the solid surfaces in a bed of granular solids. Also, the rate of loading may affect the way sand shears. A relatively rapid loading can cause a uniform sand movement while a relatively slow loading may lead only to localized sand failure at the lowest value of the shearing resistance in the sample.

EXPERIMENTAL

Plan of Experimentation

The investigation involved the operation of a laboratory-scale panel bed filter to obtain pulseback operating data. Sand was used to form the panel bed, as seen in Figures 1 and 3, and water was used as a static liquid to fill the filter case. Air was used to cause the reverse transient flow of the water through the sand panel to constitute pulseback.

The primary variables measured for each pulseback were the sand spill and the time history of the pressure drop across the panel bed. Neither of these variables was an independent variable which could be directly controlled. The variables which were controlled include the air reservoir volume, the valve orifice diameter, and the reservoir air pressure. A change in any of these variables results in a change in the total energy transmitted to cause pulseback. Also, as a parameter, two different particle sizes of sand were used separately to create the sand panel. See Figures 4 and 5 for photographs of the sand.

To provide a basis for future scale-up of the panel bed filter, the equipment configuration was varied. Air reservoirs of ~100 cm^3 and ~50 cm^3 were used, and are shown in Figure 6. Also, valves of orifice diameter 6.15 mm and 3.38 mm respectively were used and are shown in Figure 7.

To facilitate logging of the data a code was employed to specify

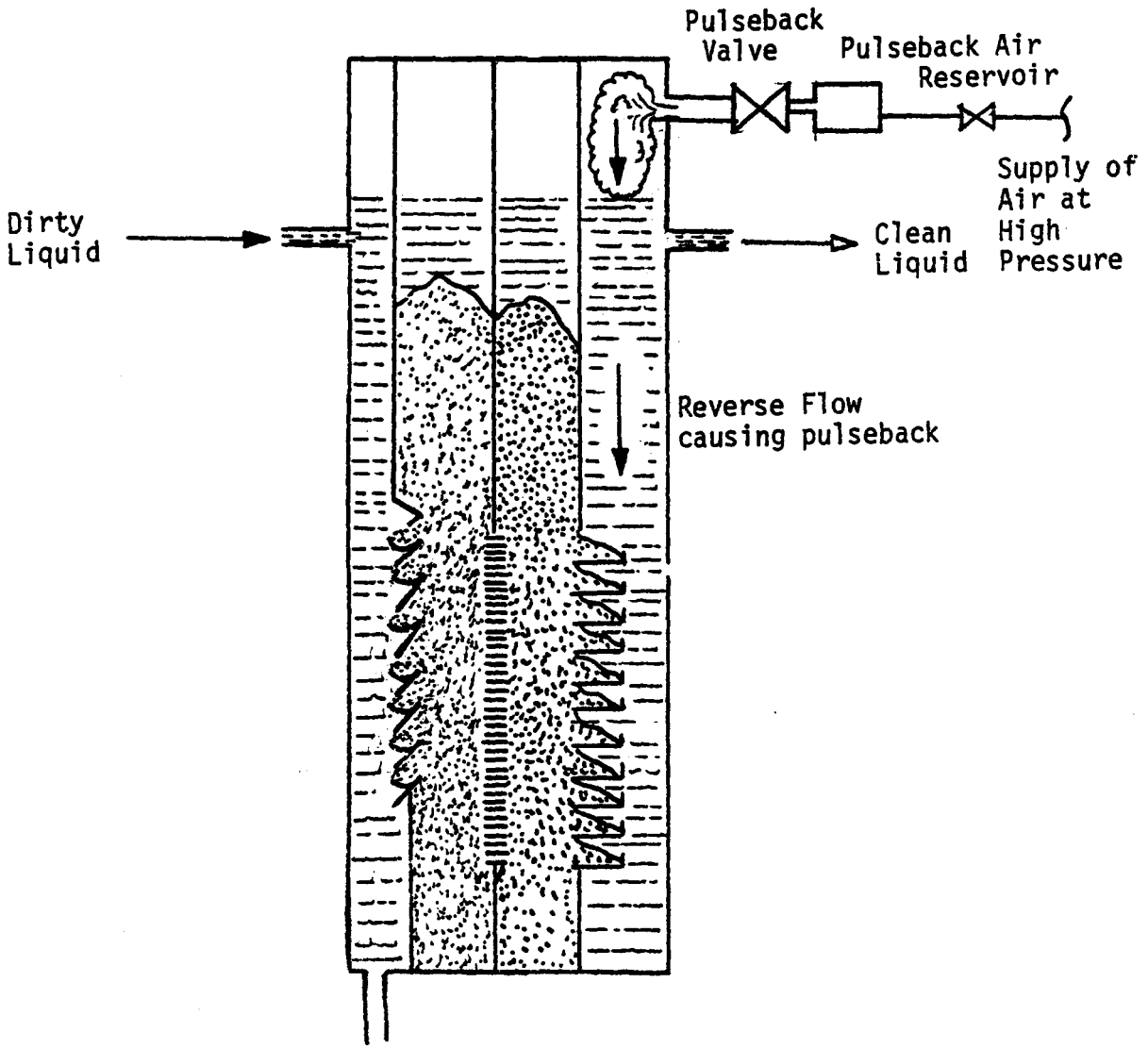

Figure 3. Schematic diagram of experimental panel bed.

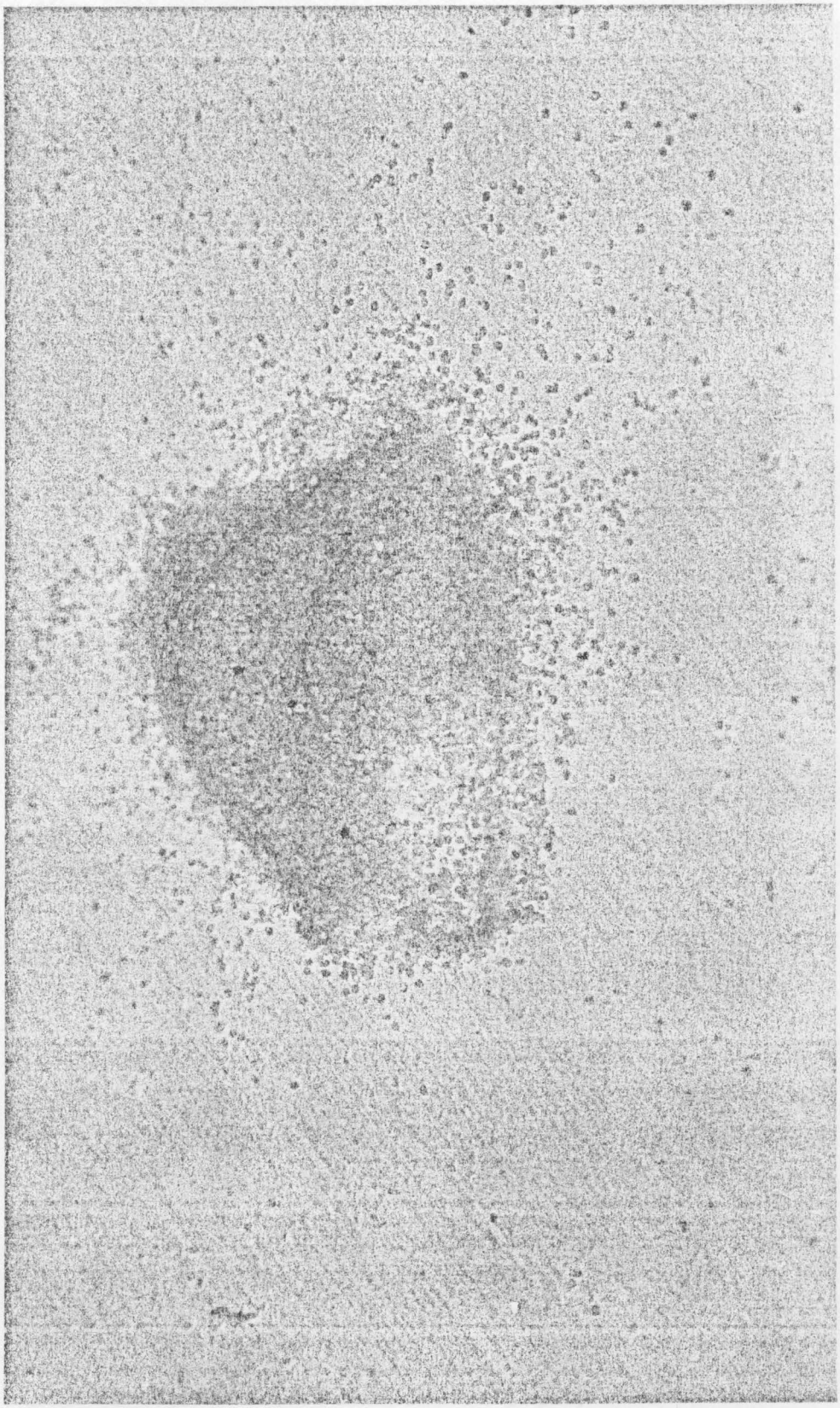

Figure 4. 20-30 mesh sand. Note the rounded shape of the particles.

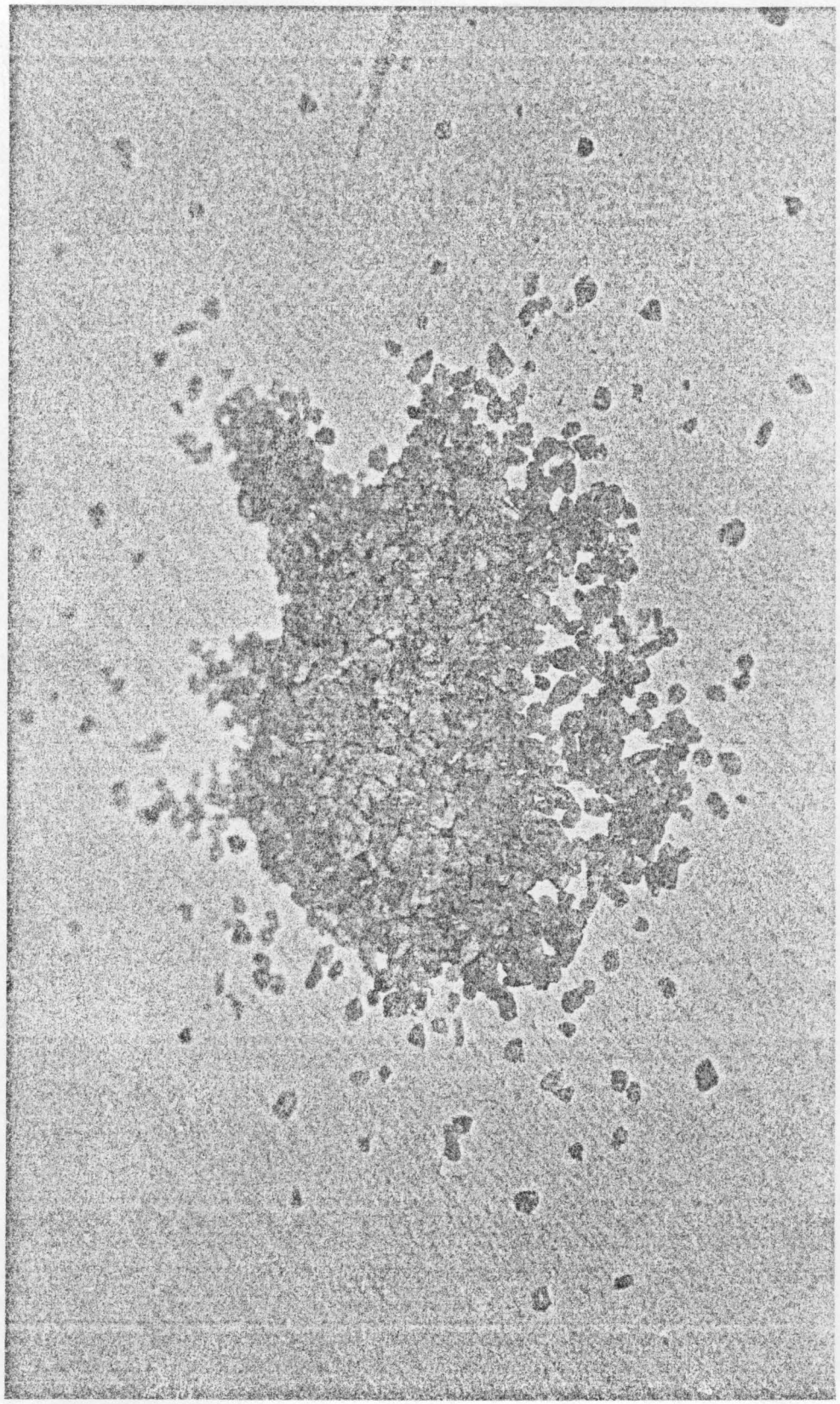

Figure 5. 8-14 mesh sand. Note the highly angular nature of the particles.

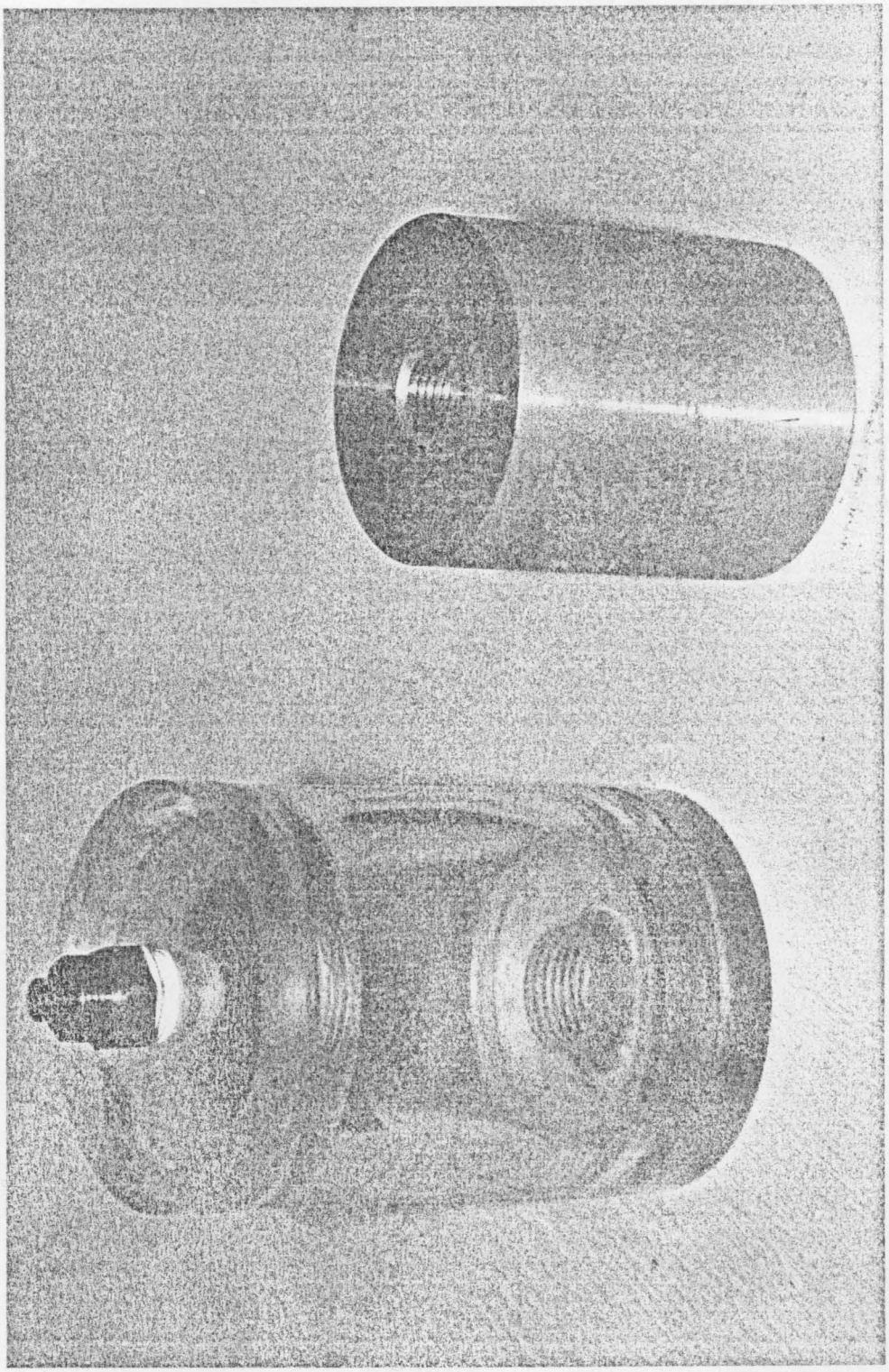

Figure 6. Air reservoirs. 103 cm^3 (left) and 51 cm^3 (right).

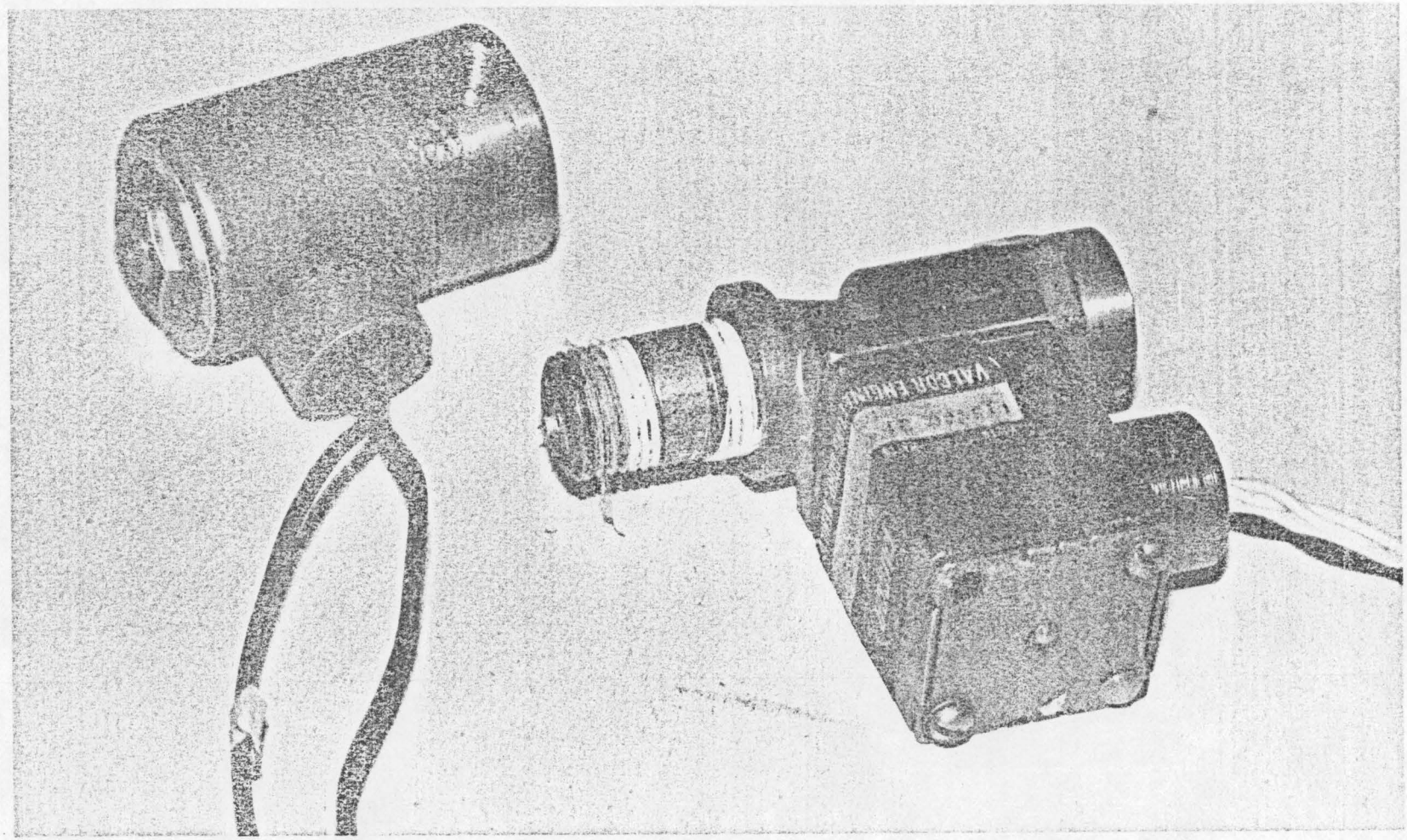

Figure 7. Solenoid valves used for pulseback. 3.38 mm valve (left) and 6.15 mm valve (right).

the particle size-reservoir-valve-air pressure configuration. Table I gives the explanation of the code symbols along with an example.

For each particle size, a series of runs was made using all possible combinations of the two air reservoirs and the two valves. At each particle size-reservoir-valve configuration the panel bed was pulsed using a series of valves for the air reservoir pressure. During each pulse the pressure drop across the panel bed was measured. After each pulse the sand which was spilled during the pulse was removed, decanted, and weighed.

Method of Procedure

Equipment Preparation. In early 1977, one of the experimental panel beds used by Lee (1975) in his studies of the panel bed filter was moved from The City College of New York to VPI & SU. (For information concerning the equipment design, see the dissertation by Lee). The equipment included the filter case, three sets of louvers, an air regulator, one air reservoir, a pressure gauge, one solenoid valve, an electrical switch, and various fittings. In the late winter of 1977 the equipment was installed in Room 217 of Randolph Hall as shown in Figure 8.

On arrival, the louvers which were made of solid brass had a surface coating of brown scale. This coating was removed by immersing the louvers into a hydrochloric acid solution of unknown concentration. Then the louvers were primed and sprayed with Rust-Oleum enamel paint. When the louvers were installed in the filter

TABLE I. Symbolic Code used in Pulseback Experiments

A = 2.362 to 1.168 mm sand (8-14 mesh)

C = 0.833 to 0.542 mm sand (20-30 mesh)

1 = 6.15 mm diameter solenoid valve orifice

2 = 3.38 mm diameter solenoid valve orifice

B = Air reservoir #1 (103 cm^3)

S = Air reservoir #2 (51.4 cm^3)

X = Reservoir air pressure (psig) (1 psig = 6.9 kPa)

Example: A-1-B-16 means 8-14 mesh sand, 6.15 mm valve, reservoir #1, with 16 psig air pressure (110.4 kPa).

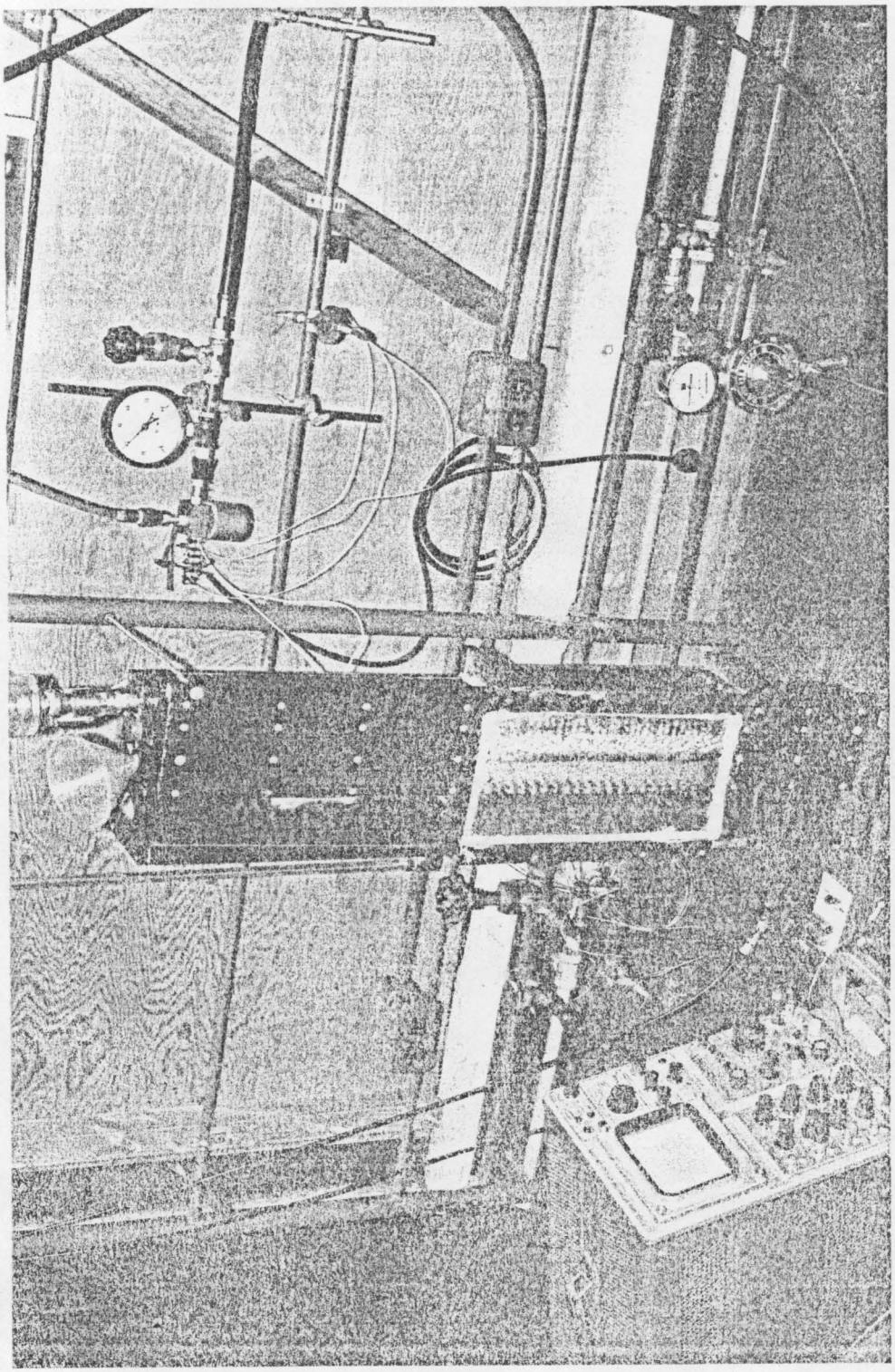

Figure 8. Complete equipment set up for pulseback.

case the paint was scarred and shortly thereafter brown tubercules formed on the louvers. Then the enamel paint was removed by applying methylene chloride to the paint and sand blasting the residue. The sand blasting technique proved to be very effective but pitted some portions of the louver metal. Finally, the louvers were primed again with Rust-Oleum Deep Red Primer and painted with Rust-Oleum Flat Paint. This method proved successful in controlling the metal degradation during the present experiments. In October, 1977, a few brown tubercules were noticed on the louvers.

Sealing the Filter Case. After the louvers were installed, the transparent glass window, shown in Figure 9, was sealed into place using Dow-Corning Silicone Caulk. Then the filter case was filled with water to test the water tightness of the filter case joints. (The details of the operating procedure are given in a later section). The filter case leaked badly at many of the joints and at the window seals.

The filter case was constructed of 12.1 mm (1/2-inch) aluminum plate and joined by Allen screws, which had been counterbored. Therefore, the filter case could be disassembled to seal the joints. While disassembling the filter case, the glass window was shattered. This was replaced by a second glass window which was also shattered. Subsequently, a piece of plexiglass was used for the transparent window and this has proved quite satisfactory.

In the first attempt to seal the filter case, a layer of Dow-Corning Silicone Caulk was used to create a quasi-gasket in the metal

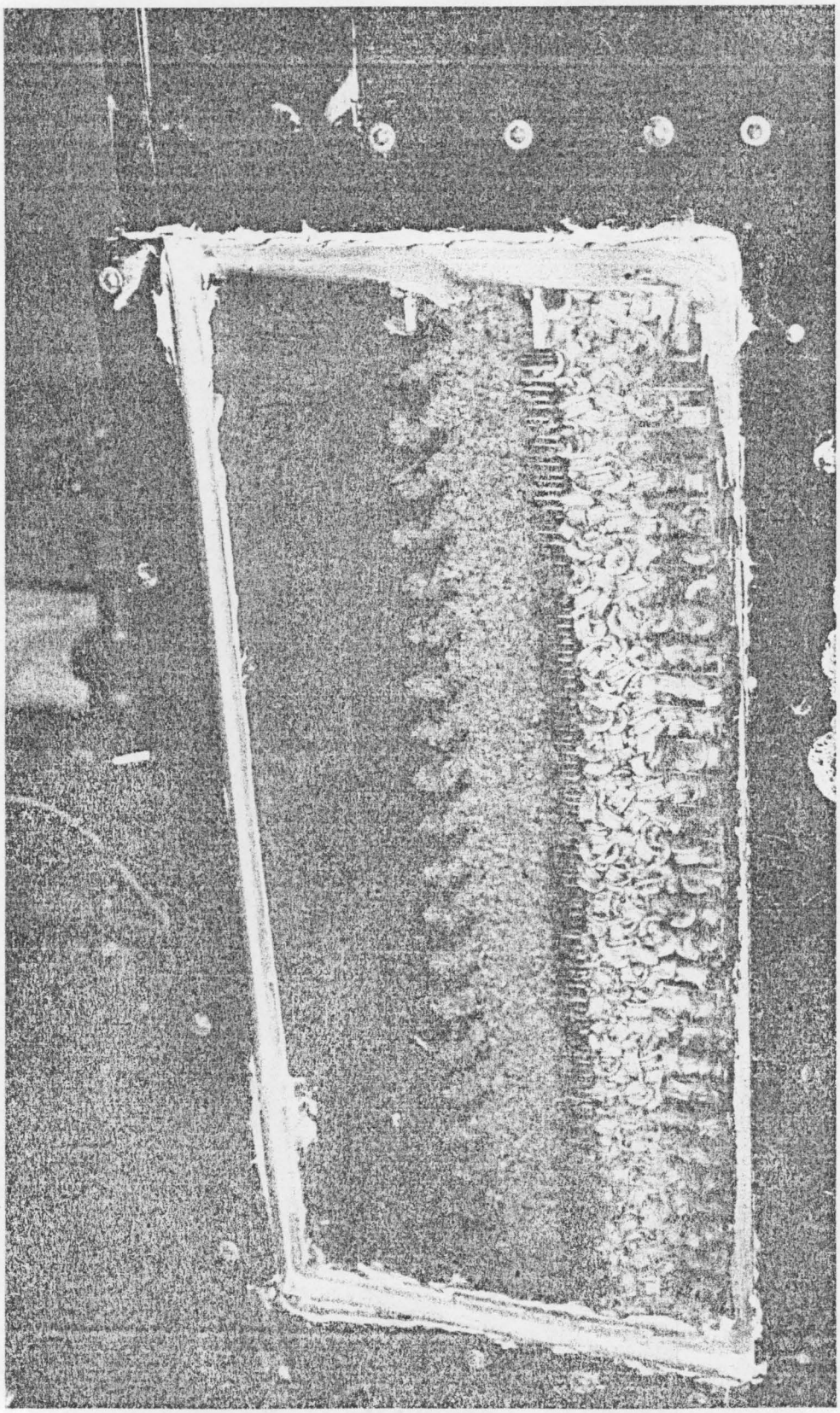

Figure 9. The panel bed filter showing the sand, support, louvers, and window.

joints. A static water test proved that the filter case was still not sealed. After disassembly, the caulk compound was removed from the metal surfaces by using a coarse wire brush operated with an electrical drill. A second attempt was made to use the caulk compound in heavier quantities to form a gasket type seal, but this too, proved ineffective. Next, gaskets were cut for all of the joints from McCord 0.4 mm (1/64 inch) gasket paper. The filter case was then reassembled with the paper gaskets in the joints, but still leaked badly during the static water test. New paper gaskets were then cut and the filter case was then reassembled using Permatex gasket compound whenever possible to help create a water-tight seal. The static water test showed considerable improvement in the effectiveness of the seals but serious leaks still existed. Finally, a combination of Plastic Filler for Aluminum and Epoxy Cement was used to fill and seal the cracks at the joints. After several crack-filling treatments the filter case was virtually leak-free under the static water test. The later pulseback experiments showed that the seals retained their integrity throughout the investigation.

Pressure Measurements. For measurements of pressure within the panel bed filter during pulseback, pressure transducers were inserted on the clean and dirty side of the panel bed. The transducer elements are shown in Figure 10. For details concerning the transducer system, see Appendix B of this thesis.

During the pulseback, the signals from the transducers were amplified by the electronic units shown in Figure 11. Then the

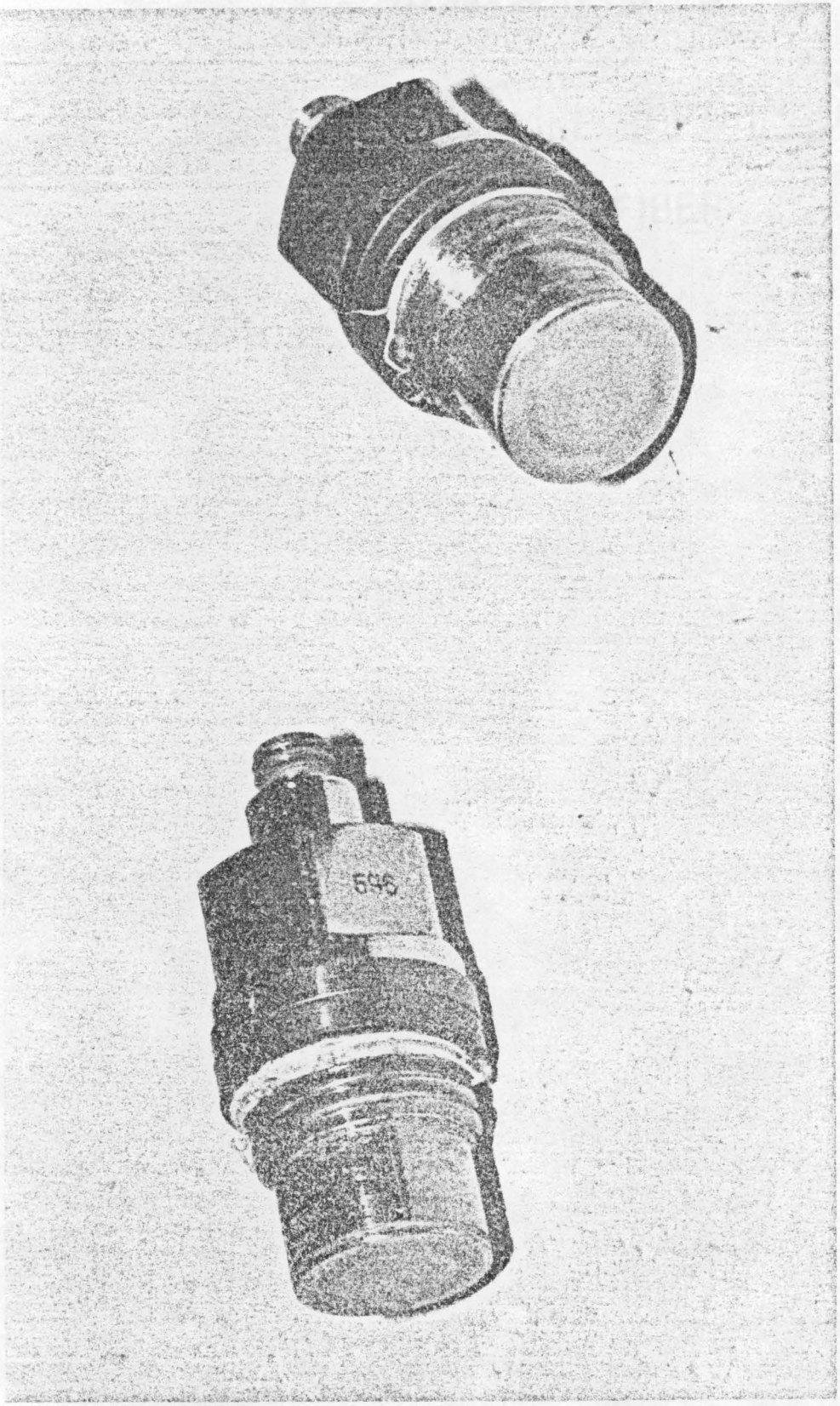

Figure 10. Transducer elements which were inserted into the filter case.

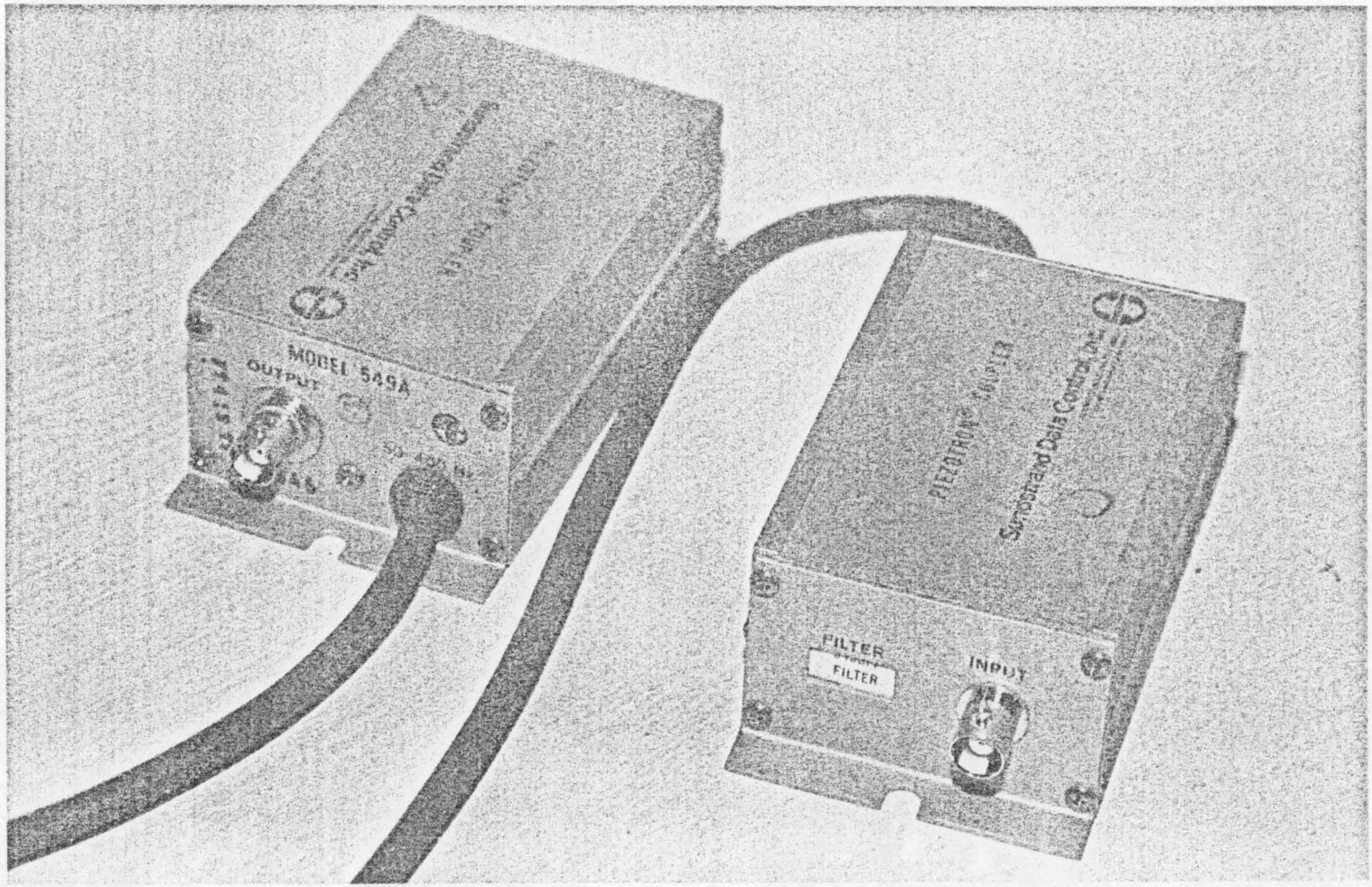

Figure 11. Electronic couplers used to transmit the transducer signals to the oscilloscope.

clean-side signal was electronically subtracted from the dirty-side signal. The difference was then transmitted to a Tektronix Four-Channel storage oscilloscope as shown in Figure 12. The pressure difference signal was then stored on the oscilloscope screen and photographed with a 35-MM camera. In this way, a permanent record of the pressure drop-versus-time history across the panel was obtained for further analysis.

During the early stages of the investigation, the amplified clean and dirty side pressure signals were transmitted directly to the oscilloscope without electronic subtraction. Analysis of this data was difficult and time-consuming. This was because the signals then had to be reproduced by hand and then subtracted by hand for display on graph paper. Therefore, the electronic subtraction device was installed. This device, as shown in Figure 13, was designed and constructed by Mr. S.C. Reid of the VPI & SU Chemical Engineering Department. The details of the device can be found in Appendix 3.

Calibration of the Transducers. To be assured of accurate pressure drop data, the pressure transducer systems were calibrated. However, the calibration procedure was not straight forward since the transducer elements were of the quartz type. A transducer of this type responds well to a change in pressure but has a natural decay in its output signal thereafter. Therefore, several methods were used in the attempts to calibrate the systems.

The first method involved measuring the electrical output of only the transducer element with an analog volt-ohmmeter. This method

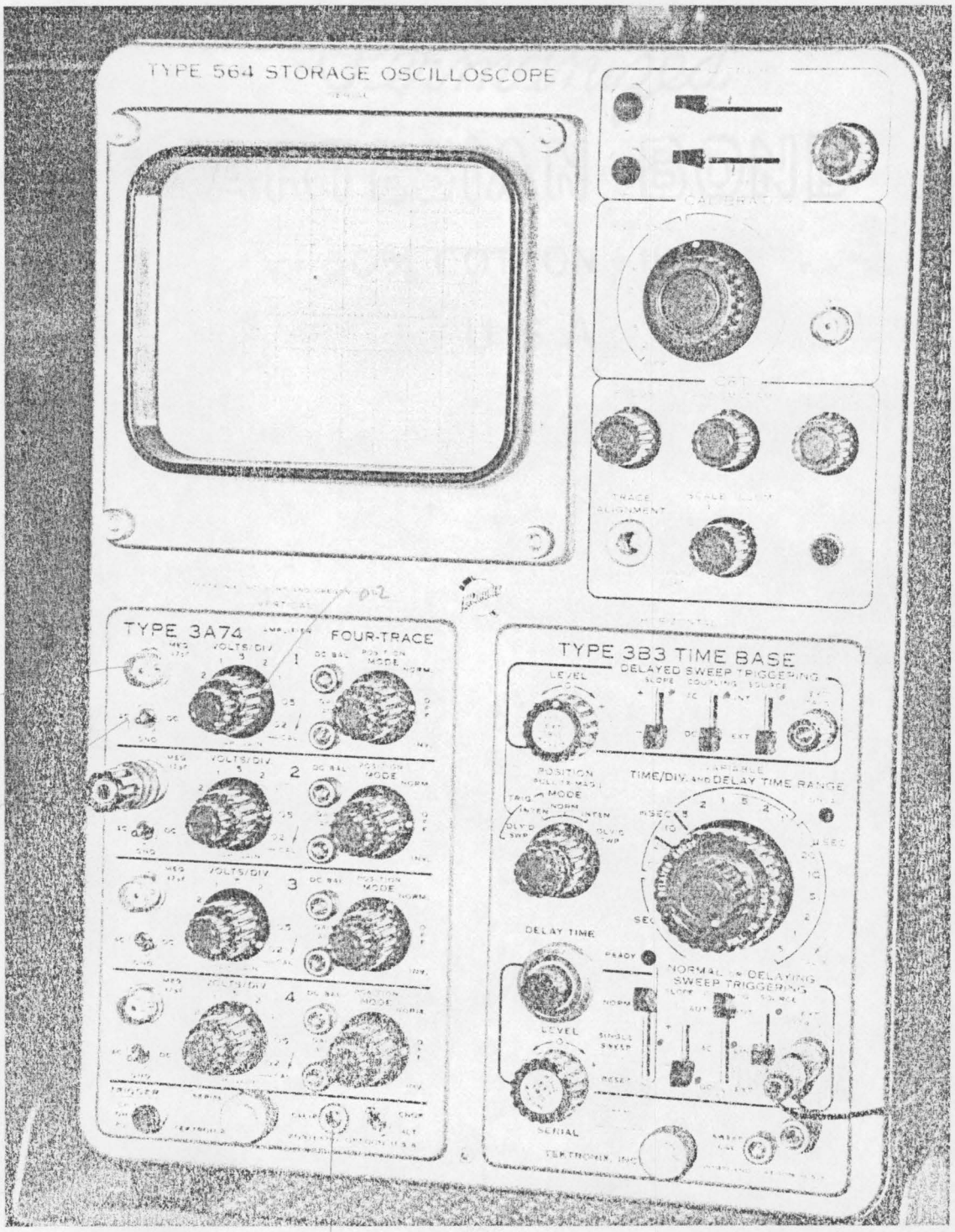

Figure 12. Oscilloscope used to display the pressure difference from the electronic subtractor.

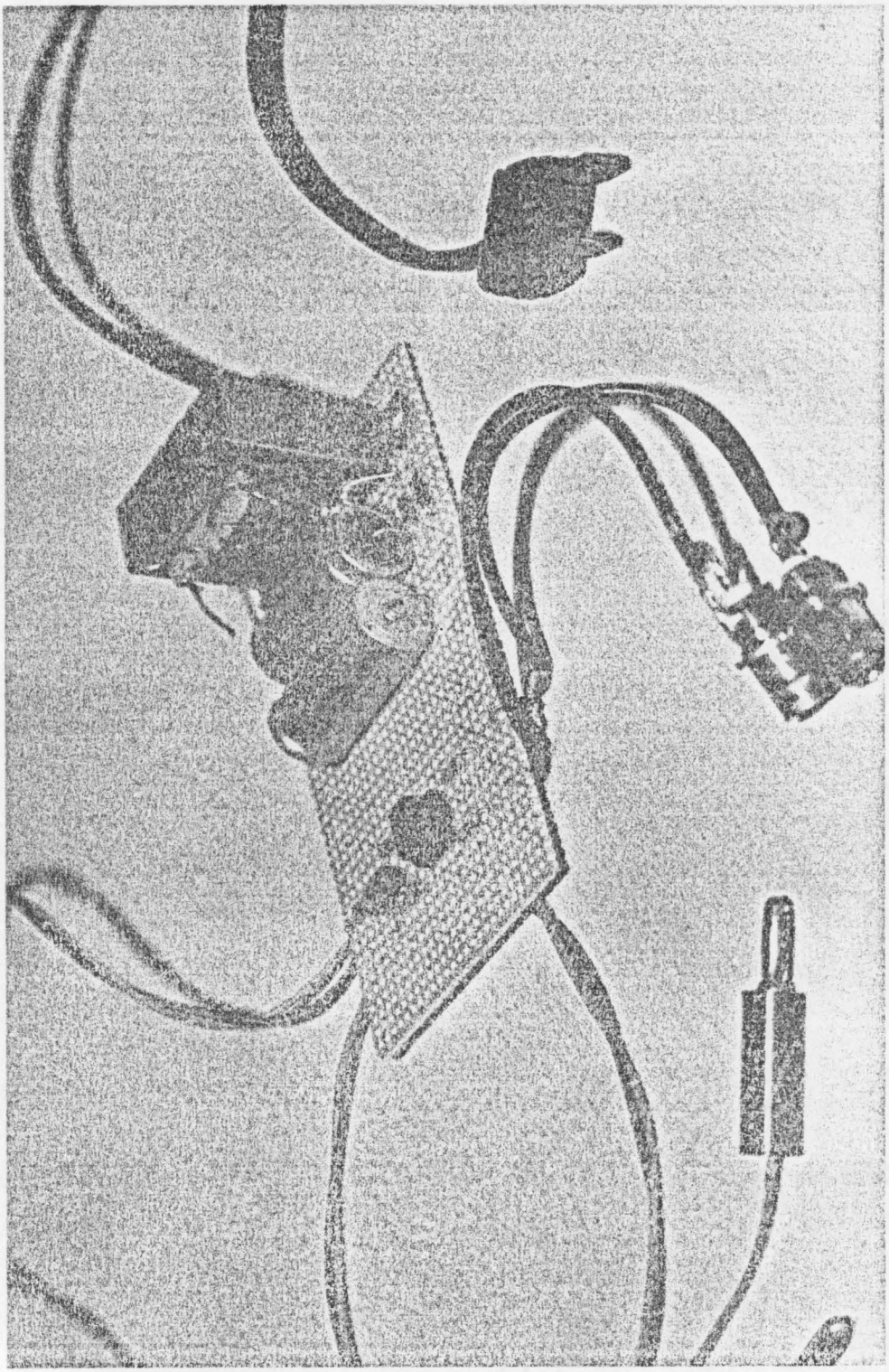

Figure 13. The electronic subtractor which receives the transducer signals and generates the pressure difference signals.

proved ineffective due to the short life of the output signal resulting from the pressure pulse. The needle on the volt-ohmmeter swung too rapidly to be read accurately. The next method involved connecting the transducer system to the available water supply so as to measure the pressure pulse when the valve was suddenly opened. The pressure signal was displayed and stored on the oscilloscope while the water pressure was read from a conventional pressure gauge. After this method was attempted several times it was discarded since the water pressure could not be read accurately from the pressure gauge. The final method involved connecting the transducer system to the available air supply via an air regulator. The air regulator fixed the maximum pressure which the transducer would measure. When the air supply valve was suddenly opened, the pressure signal was stored on the oscilloscope screen. The maximum value for each of three pressure signals was then recorded for each transducer system. Calibration curves were then constructed from these data.

Preparation for Pulseback. All letters in this section refer to Figure 14.

To prepare for the pulseback experiments the following procedure was followed:

> Initially all valves were closed except solenoid valve J. Sand was loaded through Port H. A common plastic laboratory funnel was used to facilitate the sand loading. Also, sand develops a high degree of apparent cohesion when it is wet with water.

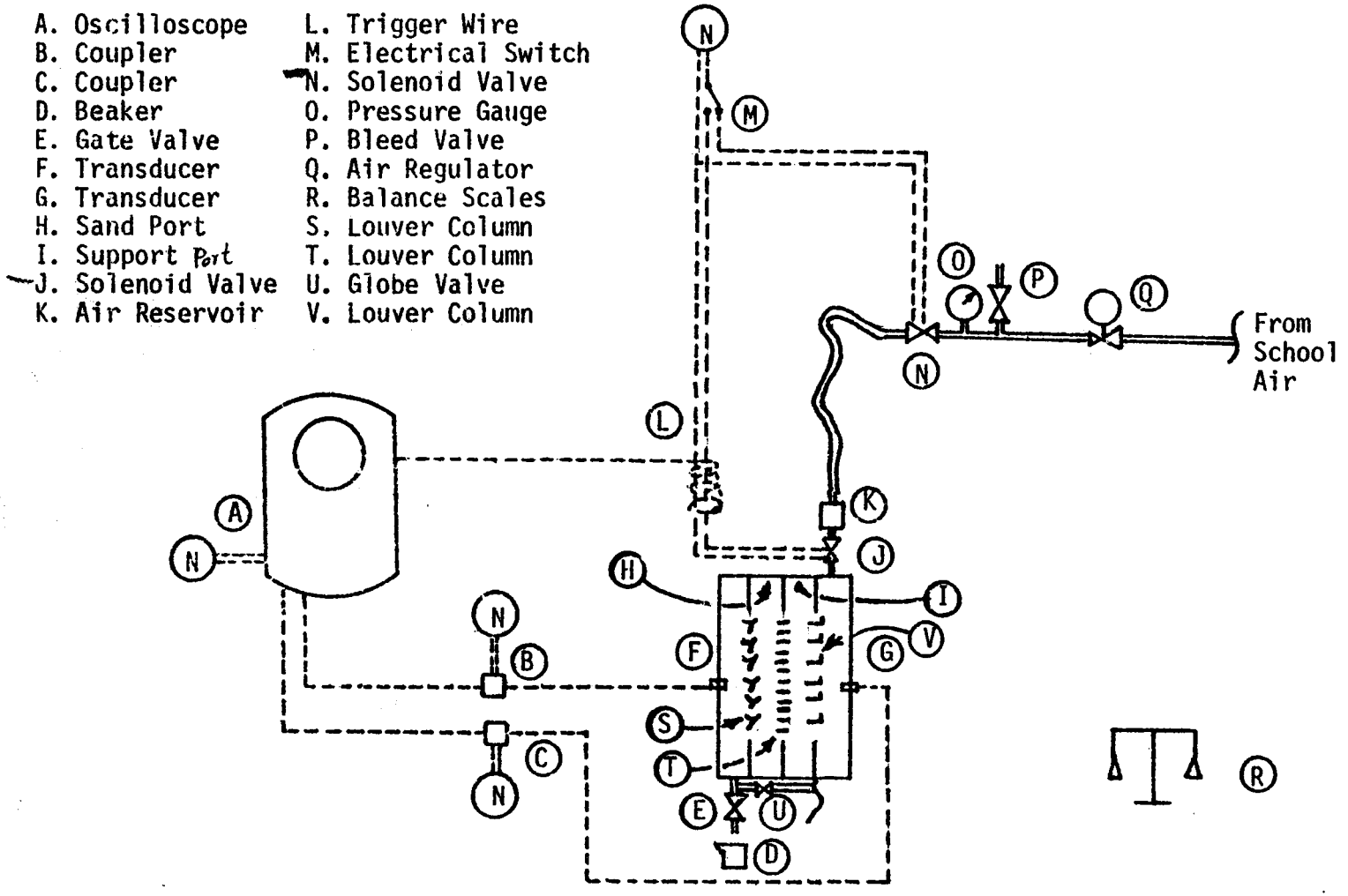

Figure 14. Schematic illustration of equipment set-up. (Dash line indicates electrical wire connection).

Therefore, the sand had to be completely dry or the sand loading process was practically impossible. The sand was allowed to free fall and rest between Louver S and Louver T. Next, the support material was loaded through Port I. A funnel was also used for this procedure. Coarse sand of 8-14 mesh and 3/8 inch Berl saddles were tried separately during the investigation. Both the sand panel and the support material were loaded until the level of each had reached the loading ports. Globe valve U was then opened to admit water into the Filter Case. When the water level reached the prescribed mark on the Sight Tube, Valve V was closed. After several glass sight tubes were broken, a piece of Tygon Flexible plastic tubing stretched to a near vertical attitude and held by a common Lab Clamp proved satisfactory and is shown in Figure 15. The chosen value for the maximum water level provided for a sufficient water seal which prevented the leakage of visible air bubbles between the louver support baffle and Louver V. The mark indicating the maximum water level was placed on the sight tube with a common red grease pencil. A higher water level allowed an excessive amount of water to escape through Surge Port H during the pulseback.

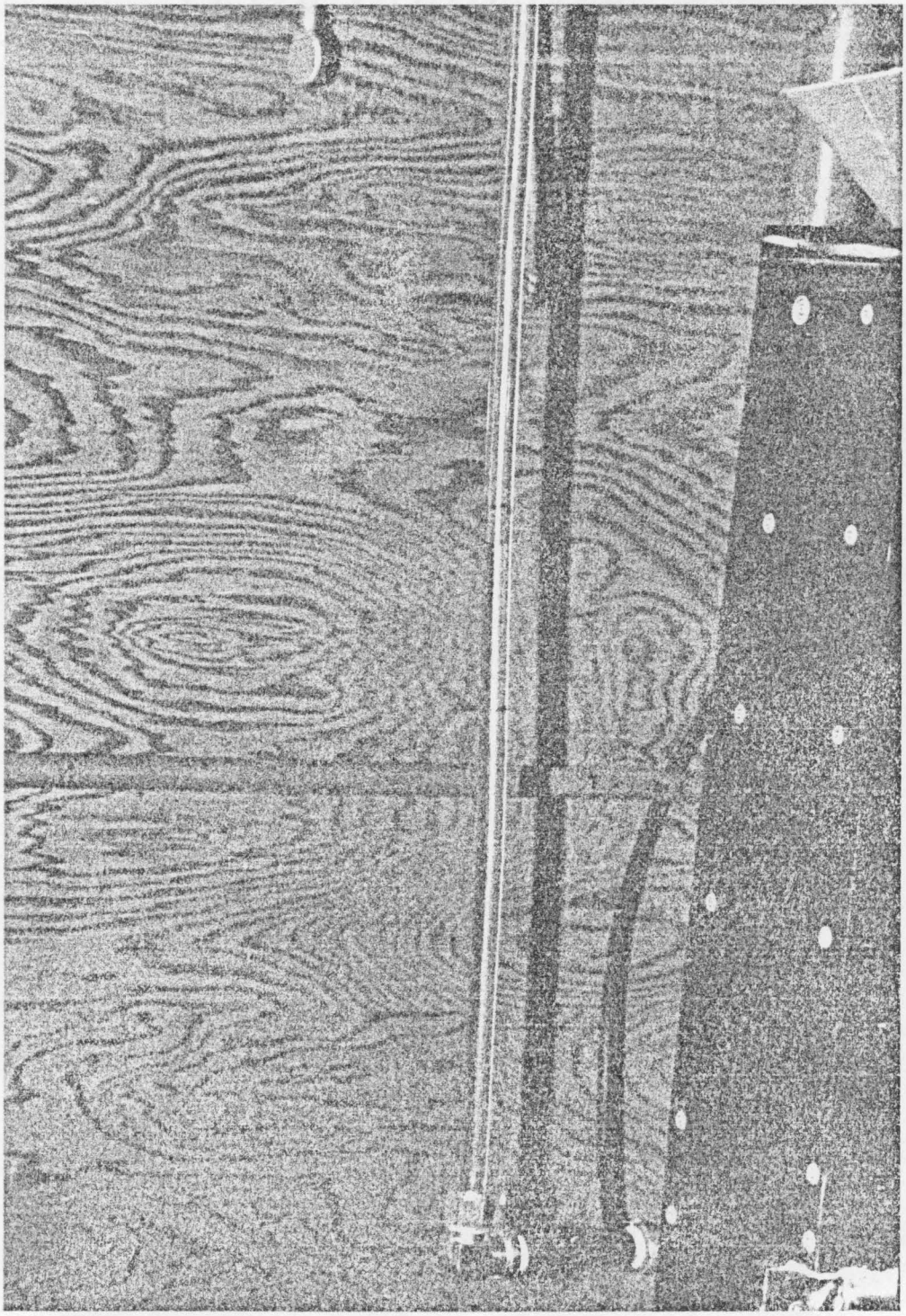

Figure 15. Sight tube of Tygon tubing.

Final Procedures. The final procedures prior to the pulseback experiments included pulsing the filter a minimum of three times at the maximum air pressure to be used at the particular particle size-reservoir-valve configuration. These initial, high-intensity pulses settled the sand and support material to the equilibrium state to be used during the pulseback experiments. (See the following section on history effects for more information). The procedure for pulsing the filter will be detailed in a subsequent section. After the settling pulses, the levels of sand and support material were inspected via Ports H and I respectively and additional sand and support material were added as required. During the pulseback experiments the sand and support levels were maintained approximately 6.35 mm below the bottom face of the top side of the filter case. After the additional sand and support were added, stoppers were inserted into Ports H and I to prevent any surge of material from these ports. Small diameter holes were bored in the stoppers to allow air to re-enter the cavities immediately above the sand and support panels after a pulseback.

Pulseback Procedure. After the filter unit had been prepared for pulseback, Oscilloscope A, the electronic subtractor and pressure signal amplifiers were switched on. Also, the power to operate Solenoid Valves J and N was switched on. A schematic drawing illustrating the electrical circuit operating the two solenoid valves is shown in Appendix 4. Next, Air Regulator Q was used to adjust the line pressure leading to Air Reservoir K. Gate Valve P was used to quickly adjust the line pressure by bleeding any excess air from the

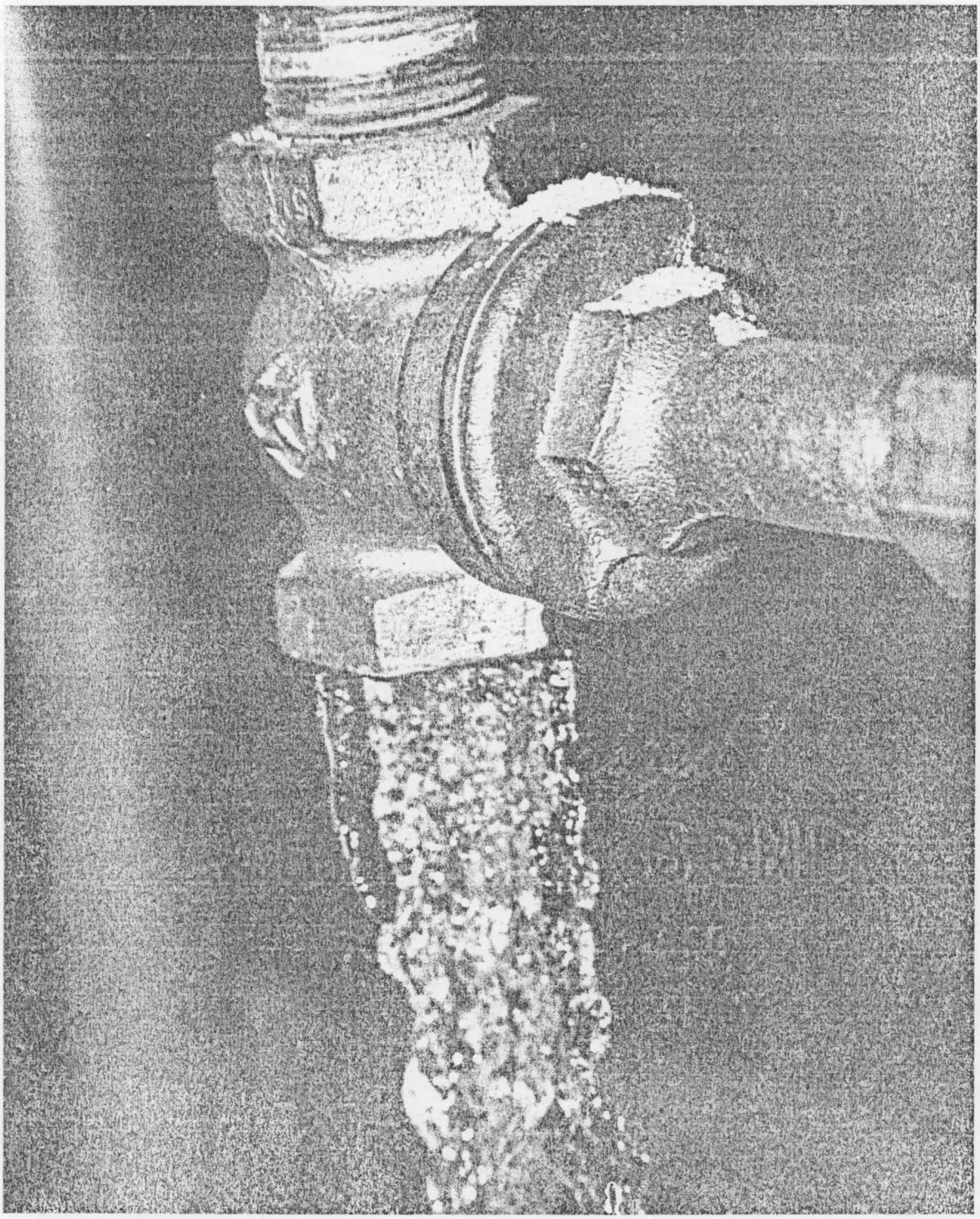

Figure 16. Draining of the sand and water from the bottom of the filter case.

line. The air reservoir pressure was monitored by reading Pressure Gauge O. Electrical Switch M was then operated to close Solenoid Valve J and open Solenoid Valve N. This allowed Air Reservoir K to fill with air at the preset line pressure. When the position of Electrical Switch M reversed, Solenoid Valve J was opened and Solenoid Valve N was closed. This allowed only the air contained in Air Reservoir K and the other fittings and tubing between the solenoid valves to be admitted to the clean side of the panel bed filter. When the air entered the air cavity above the water level on the clean side, the pressure increased in this cavity causing a flow of water in the direction from the clean side of the filter to the dirty side. Prior to the opening of Solenoid Valve J, a "trigger" signal was transmitted to the oscilloscope. This trigger signal was generated by wrapping a wire to form an induction coil around the wires carrying power to Solenoid Valve J. When Solenoid Valve J opened, the induction coil sensed the power fluctuation and transmitted the trigger signal to the oscilloscope. When the oscilloscope received the "trigger" signal, it began to display and store the pressure difference signal on the oscilloscope screen. At this point an identifying label was affixed to the oscilloscope screen and the screen was photographed with a 35 MM camera. The oscilloscope screen was then erased. During the pulseback, the sand which was spilled collected by gravity on the dirty side of Louver S. This sand was removed by opening Gate Valve E and allowing the sand-water mixture to flow from the bottom of the filter case as shown in Figure 16.

The flow was continued until the flowing stream appeared clear and free from sand and then the valve was closed. Care was taken that Gate Valve E was not opehed too suddenly nor too wide so that the sand in place behind Louver S was not disturbed. The sand-water mixture was caught in a beaker and the water was decanted, retaining the sand. Then the saturated sand was weighed on Balance R and the weight was recorded. Finally, additional water was added to the filter case by opening Valve U. When the water level reached the prescribed mark on the Sight Tube,Valve U was closed and the air reservoir pressure was adjusted for another pulseback.

A sand dumping port sealed with a rubber stopper was provided on the bottom side of the filter case for changing the sand.

Wet Sand-versus-Dry Sand. The dry weight of the sand spilled during pulseback was needed for the analysis of data. Two methods were tried to determine the dry weight of the wet sand samples.

The first method involved simply drying the wet samples. This was done by placing the wet samples on blotter paper and allowing the samples to remain undisturbed in the ambient laboratory environment for 24 hours. This method proved time consuming.

The second method involved weighing a sample of dry sand. The weight was recorded and the sample was then saturated with water. Excess water was decanted and the saturated sand sample was then weighed and the weight was recorded. Plots of wet sand weight versus dry sand weight were then made. Therefore, for any given wet sand weight, a dry sand weight was immediately available.

History Effects on the Pulseback Results. The pulseback experiments were conducted by varying the value of the air reservoir pressure downward in a decreasing sequence from the maximum pressure for a particular particle size-valve-reservoir configuration. During the early experiments it was noticed that occasionally the value of the sand spill did not vary in a decreasing sequence with the value of the air reservoir pressure. Based on the work of Lee (26) it was thought that a functional relationship should exist between the sand spill and the air reservoir pressure. Therefore, the lack of such a relationship during the early experiments prompted an investigation of the effect of the history of pulses upon the sand panel, on the value of the sand spill at a given air reservoir pressure.

This investigation involved the repeated pulsing of the panel bed at an air reservoir pressure midway in the sequence of air reservoir pressures to be tested. The panel bed was pulsed at the same pressure until the sand spill achieved an equilibrium value. Next, the panel bed was pulsed at the maximum air reservoir pressure in the sequence until the sand spill achieved an equilibrium value. Finally, after an equilibrium sand spill was achieved at the maximum air reservoir pressure, the bed was again pulsed at the lower pressure until equilibrium sand spill was reached. This procedure provided information on the effect of the degree of settling of the panel bed and if this settling could be accelerated by several initial high pressure pulses.

RESULTS AND DISCUSSION

Procedures Prior to Pulseback

Transducer System Measurement. The literature which accompanied the transducers indicated that the transducers' response was within 80-120 mv/psi with a nominal value of 100 mv/psi. The literature also stated that the transducers' response was linear over a range of pressures from 0 psi to 500 psi. The pressures used in the pulseback experiments were well within this range. Based on this information each transducer system was tested at 40 psig (276 kPa), 20 psig (138 kPa), and 0 psig (0 kPa). The results for the transducer calibration are shown in Table II. Also, the transducer system output voltage is plotted versus the applied pressure in Figures 17 and 18. Note that each transducer system response was linear throughout the range of pressures tested. Also, both transducer systems responded the same with an output of 110 mv/psi--well within the range indicated by the transducer manufacturer.

History Effects. During the early experiments of this investigation, unusual trends were detected in the sand spill data. As the value of the air reservoir pressure was decreased sequentially from 32 psig (221 kPa), the sand spill also decreased. However, when pressures as high as 20 psig (138 kPa) were reached, successive pulsebacks did not necessarily yield a net decrease in sand spill. It was thought that this unusual trend might be due to the sand in the panel settling to an equilibrium packing. Therefore, an experiment

TABLE II. Transducer System Calibration Data

Transducer	Regulator Pressure (psi)	Oscilloscope Divisions (div)	Oscilloscope Scale Factor (volts/div)	Transducer Output (mv/psi)
Clean Side	40.0	11/5	0.2	110
Clean Side	20.0	5.5/5	0.2	110
Dirty Side	40.0	11/5	0.2	110
Dirty Side	20.0	5.5/5	0.2	110

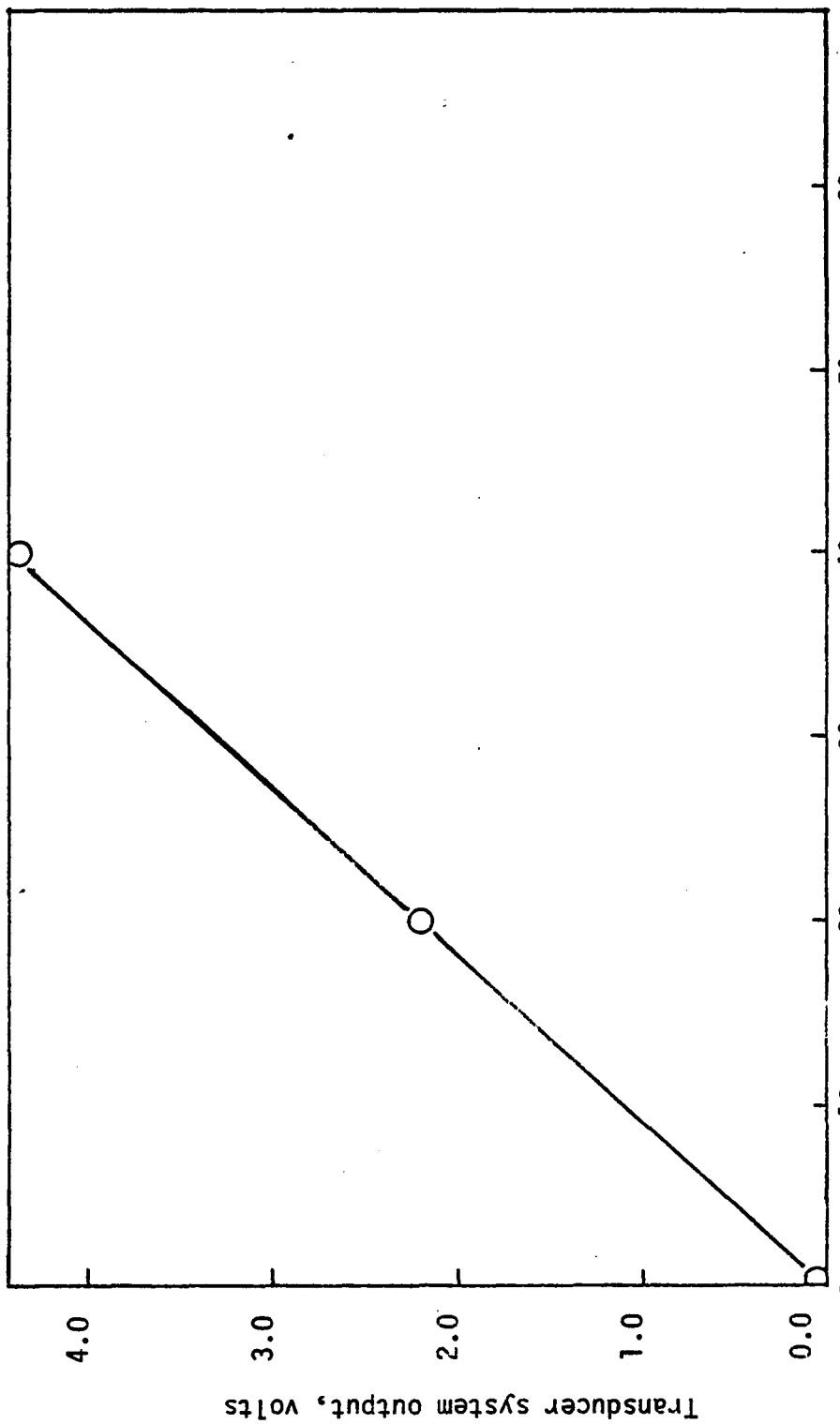

Figure 17. Dirty side transducer system calibration data.

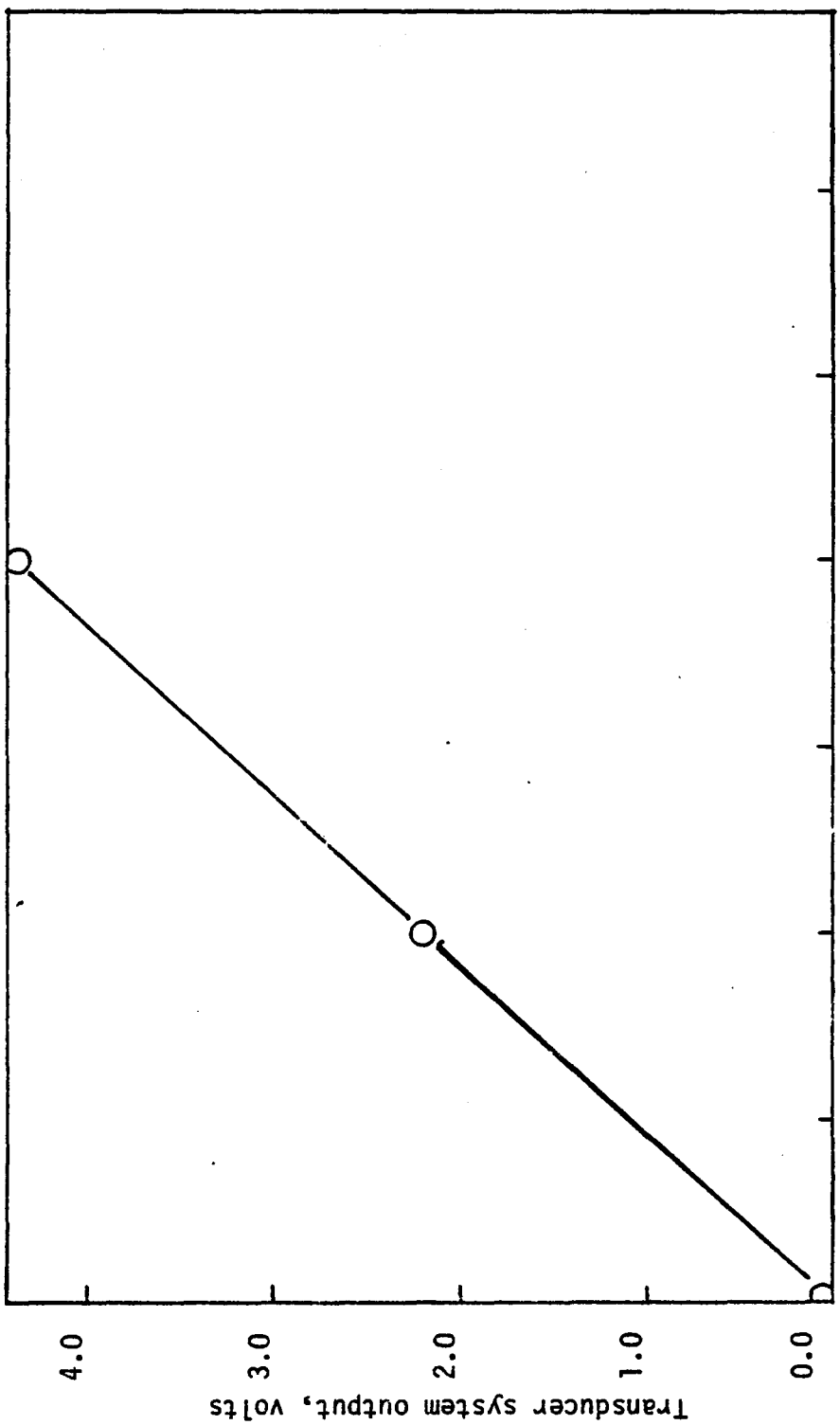

Figure 18. Clean side transducer system calibration data.

was done to determine the effects of any history of pulsebacks on the sand.

The experiment consisted of pulsing a fresh fill of sand at 16 psig (110.4kPa) until the sand spill reached an equilibrium value. The results of this experiment are shown in Figure 19. A second experiment was then done to determine if the equilibrium state could be reached in a fewer number of pulsebacks. It was thought that several relatively high pressure pulsebacks (32 psig) would settle the sand quickly and then the sand would be in an equilibrium state for any lower pressure (16 psig). Both experiments were performed with configuration A-1-B. The results of the second experiment are shown in Figure 20.

It is striking that by pulsing only at 16 psig (110 kPa), about 11 pulses were required to reach equilibrium. This was frustrating since 11 pulsebacks would empty the sand reservoir and it is thought that some of the scatter in the data was due to the necessary filling of the sand reservoir. The second experiment showed that an equilibrium state for a relatively low pressure could be reached quickly by pulsing initially at a relatively high pressure. This second, more expedient method proved helpful in subsequent pulseback experiments.

Wet Sand-versus-Dry Sand. To provide for the most rapid analysis of the pulseback data, it was necessary to have the dry weight of the sand spill samples immediately available. Therefore, experiments were done to determine the relationship between the

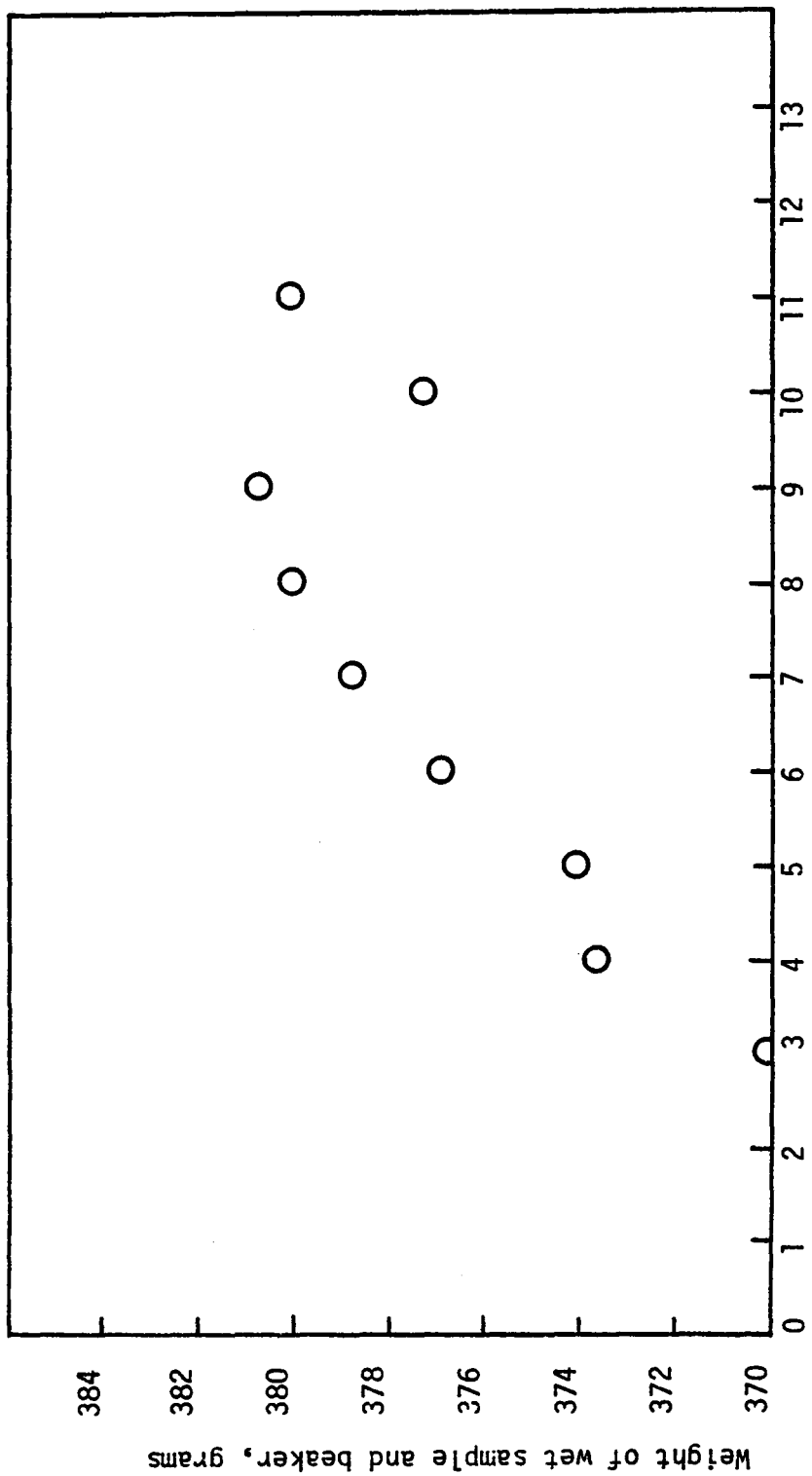

Figure 19. Approach to equilibrium state for the panel bed by pulsing at a relatively low pressure.

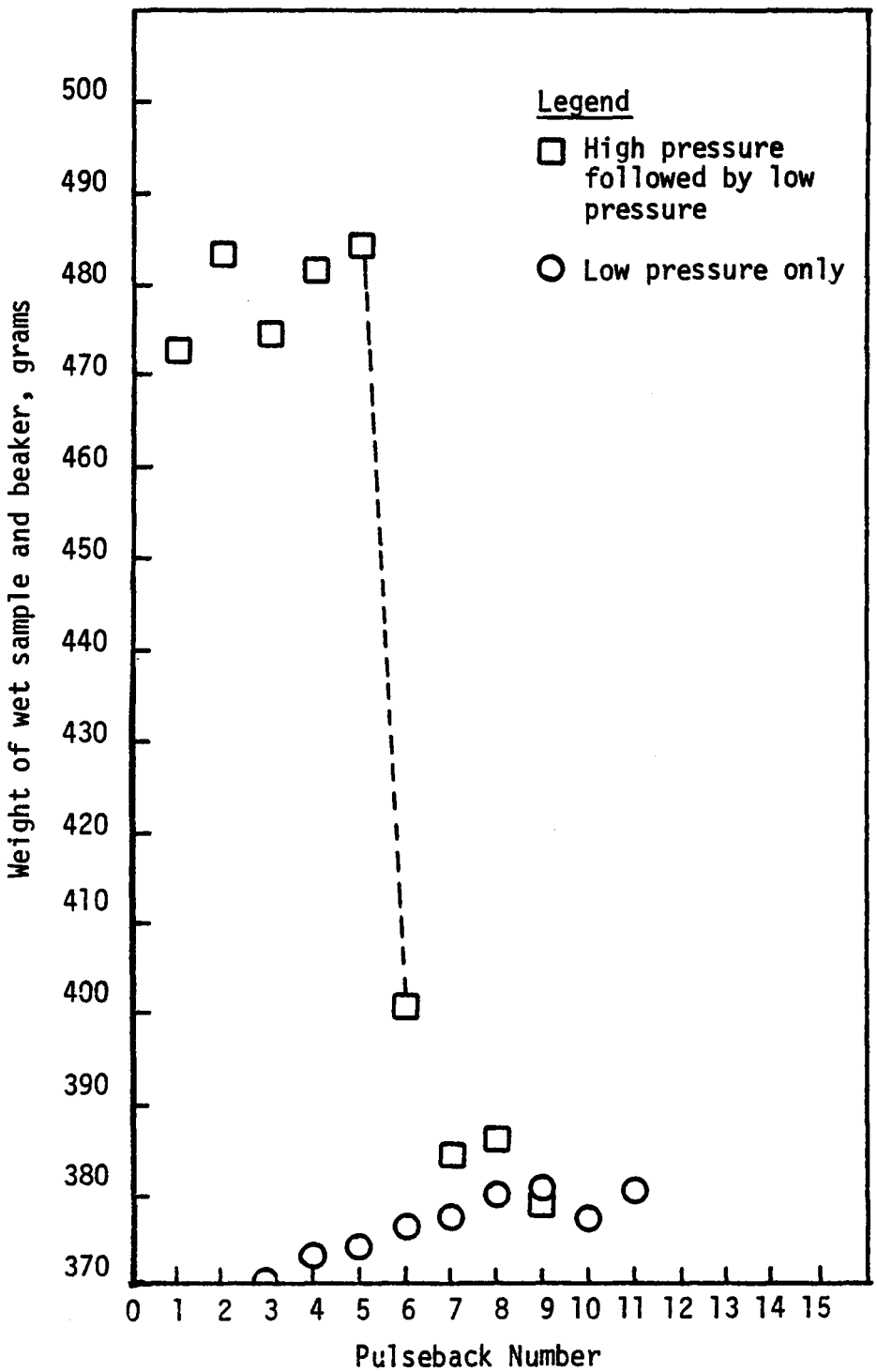

Figure 20. Comparison of approach to equilibrium of initial high pressure pulses followed by low pressure pulses, with, low pressure pulses only.

weight of saturated wet sand samples and the corresponding dry weight of the samples. The data were plotted as dry weight versus wet weight and are shown for 8-14 mesh sand in Figure 21 and for 20-30 mesh sand in Figure 22. As expected, the plots were linear with a different slope for each particle size of sand.

The dry weight-vs-wet weight data can easily be converted into porosity values for each particle size. Porosity is defined as the ratio of void volume to total volume and actual porosity values for the sands tested are shown in Table III.

Pulseback Data and Analysis

High Speed Movies. The pulseback phenomenon is a very rapid, short lived phenomenon existing at most for 0.1 seconds. Therefore, to obtain a more accurate visual description of the pulseback phenomenon, high speed movies were made of the equipment during pulseback. The following cases were filmed: C-1-B-2, C-1-B-20, A-1-B-4, and A-1-B-32. No basic differences were detected in the four cases filmed. The pulseback phenomenon occurred in the same way each time.

The pulseback phenomenon consists of a rapid but uniform flow of sand from the louvers. The sand flow has a slight upward attitude but it is thought that this is due to the cup shaped construction of the louvers. The rate of the sand flow increases very rapidly after the initiation of pulseback. As the sand commences to flow from the louvers, the sand panel separates from the central support louver

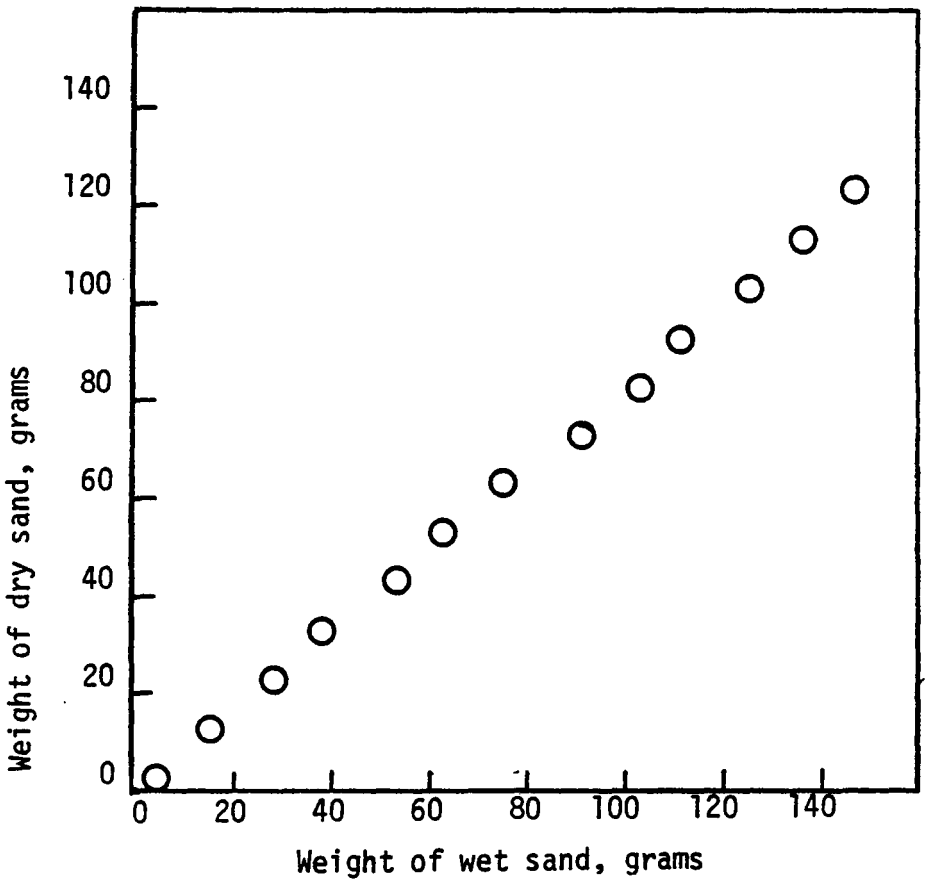

Figure 21. Relationship between 8-14 mesh wet sand and dry sand.

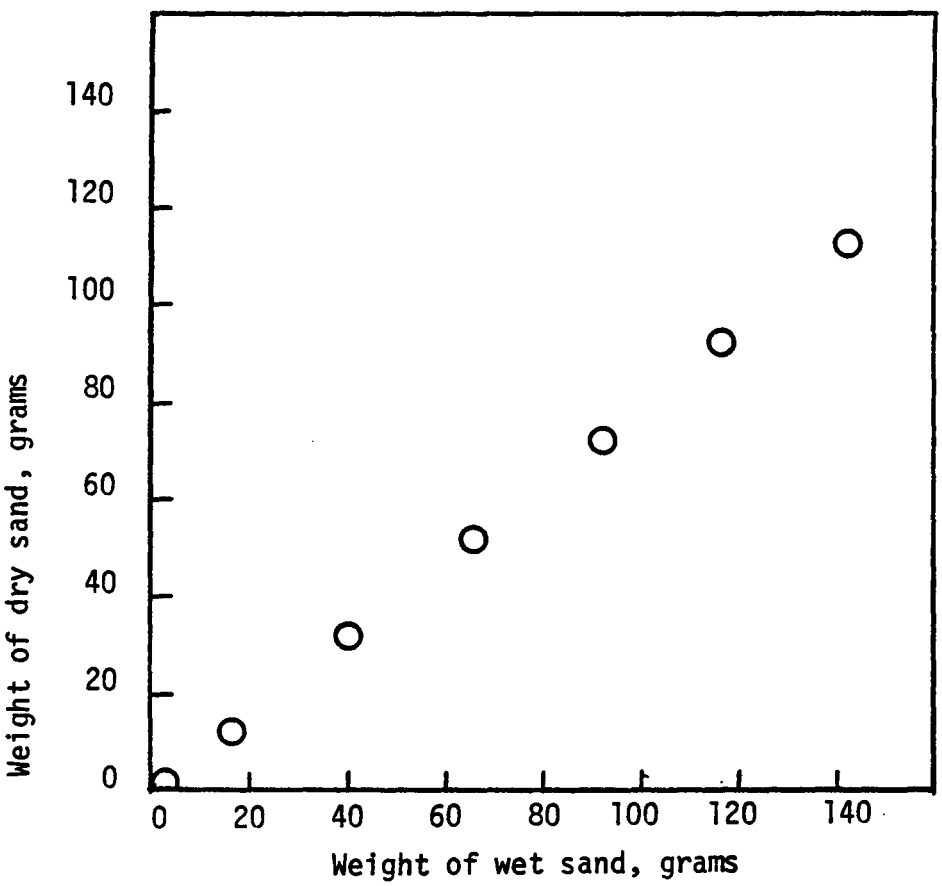

Figure 22. Relationship between 20-30 mesh wet sand and dry sand.

TABLE III. Porosity Values of Sand

Particle Size	Porosity, ε
8-14 mesh	0.40
20-30 mesh	0.508

column (i.e., column T in Figure 14). The separation distance from the support louver increases rapidly but uniformly as does the flowrate of the sand. Toward the termination of pulseback, the sand flow stops suddenly near the peak of the sand flowrate. This sudden cessation of sand flow coincides with the largest separation distance between the sand panel and the central support louver. After the sand flow abruptly stops, the sand panel "falls" or "slumps" back to its former position against the support louver. As the sand panel comes to rest against the support louver the sand descends from the supply chamber above the sand panel into the sand panel. At this point the sand panel is fully loaded with sand and is ready for another pulse.

The sand flow commences with a motion which can be described as a "jump" or "push" of the sand particles. Lee (27) described this motion as "body movement". The sand which then flows, travels with almost homogeneous characteristics. The flowing sand particles appear to be surrounded by water and are more widely separated than the particles in the sand panel which do not flow. The sand which flows appears to be in a quasi-fluidized state. Therefore, pulseback appears to be something more than a mere translation of the sand panel.

Pulseback Data. The data collected during the pulseback experiments consists of the pressure drop across the panel (ΔP) versus time (t) history and the sand spill for each pulseback. Also recorded was the particle size-valve-reservoir configuration along

with the air reservoir pressure. The ΔP-vs-t oscilloscope signals were photographed and they are reproduced in Figures 23 through 30. For these graphs, time is represented on the abscissa and ΔP is represented on the ordinate. The scale factors used in recording the ΔP-vs-t signals are given in Table IV. Other pulseback data are given in Table V.

Without exception, the ΔP-vs-t graphs exhibit two or more peaks. This is probably due to the way in which the equipment was originally designed. The design causes the water level on each side of the sand panel to oscillate much like the fluid in a manometer. An attempt has been made to model this phenomenon and is shown in Appendix E.

Ergun (28) has derived the following model which describes the pressure drop of a fluid flowing through a bed of particles:

$$\frac{G_c dp^3 \varepsilon}{\mu^2 (1-\varepsilon)^3} \left(\frac{-\Delta P}{L} \right) = a \left[\frac{dp U_o \rho}{\mu (1-\varepsilon)} \right] + b \left[\frac{dp U_o \rho}{\mu (1-\varepsilon)} \right]^2 \qquad (6)$$

where: dp = b/av = effective particle diameter, L

av = surface area of particle/volume of particle, L^{-1}

ε = void fraction of bed (porosity), dimensionless

U_o = superficial velocity (mean velocity in the absence of packing), L/θ

ρ = density of fluid, M/L^3

μ = viscosity of fluid, M/Lθ

P = gauge pressure, F/L^2

L = bed depth, L

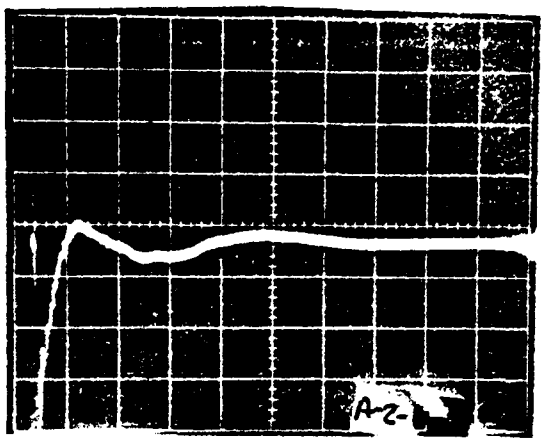

A-2-B-2

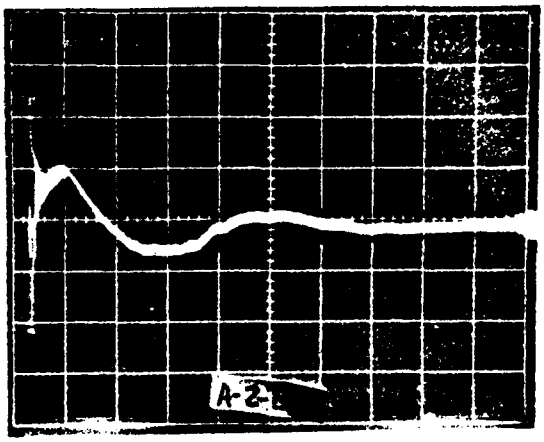

A-2-B-4

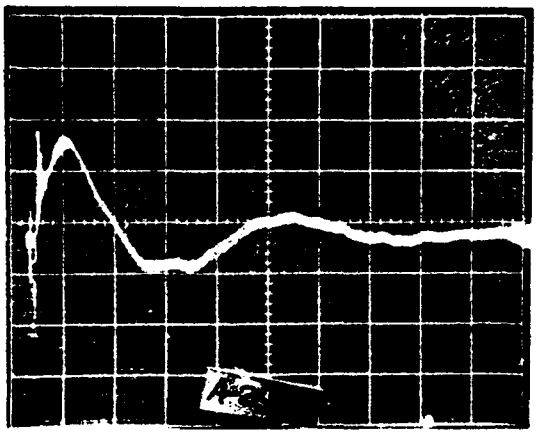

A-2-B-8

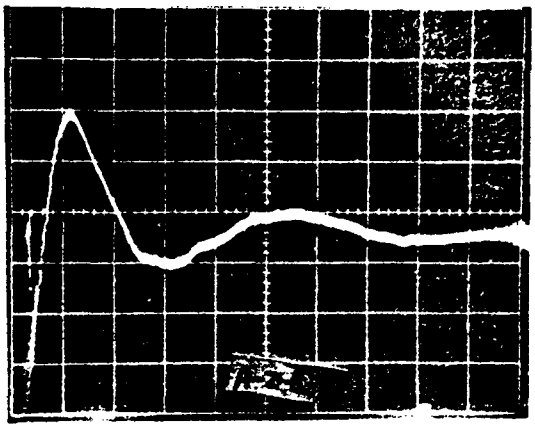

A-2-B-12

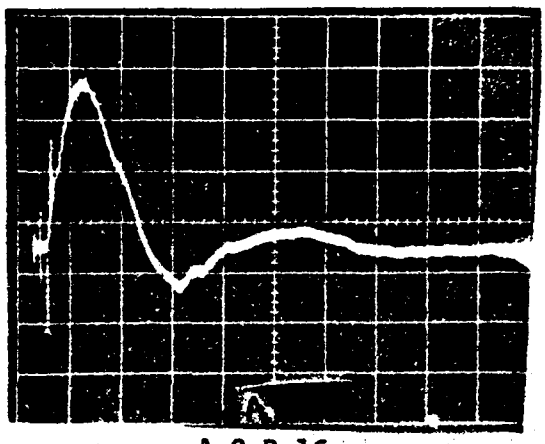

A-2-B-16

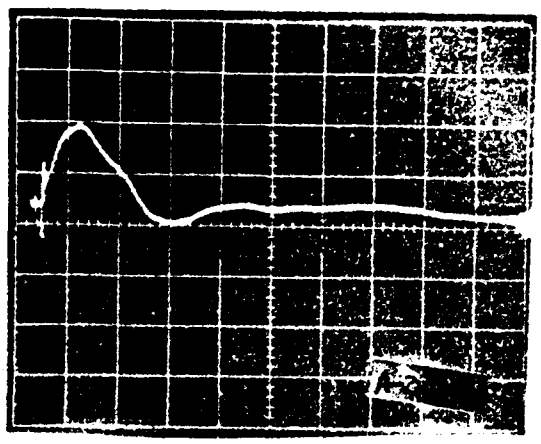

A-2-B-20

Figure 23. ΔP-vs-t graphs for A-2-B.

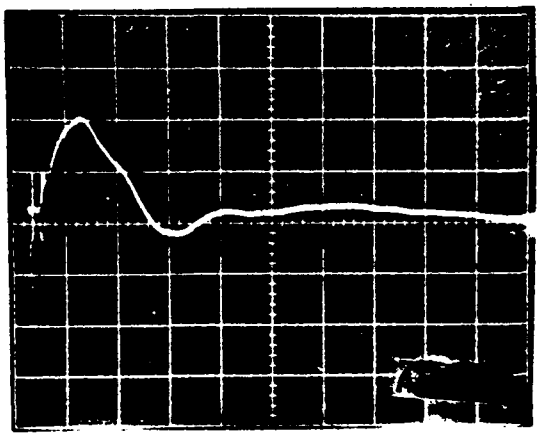

A-2-B-24

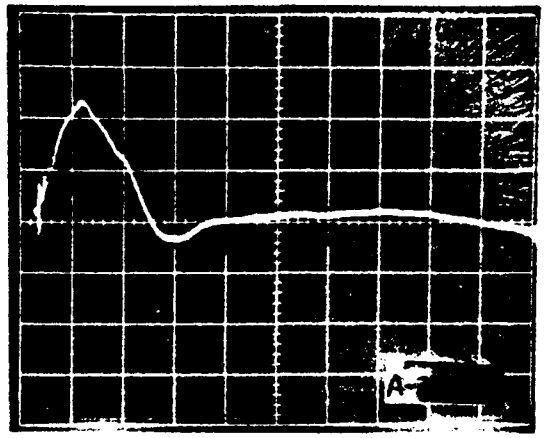

A-2-B-28

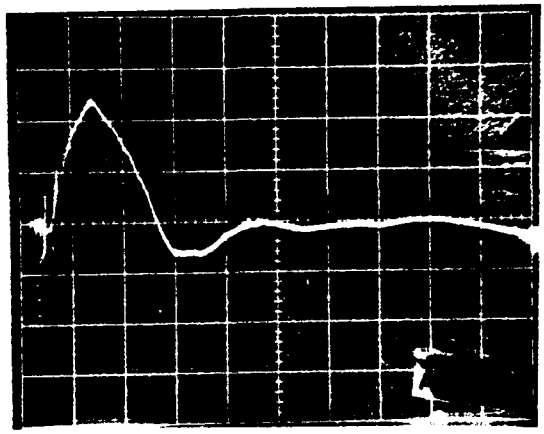

A-2-B-32

Figure 23 - continued.

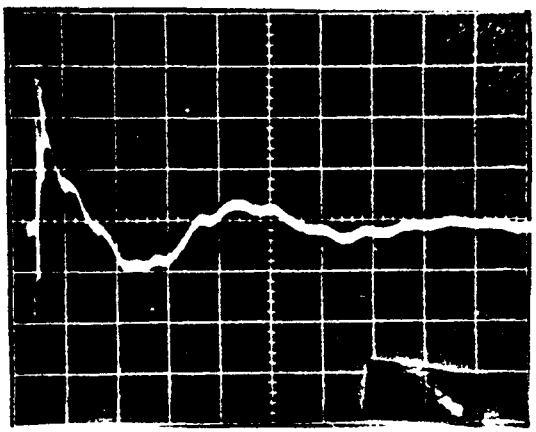

A-1-B-2

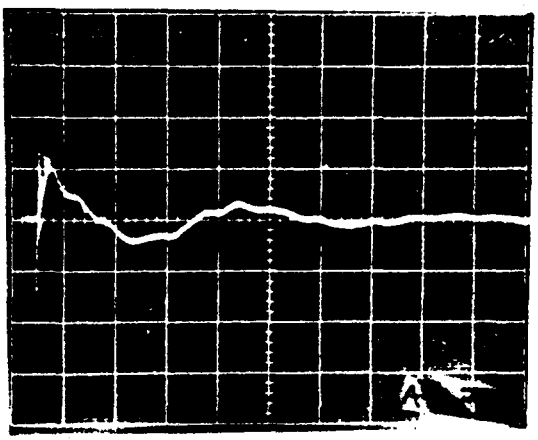

A-1-B-4

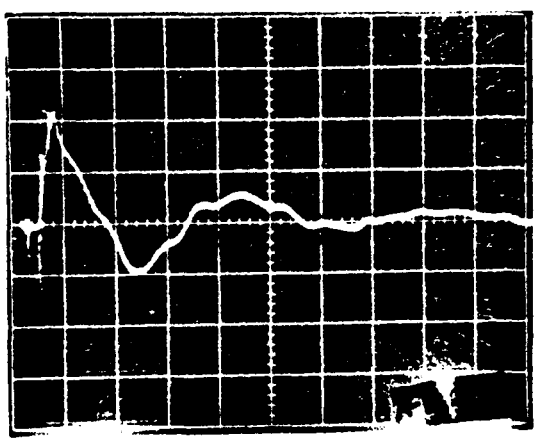

A-1-B-8

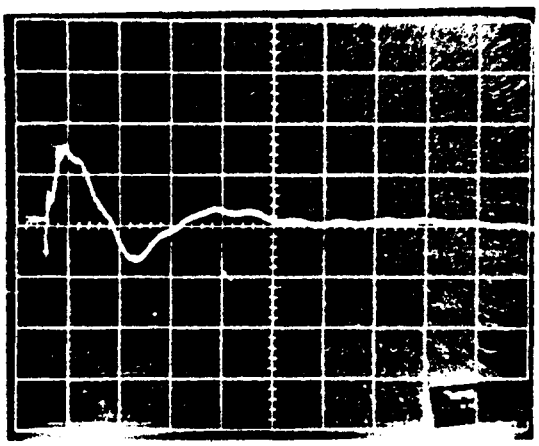

A-1-B-12

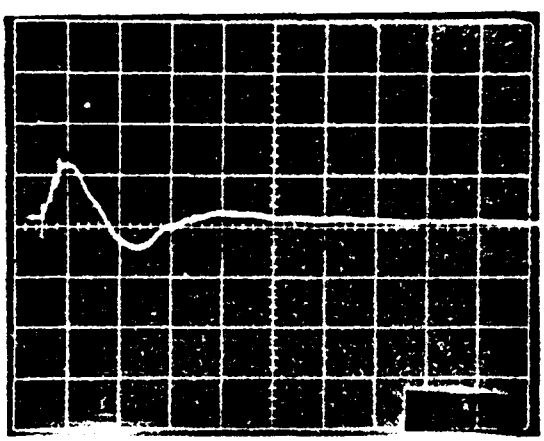

A-1-B-16

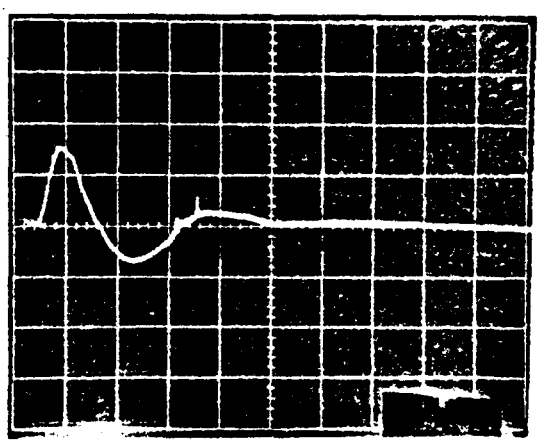

A-1-B-20

Figure 24. ΔP-vs-t graphs for A-1-B.

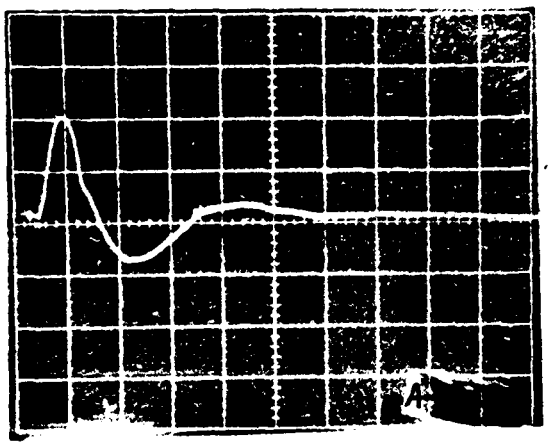

A-1-B-24

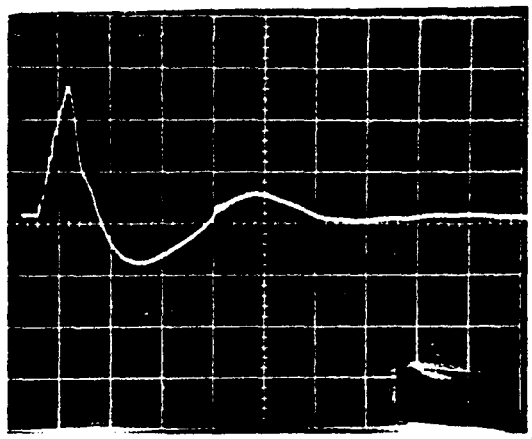

A-1-B-28

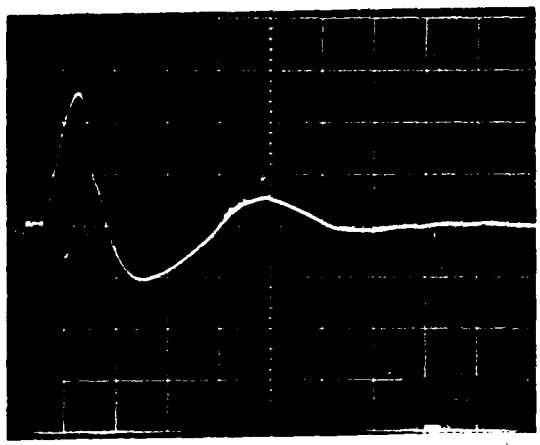

A-1-B-32

Figure 24 - continued.

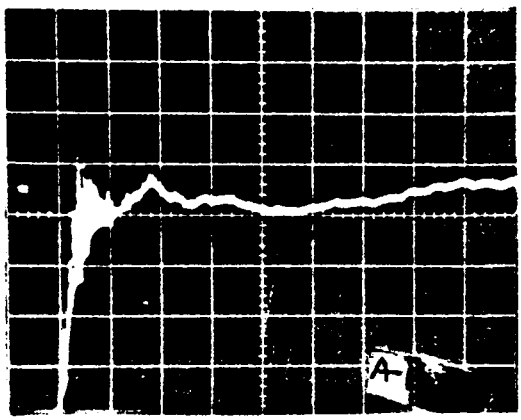

A-1-S-2

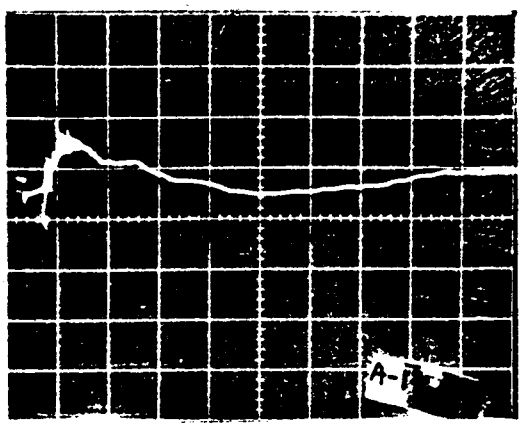

A-1-S-4

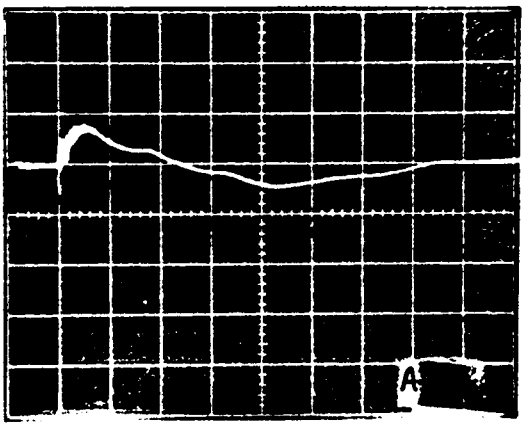

A-1-S-8

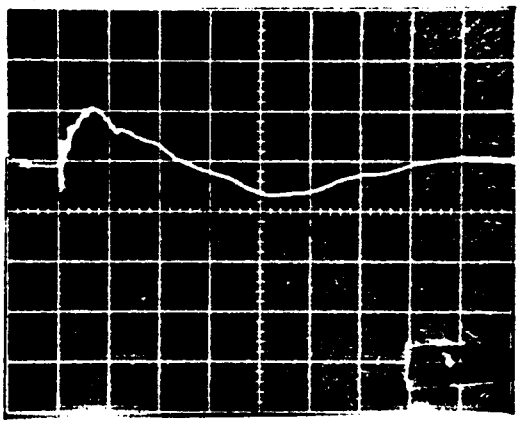

A-1-S-12

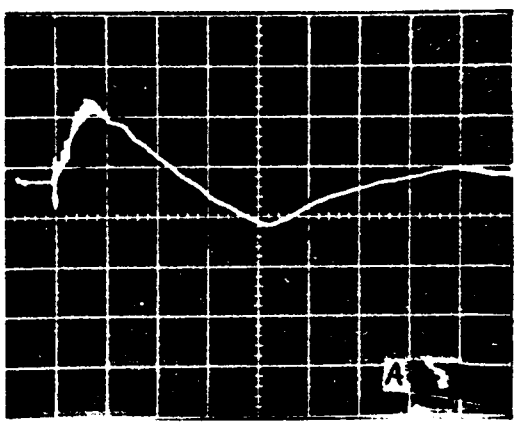

A-1-S-16

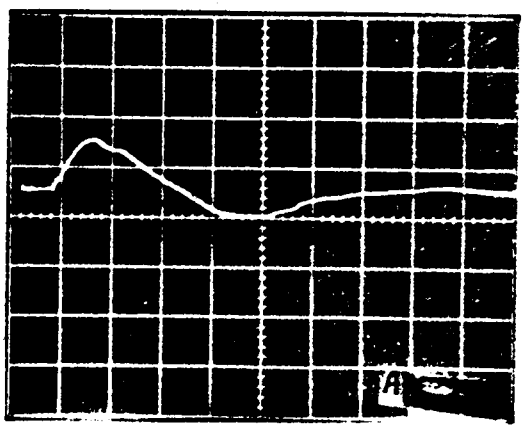

A-1-S-20

Figure 25. ΔP-vs-t graphs for A-1-S.

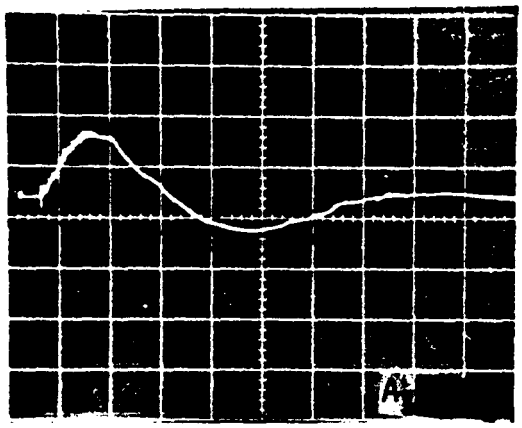

A-1-S-24

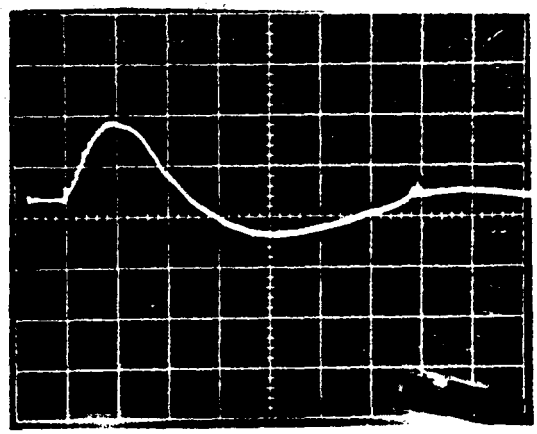

A-1-S-28

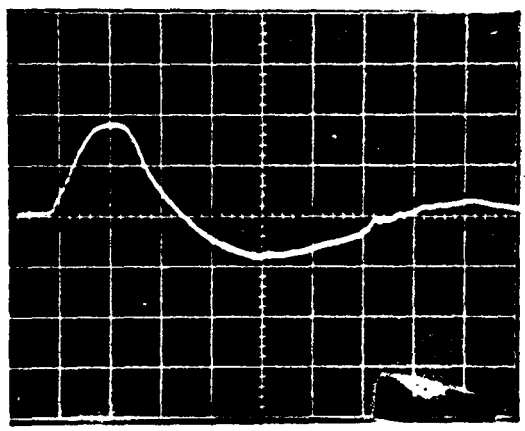

A-1-S-32

Figure 25 - continued.

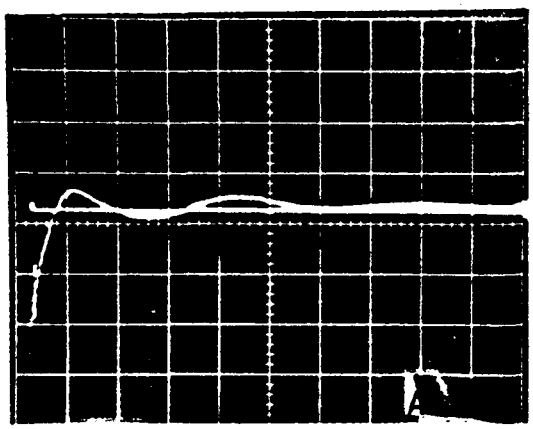

A-2-S-4

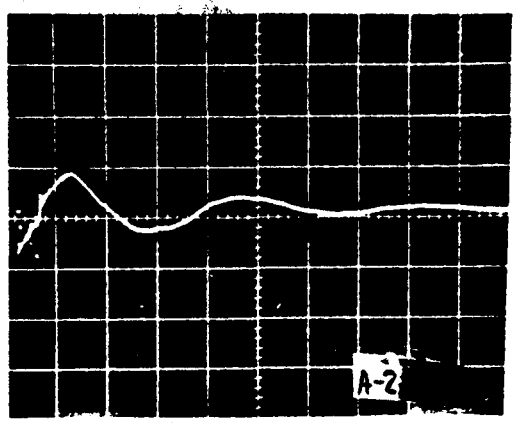

A-2-S-8

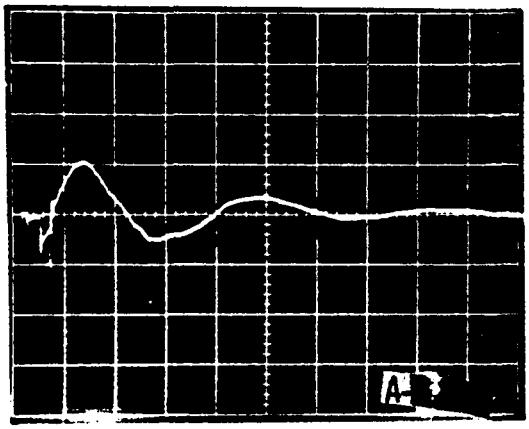

A-2-S-12

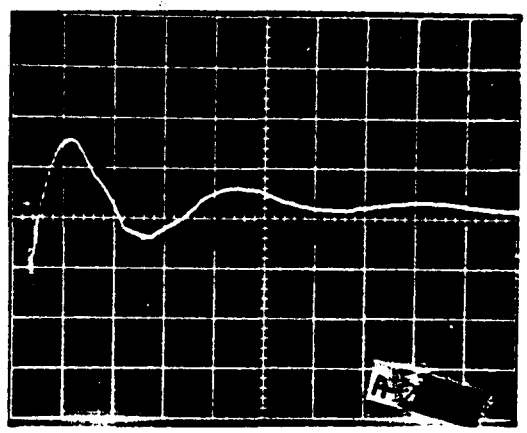

A-2-S-16

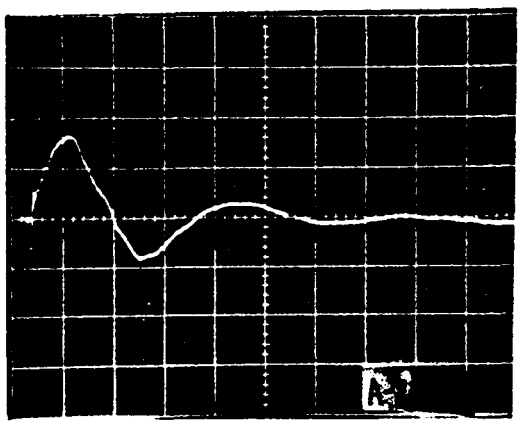

A-2-S-20

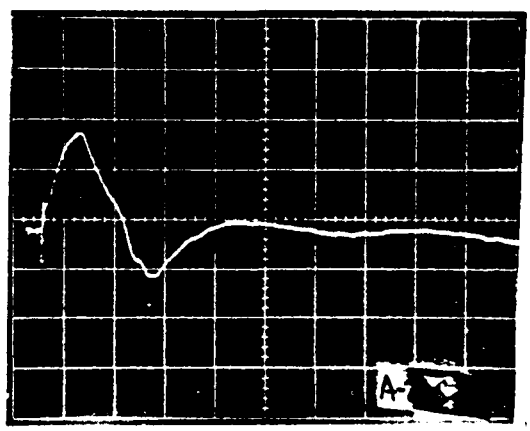

A-2-S-24

Figure 26. ΔP-vs-t graphs for A-2-S.

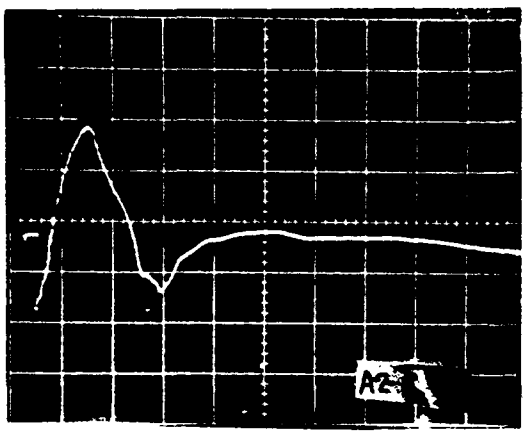

A-2-S-28

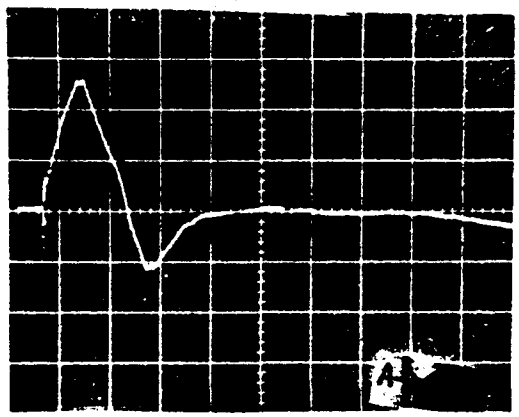

A-2-S-32

Figure 26 - continued.

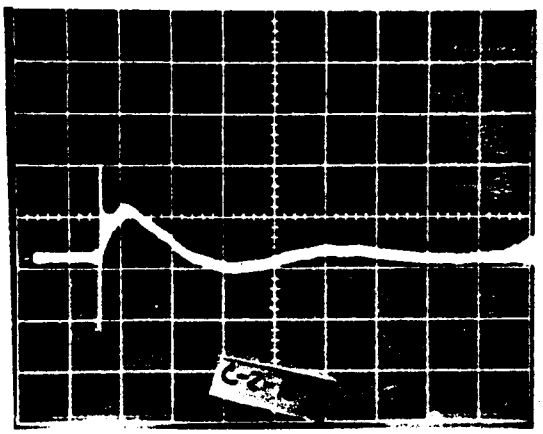

C-2-B-2

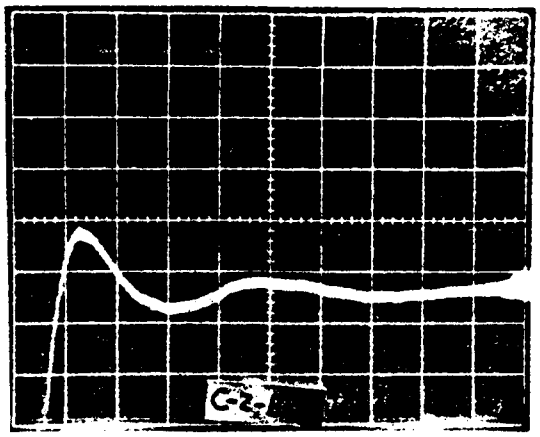

C-2-B-4

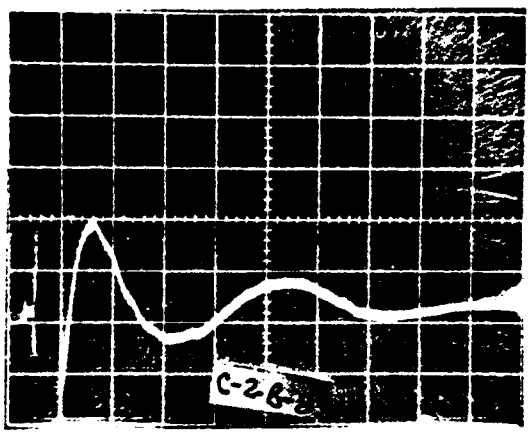

C-2-B-8

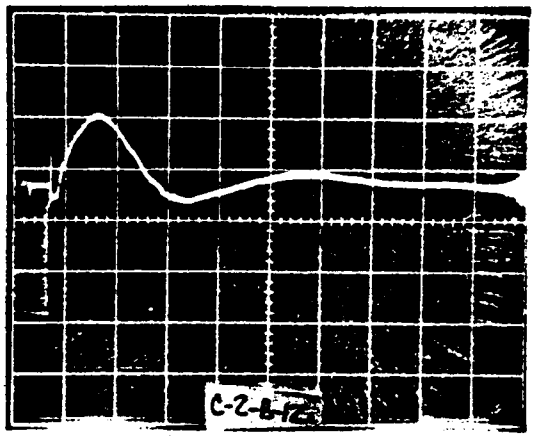

C-2-B-12

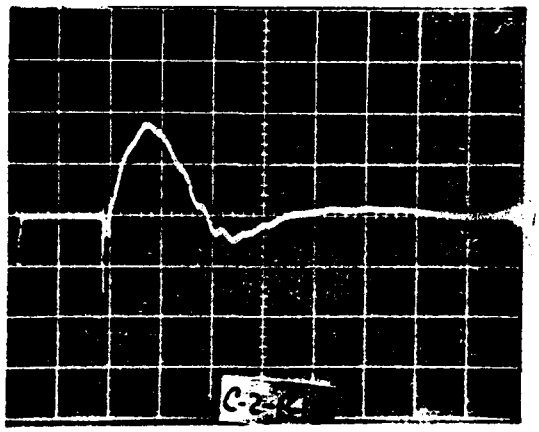

C-2-B-16

Figure 27. ΔP-vs-t graphs for C-2-B.

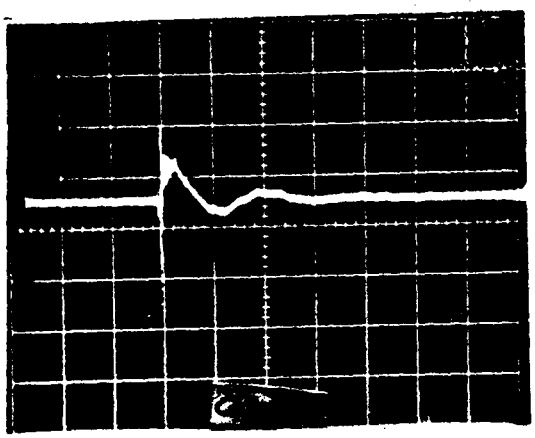

C-2-S-2

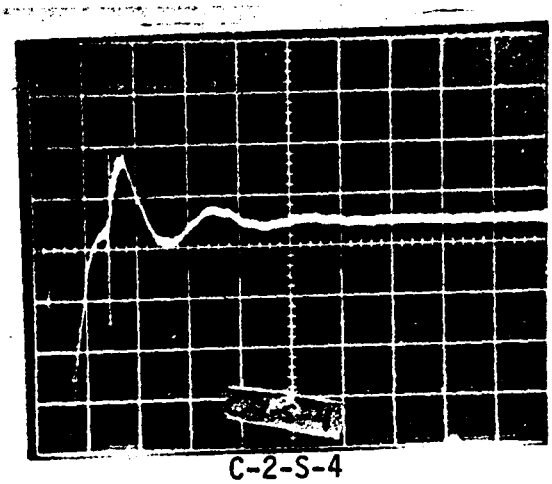

C-2-S-4

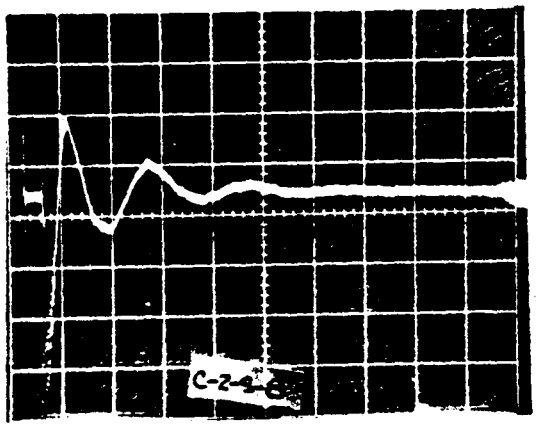

C-2-S-8

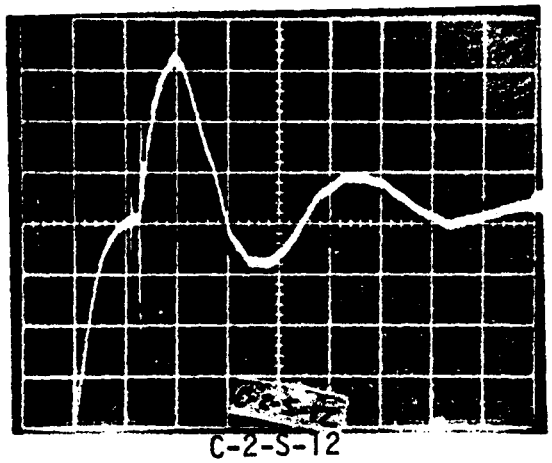

C-2-S-12

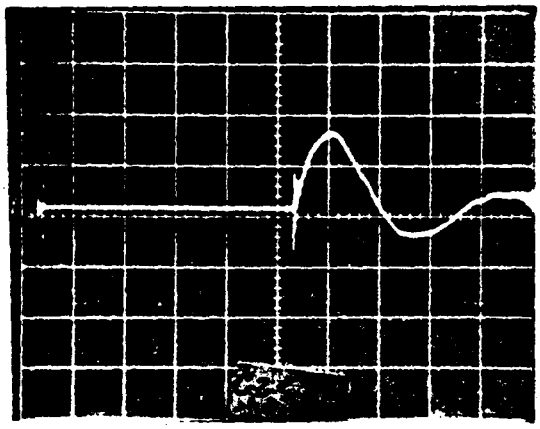

C-2-S-16

Figure 28. ΔP-vs-t graphs for C-2-S.

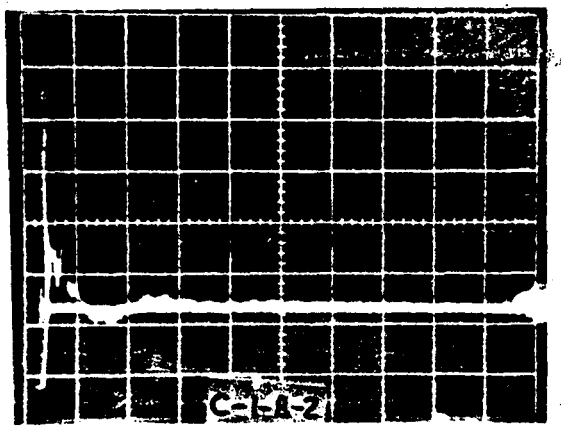

C-1-B-2

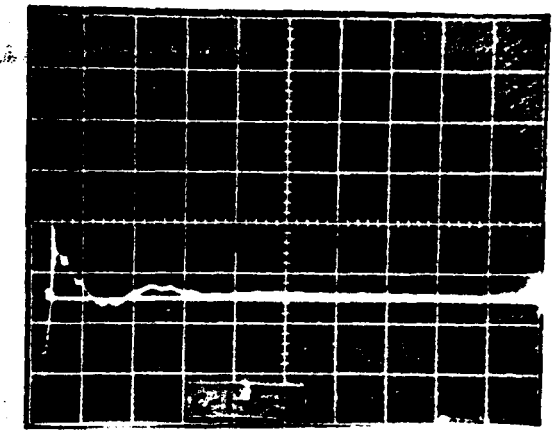

C-1-B-4

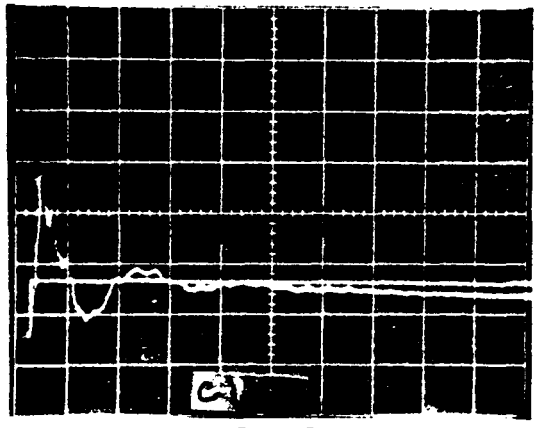

C-1-B-8

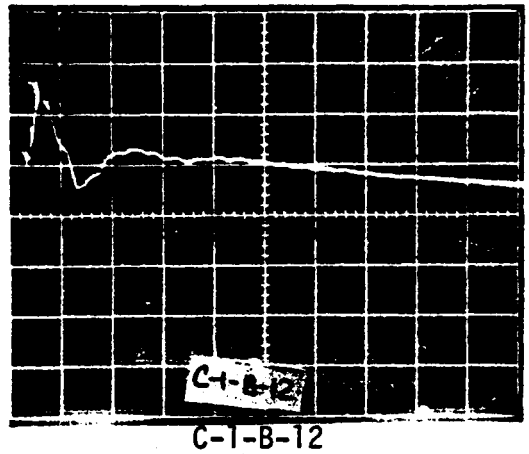

C-1-B-12

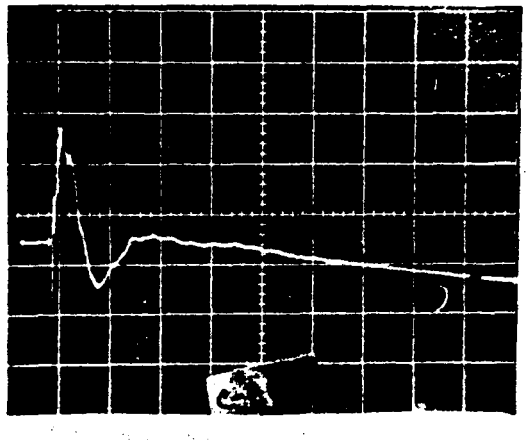

C-1-B-16

Figure 29. ΔP-vs-t graphs for C-1-B.

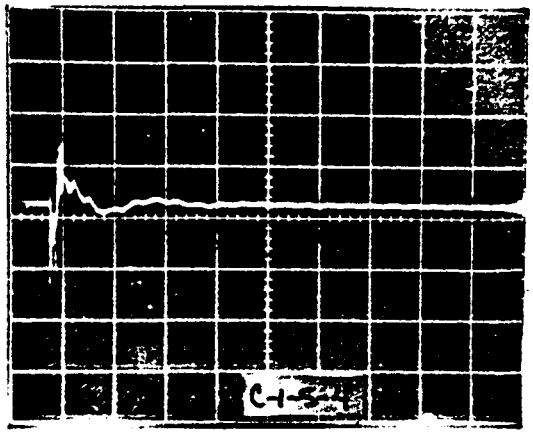

C-1-S-4

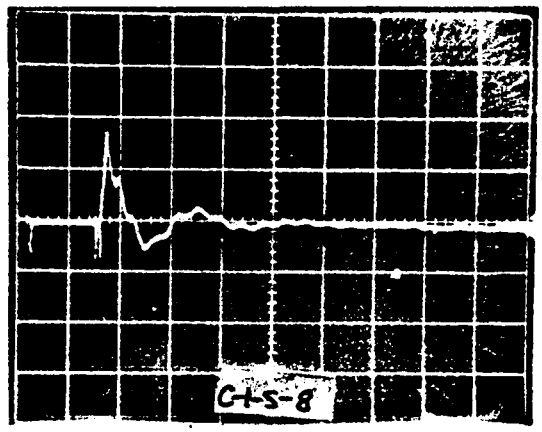

C-1-S-8

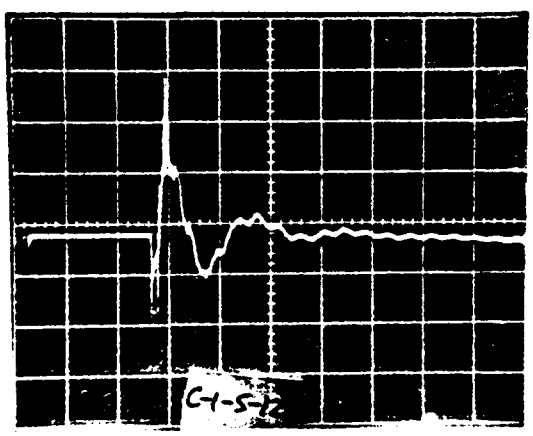

C-1-S-12

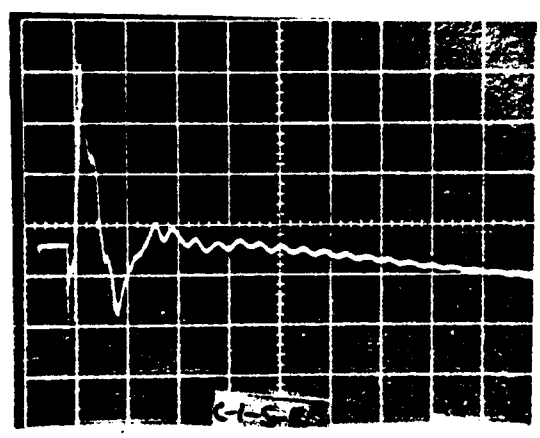

C-1-S-16

Figure 30. ΔP-vs-t graphs for C-1-S.

TABLE IV. Scale Factors for ΔP-vs-t Graphs Found in Figures 23 through 30.

Pulseback Code	Ordinate Scale Factor psi/Division(1)	Abscissa Scale Factor Milliseconds/Division(1)
A-2-B-2	0.182	50
A-2-B-4	0.182	50
A-2-B-8	0.182	50
A-2-B-12	0.182	50
A-2-B-16	0.182	50
A-2-B-20	0.455	50
A-2-B-24	0.455	50
A-2-B-28	0.455	50
A-2-B-32	0.455	50
A-1-B-2	0.182	50
A-1-B-4	0.455	50
A-1-B-8	0.455	50
A-1-B-12	0.090	50
A-1-B-16	1.818	50
A-1-B-20	1.818	50
A-1-B-24	1.818	50
A-1-B-28	1.818	50
A-1-B-32	1.818	50

TABLE IV - continued.

Scale Factors for ΔP-vs-t Graphs
Found in Figures 23 through 30.

Pulseback Code	Ordinate Scale Factor psi/Division(1)	Abscissa Scale Factor Milliseconds/Division(1)
A-1-S-2	0.182	20
A-1-S-4	0.455	20
A-1-S-8	0.909	20
A-1-S-12	0.909	20
A-1-S-16	0.909	20
A-1-S-20	1.818	20
A-1-S-24	1.818	20
A-1-S-28	1.818	20
A-1-S-32	1.818	20
A-2-S-2	0.182	50
A-2-S-4	0.182	50
A-2-S-8	0.182	50
A-2-S-12	0.455	50
A-2-S-16	0.455	50
A-2-S-20	0.455	50
A-2-S-24	0.455	50
A-2-S-28	0.455	50
A-2-S-32	0.455	50

TABLE IV - continued.

Scale Factors for ΔP-vs-t Graphs
Found in Figures 23 through 30.

Pulseback Code	Ordinate Scale Factor psi/Division(1)	Abscissa Scale Factor Milliseconds/Division(1)
C-2-B-2	0.182	50
C-2-B-4	0.182	50
C-2-B-8	0.182	50
C-2-B-12	0.455	50
C-2-B-16	0.455	50
C-2-S-2	0.182	100
C-2-S-4	0.182	100
C-2-S-8	0.182	100
C-2-S-12	0.182	50
C-2-S-16	0.455	50
C-1-B-2	0.182	100
C-1-B-4	0.455	100
C-1-B-8	0.455	100
C-1-B-12	0.909	100
C-1-B-16	0.909	100

TABLE IV - continued.

Scale Factors for ΔP-vs-t Graphs
Found in Figures 23 through 30.

Pulseback Code	Ordinate Scale Factor psi/Division(1)	Abscissa Scale Factor Milliseconds/Division(1)
C-1-S-2	0.182	100
C-1-S-4	0.455	100
C-1-S-8	0.455	100
C-1-S-12	0.455	100
C-1-S-16	0.455	100

TABLE V. Pulseback Data

Note: The Sand Spill is based on a projected louver area of 232.3 cm^2.

Pulseback Code	Wt.of Dry Sand Spill D grams	Spill S gm/cm^2	Peak Pressure Drop ΔP_p cm of Water	Duration Time t_f sec	Average Pressure Drop ΔP_{av} cm of Water	Average Spill Rate Q gm/sec	Natural Log of ΔP_{av} Ln (ΔP_{av})	Natural Log of Q Ln (Q)	Empirical Constant C	Value of Pressure Drop Function
A-1-B-2	1.66	0.007	26.84	0.05714	13.42	29	2.597	3.349	1.58	10.338
A-1-B-4	12.50	0.054	36.75	0.0607	18.38	207	2.911	5.33	1.58	18.042
A-1-B-8	32.00	0.138	67.11	0.06786	33.56	473	3.513	6.159	1.58	52.232
A-1-B-12	67.04	0.289	89.48	0.064286	44.74	1045	3.800	6.952	1.58	77.955
A-1-B-16	108.82	0.469	127.83	0.064286	63.92	1696	4.158	7.436	1.58	136.961
A-1-B-20	138.82	0.598	178.97	0.05714	89.49	2433	4.494	7.797	1.58	207.173
A-1-B-24	162.77	0.701	242.89	0.06071	121.45	2685	4.799	7.895	1.58	356.621
A-1-B-28	201.34	0.867	306.80	0.06071	153.40	3320	5.033	8.108	1.58	515.812
A-1-B-32	223.75	0.964	325.98	0.06429	162.99	3486	5.094	8.157	1.58	601.153
A-1-S-2	1.45	0.006	6.39	(1)	3.20				1.58	
A-1-S-4	3.75	0.016	25.97	0.04	12.99	93	2.564	4.533	1.58	6.87
A-1-S-8	17.18	0.052	60.72	0.04429	30.36	273	3.413	5.609	1.58	29.105

TABLE V - continued.

Pulseback Data

Note: The Sand Spill is based on a projected louver area of 232.3 cm^2.

Pulseback Code	Wt.of Dry Sand Spill D grams	Spill S gm/cm^2	Peak Pressure Drop ΔP_p cm of Water	Duration Time t_f sec	Average Pressure Drop ΔP_{av} cm of Water	Average Spill Rate Q gm/sec	Natural Log of ΔP_{av} Ln (ΔP_{av})	Natural Log of Q Ln (Q)	Empirical Constant C	Value of Pressure Drop Function
A-1-S-12	25.88	0.111	67.11	0.04714	33.36	546	3.513	6.305	1.58	36.284
A-1-S-16	50.50	0.218	99.07	0.05429	49.54	934	3.903	6.839	1.58	77.323
A-1-S-20	76.68	0.330	127.83	0.4857	63.92	1580	4.158	7.365	1.58	103.478
A-1-S-24	94.91	0.409	159.79	0.051429	79.90	1848	4.381	7.522	1.58	155.889
A-1-S-28	121.66	0.524	185.36	0.04857	92.68	2507	4.529	7.827	1.58	186.137
A-1-S-32	135.12	0.582	249.28	0.05143	124.64	2785	4.825	7.932	1.58	314.762
A-2-S-4	1.96	0.008	5.75	0.05	2.88	37	3.616	3.616	1.58	0.793
A-2-S-8	10.82	0.047	8.95	0.075	4.48	146	4.982	4.982	1.58	2.393
A-2-S-12	18.69	0.081	35.15	0.075	17.58	251	5.526	5.526	1.58	20.779
A-2-S-16	33.42	0.144	41.55	0.07857	20.78	426	6.055	6.055	1.58	28.353
A-2-S-20	54.65	0.235	51.13	0.08214	25.57	665	6.500	6.500	1.58	41.140

TABLE V - continued.

Pulseback Data

Note: The Sand Spill is based on a projected louver area of 232.3 cm^2.

Pulseback Code	Wt.of Dry Sand Spill D grams	Spill S gm/cm^2	Peak Pressure Drop ΔP_p cm of Water	Duration Time t_f sec	Average Pressure Drop ΔP_{av} cm of Water	Average Spill Rate Q gm/sec	Natural Log of ΔP_{av} Ln (ΔP_{av})	Natural Log of Q Ln (Q)	Empirical Constant C	Value of Pressure Drop Function
A-2-S-24	64.09	0.276	62.32	0.07679	31.16	835	6.728	6.728	1.58	52.579
A-2-S-28	88.67	0.382	65.52	0.075	32.76	1184	7.077	7.077	1.58	55.582
A-2-S-32	105.33	0.454	79.90	0.08214	39.95	1286	7.159	7.159	1.58	83.287
A-2-B-2	1.66	0.007	3.84	0.039286	1.92	41	-0.427	3.724	1.58	0.329
A-2-B-4	3.43	0.015	13.42	0.06786	6.71	51	1.904	3.939	1.58	4.161
A-2-B-8	17.5	0.075	23.65	0.0750	11.83	233	2.470	5.449	1.58	11.110
A-2-B-12	23.59	0.102	28.76	0.067857	14.38	350	2.666	5.856	1.58	13.692
A-2-B-16	44.35	0.191	38.99	0.085714	19.50	518	2.970	6.250	1.58	27.970
A-2-B-20	74.46	0.321	47.94	0.10	23.99	746	3.177	6.615	1.58	45.238
A-2-B-24	97.70	0.421	54.33	0.10357	27.17	945	3.302	6.851	1.58	57.095
A-2-B-28	189.75	0.602	63.92	0.11071	31.96	1264	3.464	7.142	1.58	78.903
A-2-B-32	150.59	0.649	76.70	0.10357	38.35	1457	3.647	7.284	1.58	98.449

TABLE V - continued.

Pulseback Data

Note: The Sand Spill is based on a projected louver area of 232.3 cm^2.

Pulseback Code	Wt.of Dry Sand Spill D grams	Spill S gm/cm^2	Peak Pressure Drop ΔP_p cm of Water	Duration Time t_f sec	Average Pressure Drop ΔP_{av} cm of Water	Average Spill Rate Q gm/sec	Natural Log of ΔP_{av} Ln (ΔP_{av})	Natural Log of Q Ln (Q)	Empirical Constant C	Value of Pressure Drop Function
C-2-B-2	30.34	0.131	12.15	0.0893	6.08	341	1.804	5.831	1.85	8.000
C-2-B-4	38.65	0.160	16.62	0.06857	8.31	563	2.117	6.332	1.85	10.796
C-2-B-8	114.01	0.491	21.74	0.0607	10.87	1879	2.386	7.539	1.85	15.497
C-2-B-12	179.53	0.773	41.55	0.10357	20.78	1734	3.034	7.458	1.85	84.852
C-2-B-16	256.54	1.105	63.92	0.1	31.96	2567	3.464	7.850	1.85	177.888
C-2-S-2	8.17	0.035	10.23	0.07857	5.12	104	1.632	4.644	1.85	5.165
C-2-S-4	31.02	0.134	15.35	0.07857	7.68	395	2.038	5.979	1.85	10.721
C-2-S-8	72.51	0.312	17.26	0.05714	8.63	1269	2.155	7.146	1.85	9.630
C-2-S-12	126.11	0.543	38.99	0.0875	19.50	1441	2.970	7.273	1.85	63.933
C-2-S-16	172.23	0.742	44.74	0.0875	22.37	1968	3.108	7.585	1.85	81.900

TABLE V - continued.

Pulseback Data

Note: The Sand Spill is based on a projected louver area of 232.3 cm^2.

Pulseback Code	Wt.of Dry Sand Spill D grams	Spill S gm/cm^2	Peak Pressure Drop ΔP_p cm of Water	Duration Time t_f sec	Average Pressure Drop ΔP_{av} cm of Water	Average Spill Rate Q gm/sec	Natural Log of ΔP_{av} Ln (ΔP_{av})	Natural Log of Q Ln (Q)	Empirical Constant C	Value of Pressure Drop Function
C-1-S-4	36.78	0.152	31.96	0.01429	15.98	2568	2.771	7.851	1.85	7.300
C-1-S-8	92.61	0.399	52.73	0.01429	26.37	6486	3.272	8.777	1.85	17.987
C-1-S-12	125.23	0.539	89.48	0.01429	44.74	8762	3.801	9.078	1.85	46.574
C-1-S-16	206.87	0.891	105.46	0.02857	52.73	7244	3.965	8.888	1.85	125.161
C-1-B-2	36.61	0.158	19.50	0.06428	9.75	571	2.986	6.347	1.85	48.364
C-1-B-4	49.36	0.213	22.27	0.07857	11.14	630	3.108	6.445	1.85	73.538
C-1-B-8	145.16	0.625	68.71	0.071428	34.36	2033	3.537	7.617	1.85	144.712
C-1-B-12	222.55	0.959	83.09	0.07857	41.55	2835	3.727	7.950	1.85	224.101
C-1-B-16	300.07	1.292	134.23	0.07128	67.12	4202	4.206	8.343	1.85	483.056

TABLE VI. References for Sand-Water Flow Investigations

Investigation	Reference Number
Sand particles < 1 mm	29
Particles < 1/3 pipe diameter	30
Velocity data for sand flow	31
General correlation for particles 40 micron 2mm	32
Thorough general discussion	33

a = 150 (empirical constant), dimensionless

b = 1.75 (empirical constant), dimensionless

As expected, the ΔP and the fluid velocity (U_o) are coupled. However, note also that the ΔP is a strong function of the porosity (ε). This means that for a given value for U_o, a change in ε will result in a change in ΔP. This relationship between ΔP and ε is thought to be responsible for the skewness and occasional inflection points present in the ΔP-vs-t graphs. Recall that definite changes in ε were detected during pulseback by viewing the high speed movies.

Pulseback Data Analysis. A number of studies have been conducted concerning the movement of solid particles in a flowing liquid stream. Table VI enumerates the more notable investigations of this subject. Almost all of these investigations yielded an empirical correlation of the variables involved. No studies have yielded any physico-chemical models of the phenomenon; presumably, this is due to the tremendous complexity of the problem. Moreover, the only attempts at a mechanistic explanation come from the soil mechanics literature. Therefore, the analysis of the data collected in this investigation generally followed the empirical route.

The work of the investigators listed in Table VI has generally implied that the mass flow rate of solids (Q) is proportional to some power of the applied pressure drop (ΔP):

$$Q = d\ (\Delta P)^c \qquad (7)$$

where: Q = mass flow rate of solids, M/θ

ΔP = applied pressure drop across solids

d,c = empirical constants.

It appears that equation (7) above should be suitable to correlate the pulseback data. All that is needed is data regarding the relationship between Q and ΔP at any instant in time. Unfortunately, Q versus time data are not available. However, it follows from equation (7) that the average sand flow rate (Q_{av}) and the average pressure drop (ΔP_{av}) should have the same functional relationship as Q and ΔP:

$$Q_{av} = d\ (\Delta P_{av})^c \tag{8}$$

Numerical values for Q_{av} and ΔP_{av} can easily be computed from the pulseback data.

Computing Q_{av} and ΔP_{av}. Consider a general ΔP-vs-t graph as shown in Figure 31. It can be assumed that the major portion, if not all, of the sand spill occurs between 0 seconds and t_f. This is particularly obvious in the high speed movies where the water flows in a reverse direction after time, t_f. The flow of water in this direction, from dirty face to clean face, can never cause a sand spill.

Therefore, from the sand spill data, Q_{av} may be computed:

$$Q_{av} = \text{spill}/t_f \tag{9}$$

where: spill = ratio of sand spill to projected louver area, M/L^2

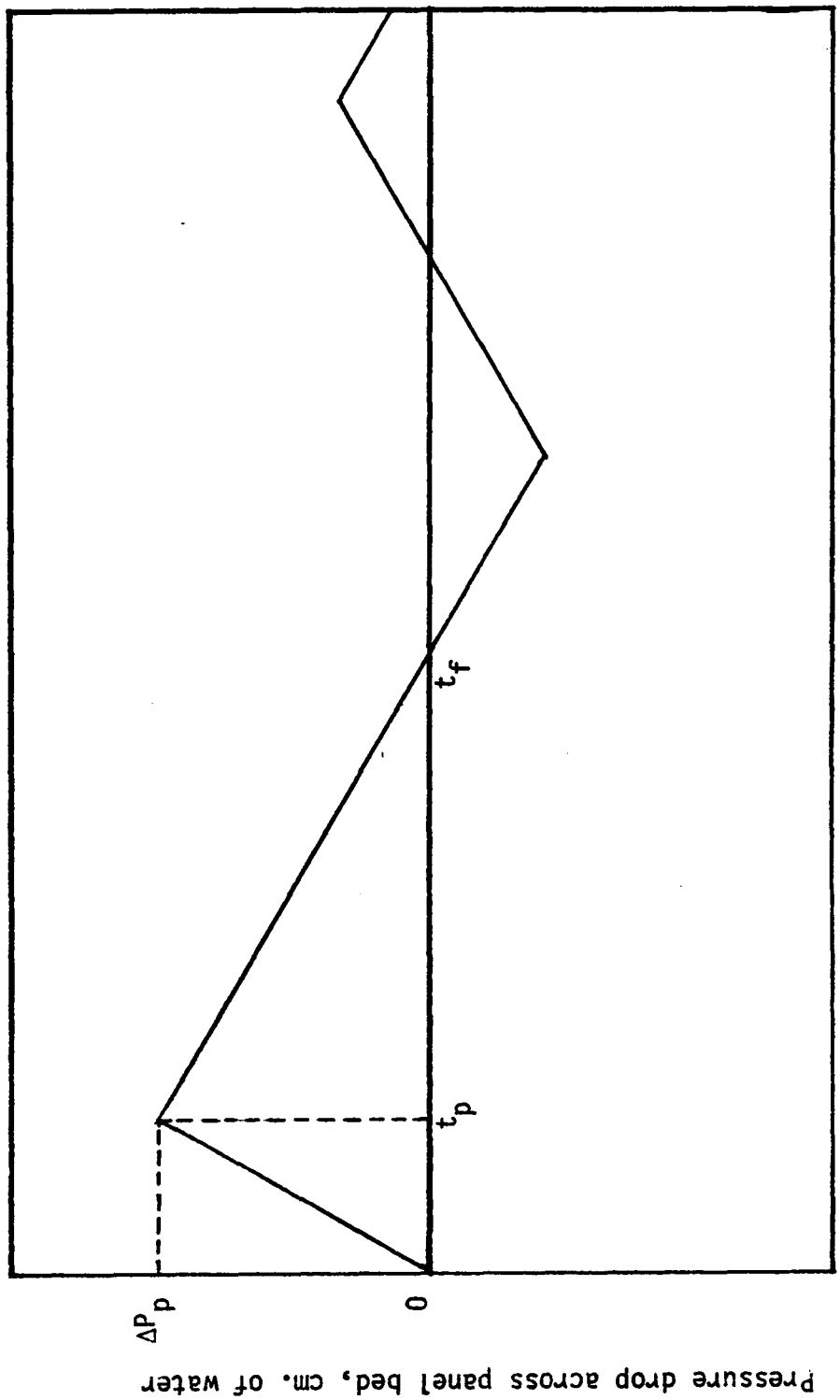

Figure 31. Schematic example of typical (ΔP-vs-t) graph.

Moreover, ΔP_{av} may be computed by using the definition for average:

$$\Delta P_{av} = \int_o^{t_f} \Delta P(t)dt / \int_o^{t_f} dt \tag{10}$$

Of course,

$$\int_o^{t_f} dt = t_f \tag{11}$$

Also,

$$\int_o^{t_f} \Delta P(t)dt = \int_o^{t_p} \Delta P(t)dt + \int_{t_p}^{t_f} \Delta P(t)dt \tag{12}$$

Due to the triangular character of the $\Delta P(t)$ function:

$$\int_o^{t_p} \Delta P(t)dt = 1/2\ \Delta P_p t_p \tag{13}$$

and

$$\int_{t_p}^{t_f} \Delta P(t)dt = 1/2\ \Delta P_p\ (t_f - t_p) \tag{14}$$

Therefore,

$$\int_o^{t_f} \Delta P(t)dt = 1/2\ \Delta P_p t_f \tag{15}$$

and,

$$\Delta P_{av} = 1/2\ \Delta P_p \tag{16}$$

Now, by inserting expressions (9) and (16) into equation (8), we have:

$$spill/t_f = d\ (1/2\ \Delta P_p)^c \tag{17}$$

By taking the logarithm of both sides of equation (17), we obtain the following expression:

$$\ln (spill/t_f) = c \ln (1/2\ \Delta P_p) + \ln (d) \qquad (18)$$

When equation (18) is plotted on rectangular coordinates, it should yield a straight line and c may be determined.

Pulseback data for each particle size have been plotted according to equation (18) and are shown in Figures 32 and 33. The values for c are shown in Table VII.

The pulseback data plotted in Figures 31 and 32 will yield a perfect straight line only if the average porosity for each pulse: (1) is a constant, or, (2) if the average porosity for a given pulse does not affect the amount of sand spill. Item one above is obviously not true in the high speed movies. Item two above appears to be reasonably true except for the lower values for $\ln (1/2\ \Delta P_p)$.

The final form for correlating the pulseback data can be obtained by an integration of equation (7):

$$\int_o^{t_f} Q dt = \int_o^{t_f} d\ (\Delta P)^c\ dt \qquad (19)$$

As before,

$$\int_o^{t_f} Q dt = spill \qquad (20)$$

Also,

$$\int_o^{t_f} d\ (\Delta P)^c\ dt = d\ (1/2\ \Delta P_p)^c\ t_f \qquad (21)$$

TABLE VII. Values of the Empirical Constant C

Particle Size	C
8-14 mesh	1.58
20-30 mesh	1.80

Therefore, combining equation (20) and (21):

$$\text{Spill} = d\,(1/2\,\Delta P_p)^c\,t_f \qquad (22)$$

The pulseback data are plotted according to equation (22) for each particle size-valve-reservoir, configuration in Figures 34 through 41.

Note that for the lower regions of the abscissa in Figures 34 through 41 the data are practically linear. This is particularly true for the 8-14 mesh sand which did not appear to flow as homogeneously as the 20-30 mesh sand. Also, for both particle sizes, the data converge to the origin which indicates that the sands under water exhibit no "yield-point" in the pulseback situation. This is not to say that soil mechanics does not predict a theoretical yield point for a slope of sand under water. However, in the pulseback situation this yield point appears to be quite small.

Another important point to consider from Figures 34 through 41 concerns the higher region of the abscissa. For high values of the abscissa, the available data become quite nonlinear. This nonlinearity occurs because the maximum amount of sand in the sand panel available for pulseback is exceeded at high values of the abscissa. Therefore, if no sand is allowed to enter the sand panel during pulseback then a maximum value for the spill should exist. Indeed, a quasi-maximum for spill can be detected in Figures 34 through 41. This inflection point is more obvious for the 8-14 mesh sand. Table VIII gives the approximate maximum spill for each particle size.

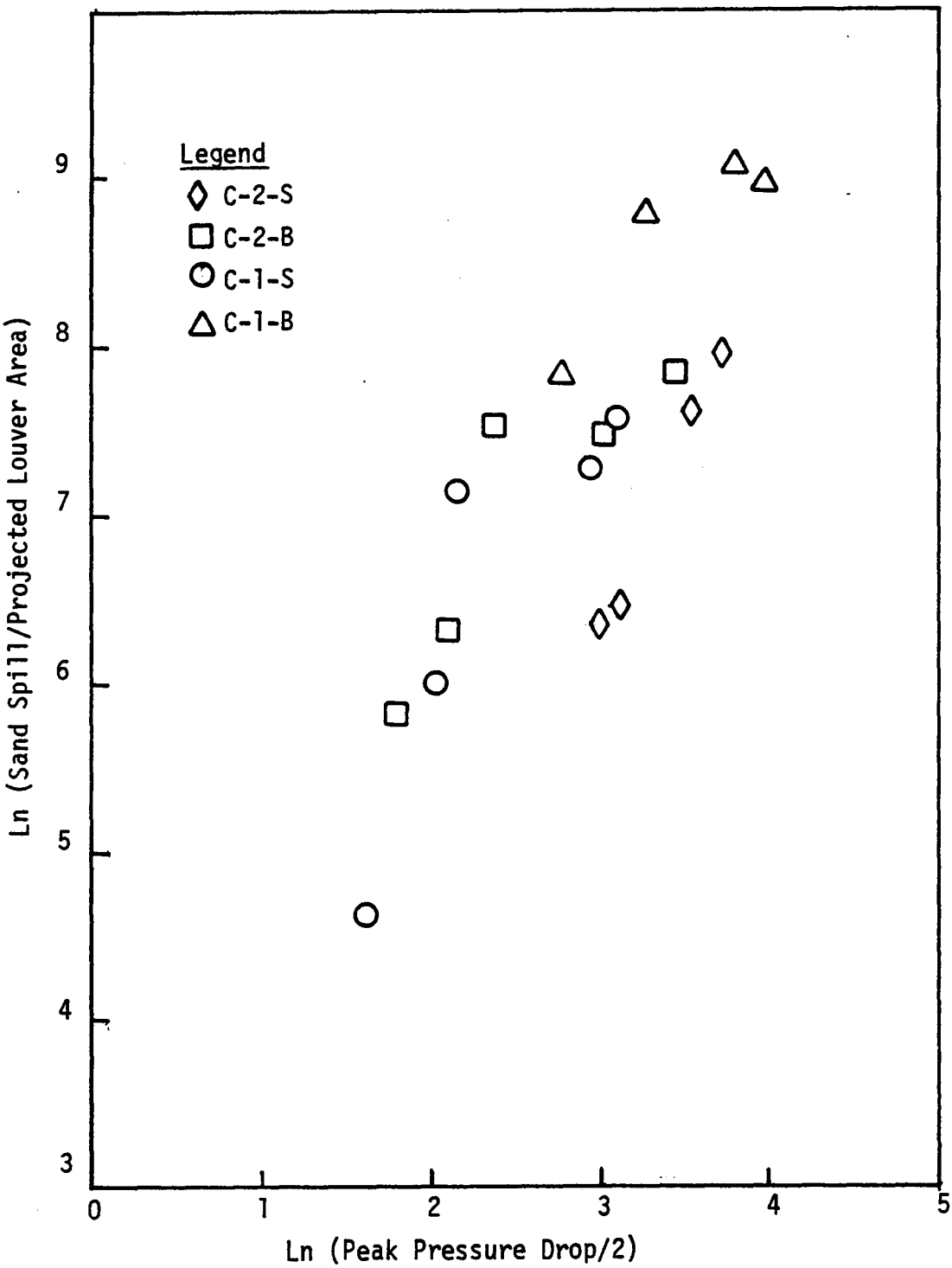

Figure 32. Plot of average pulseback data for 20-30 mesh sand to obtain the parameter, C, for the final correlation.

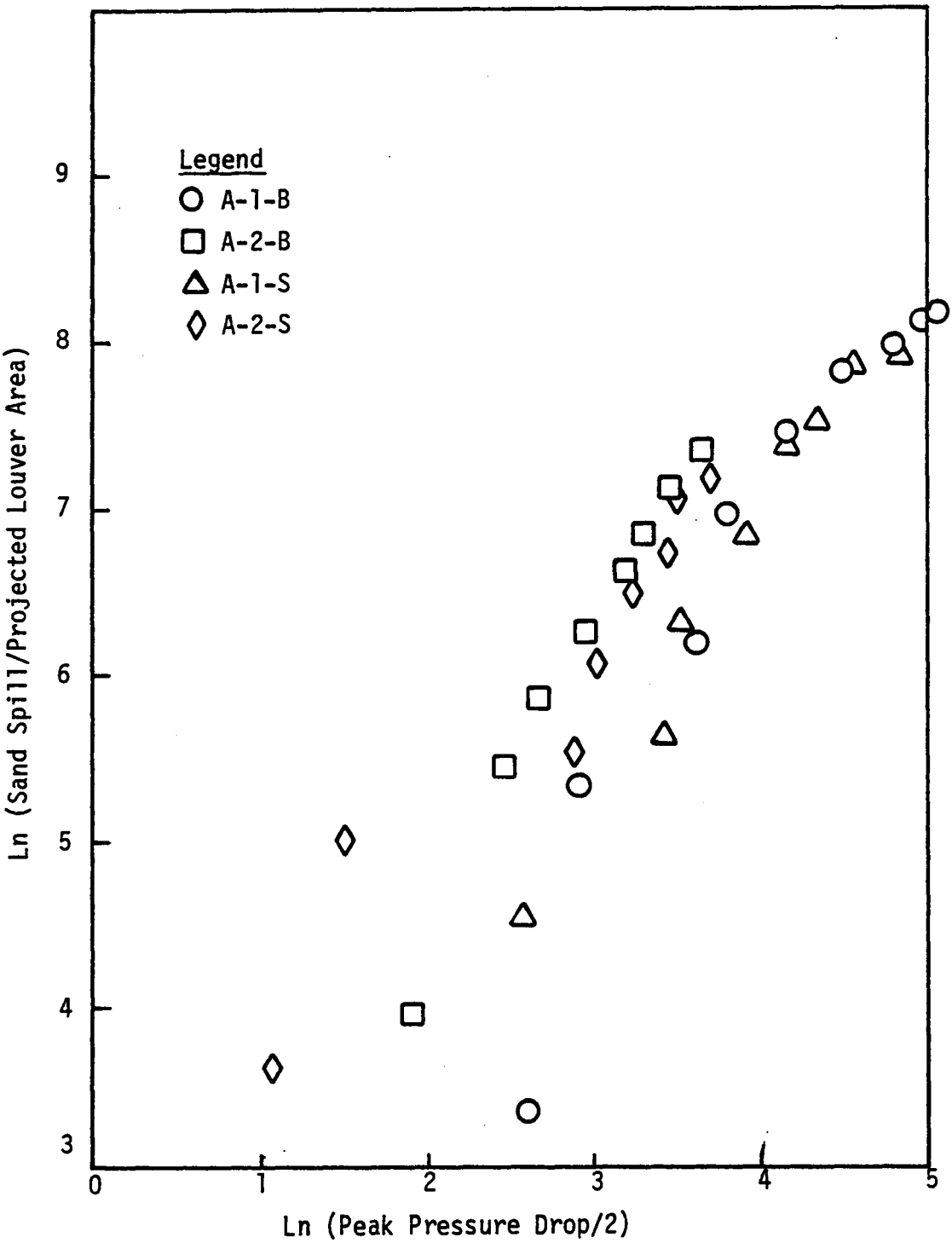

Figure 33. Plot of pulseback data for 8-14 mesh sand to obtain the parameter, C, for the final correlation.

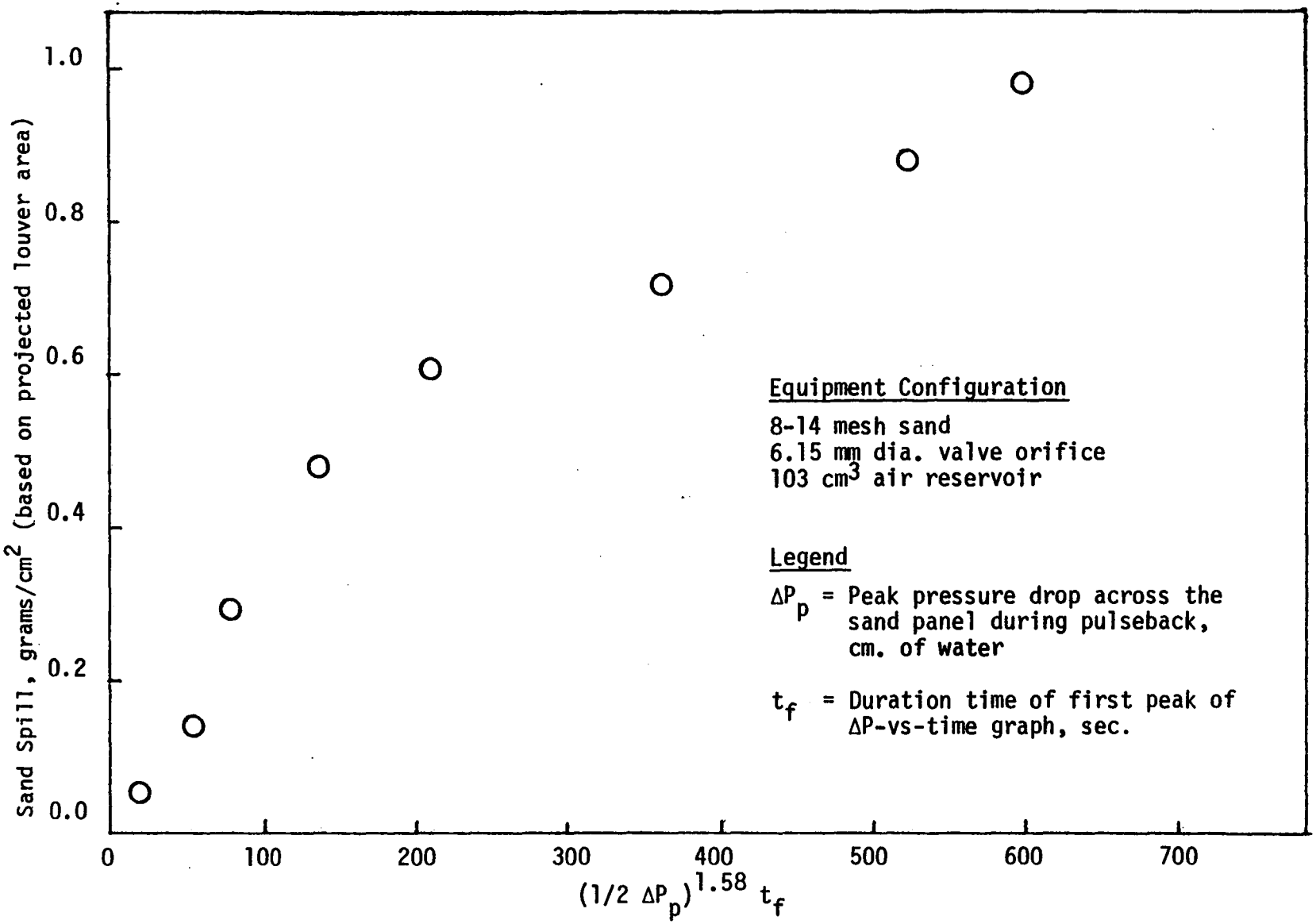

Figure 34. Sand Spill-versus-Pressure Drop Function.

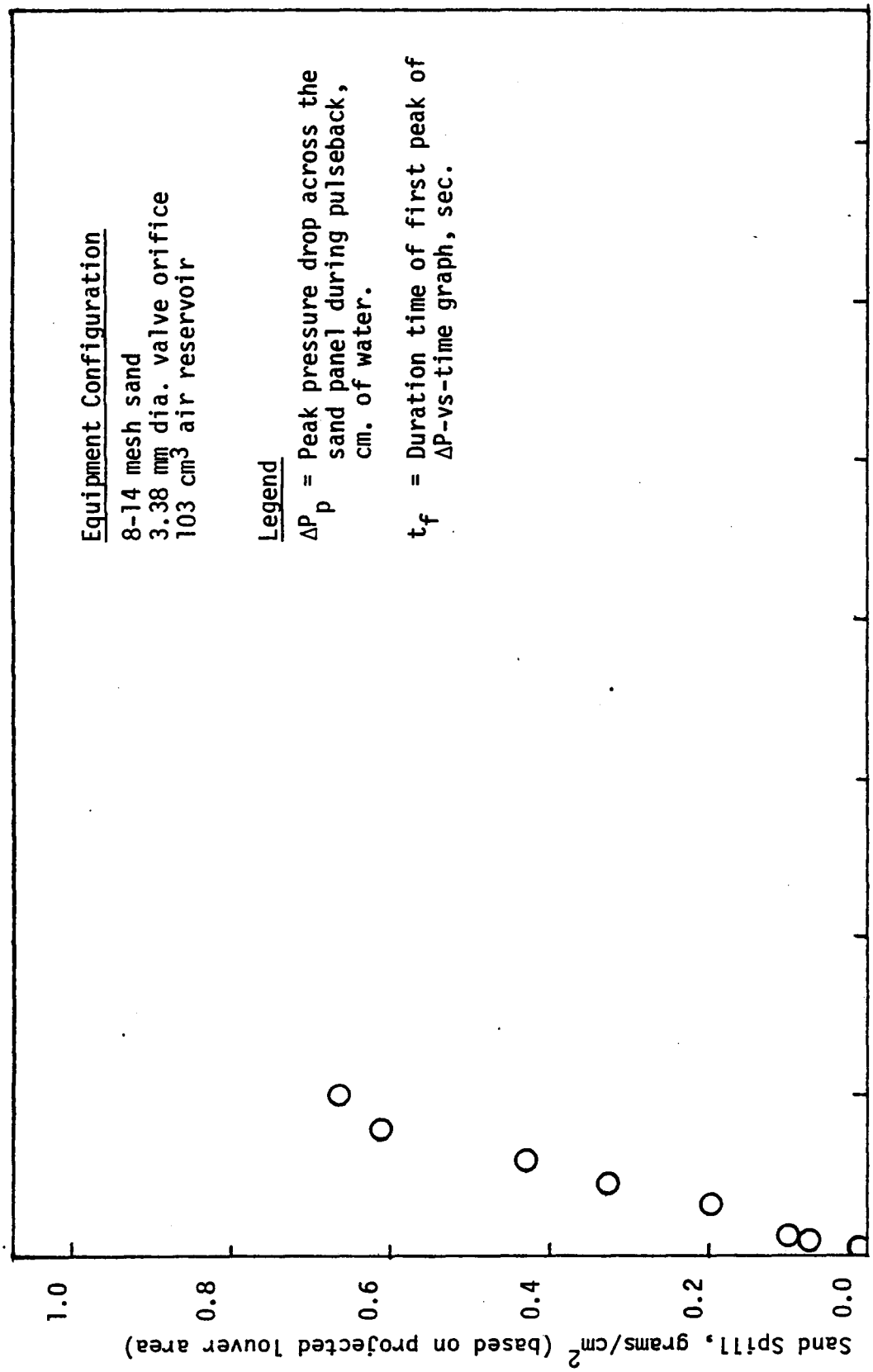

Figure 35. Sand Spill-versus-Pressure Drop Function.

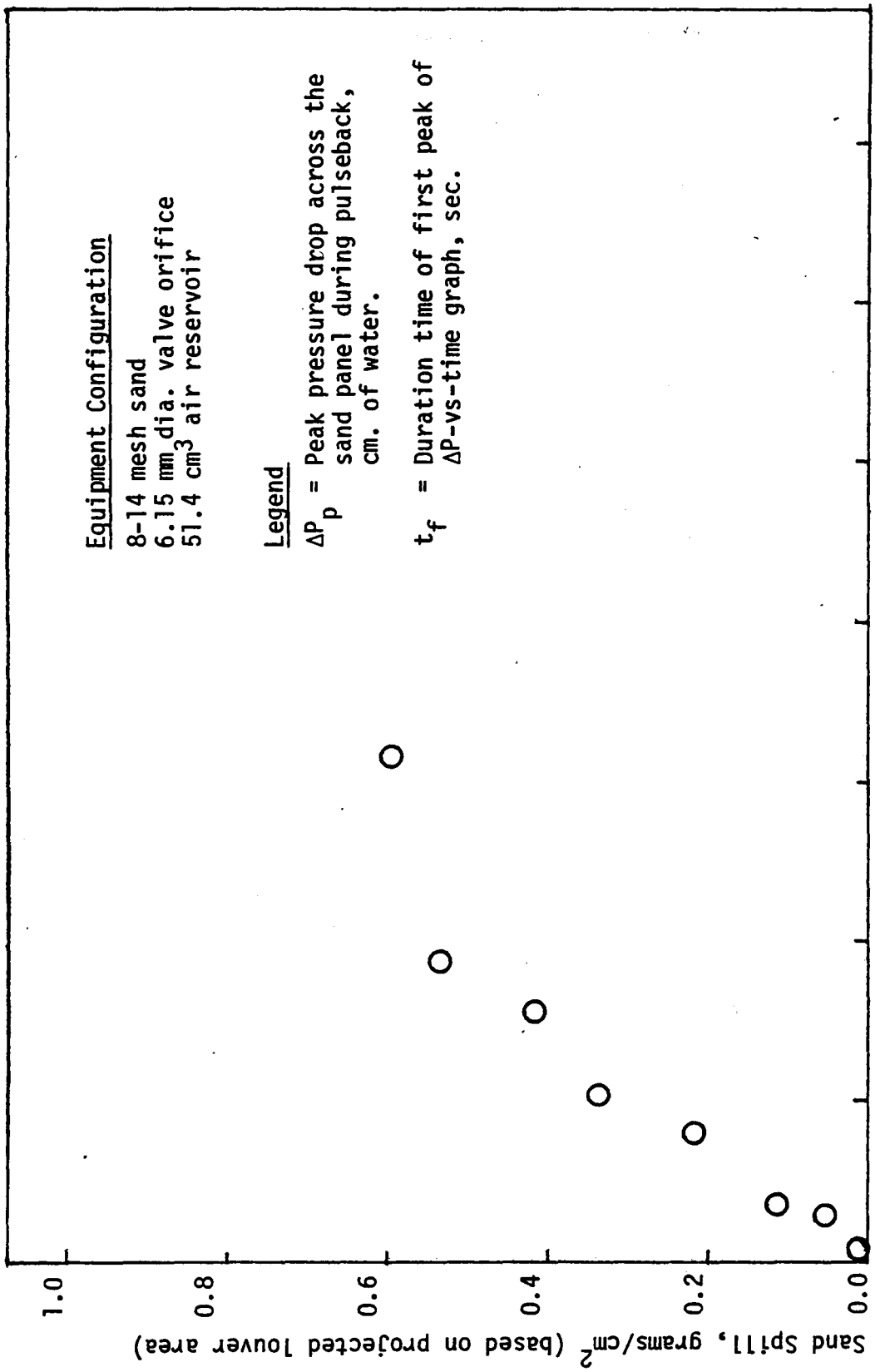

Figure 36. Sand Spill-versus-Pressure Drop Function.

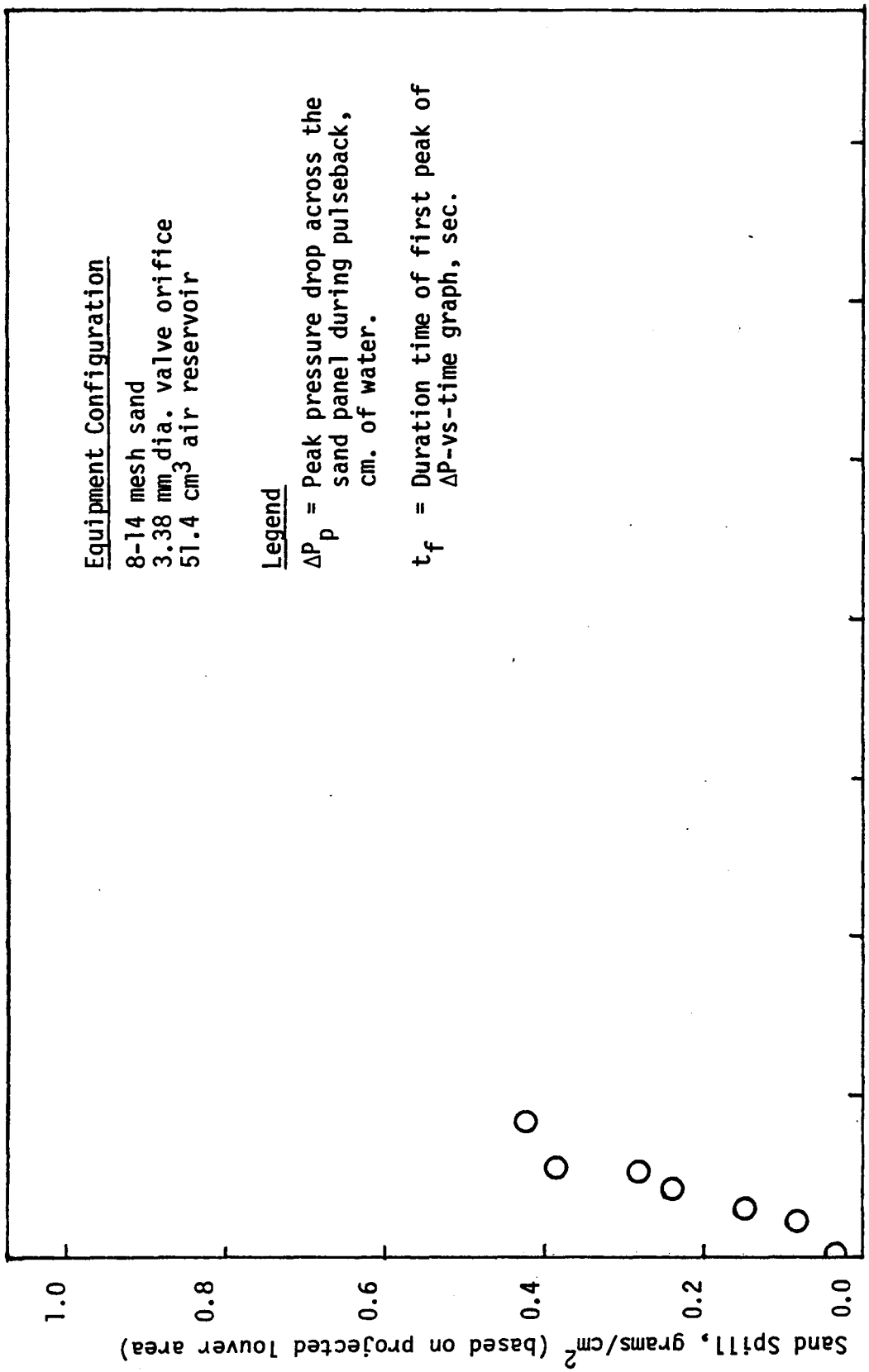

Figure 37. Sand Spill-versus-Pressure Drop Function.

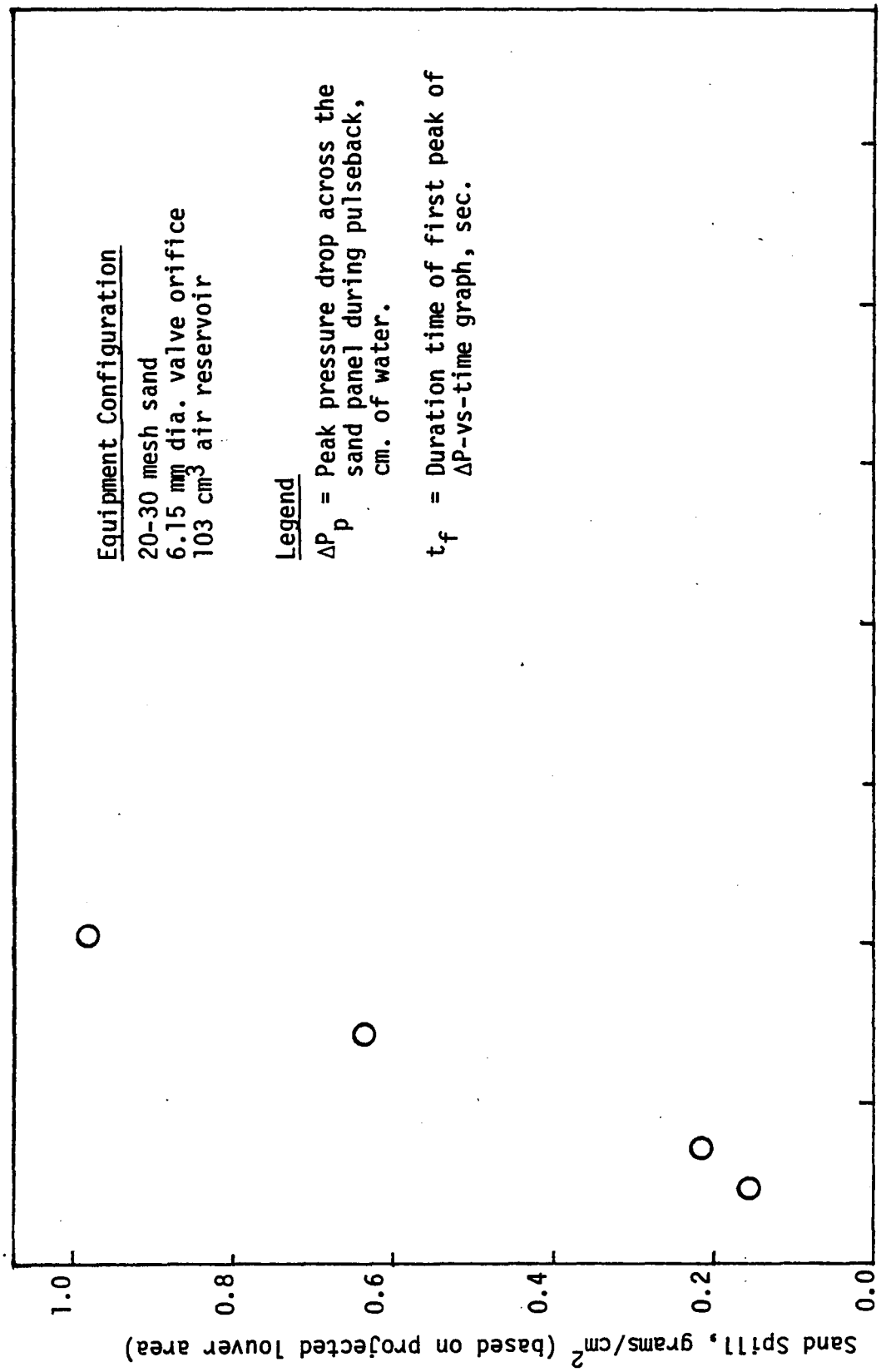

Figure 38. SAnd Spill-versus-Pressure Drop Function.

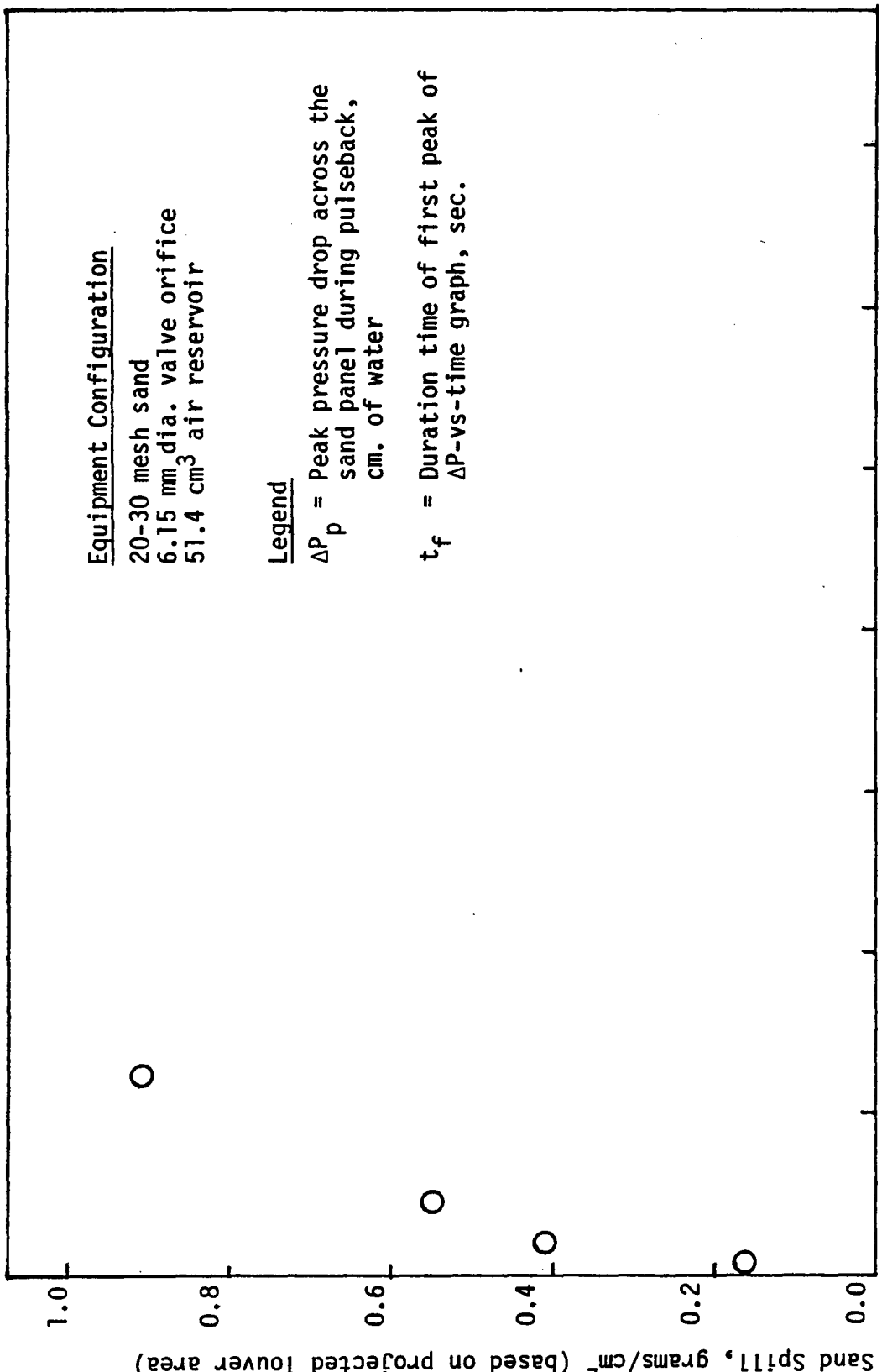

Figure 39. Sand Spill-versus-Pressure Drop Function.

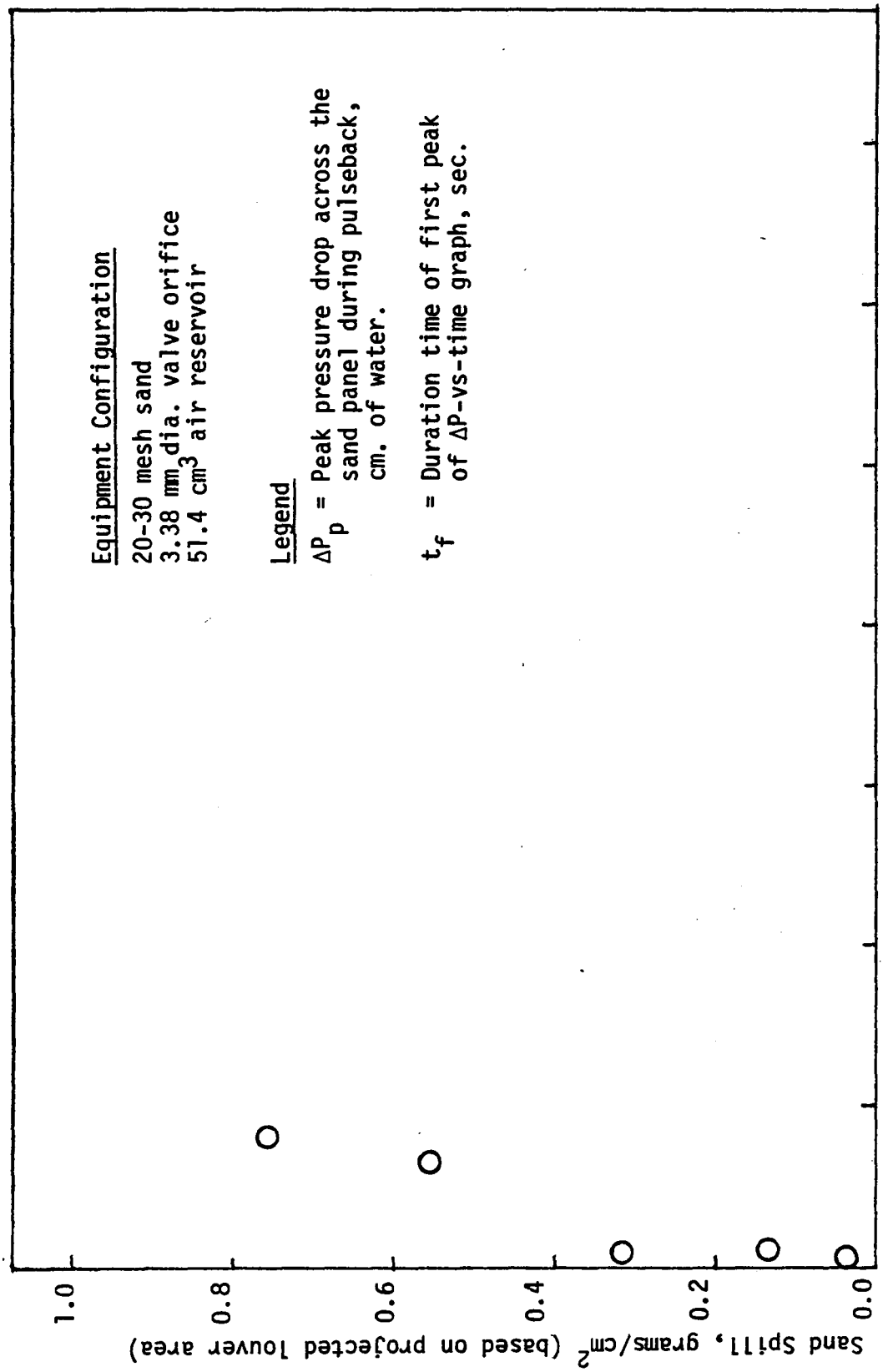

Figure 40. Sand Spill-versus-Pressure Drop Function.

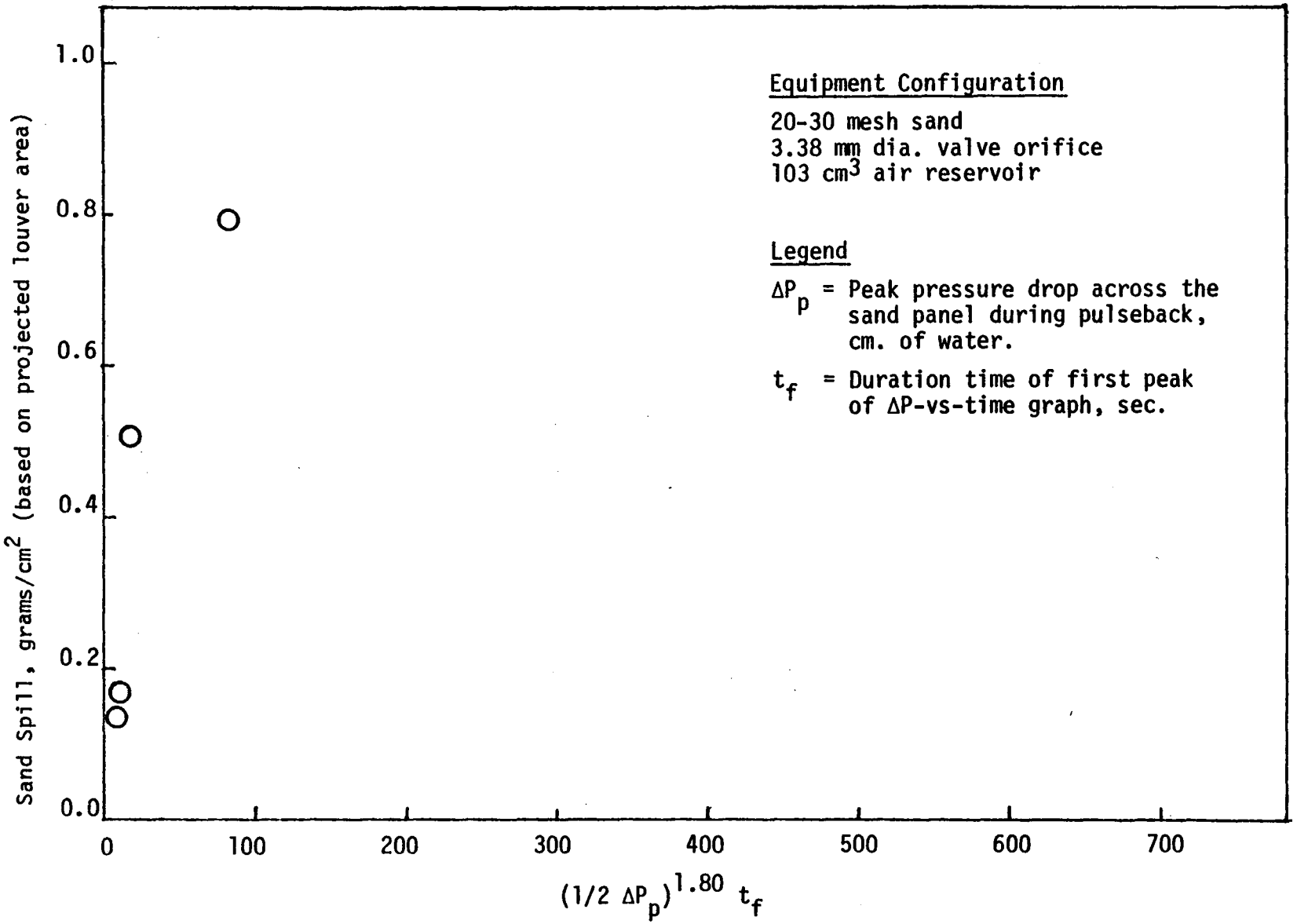

Figure 41. Sand Spill-versus-Pressure Drop Function.

TABLE VIII. Maximum Spill Values

Particle Size	Maximum Spill, gm/cm^2
8-14 mesh	0.6
20-30 mesh	0.55

Other models were used to try and correlate the pulseback data. However, none of these other models had the success of the final model as expressed in equation (22). The model used by Lee has been detailed in Appendix F for reference.

CONCLUSIONS

1. The sudden introduction of air from a high pressure source into the clean side of the panel bed case causes a surge flow of water across the bed into the "dirty" side, i.e., causes a "pulseback" of the panel bed.

2. For a relatively wide range of parameters governing the intensity of the pulseback (i.e., size of high pressure source, size of valve opening connecting the source to the panel bed cases, and air pressure), the pulseback causes a mass movement of sand in the panel bed toward the dirty side. The mass movement creates a spill of sand from each liquid-entry surface of the panel bed that appears to be substantially uniform.

3. The size of the sand spill is a function of the peak pressure drop across the panel bed during the pulseback, and is also a function of the duration of the pressure pulse creating the reverse surge flow.

4. A pulseback with too long a duration, roughly greater than about 100 milliseconds, commences with a mass movement and a substantially uniform spill, but degenerates at a later time to a spill concentrated upon the topmost liquid-entry surface or few surfaces of the panel bed.

RECOMMENDATIONS

A. The information of pulseback given here is adequate for design of experiments using the panel bed to filter dirt from a liquid or to conduct an adsorption, such as phenol on active carbon.

B. Before the design of a commercial device, it would be necessary to build and test a panel bed of appreciably greater height, such as, for example, three meters.

C. If further experiments on pulseback are undertaken, their accuracy could be improved according to the following recommendations:

   1. To prevent the oscillation of the water level, an outlet to a surge vessel should be provided at the height of the water level on the dirty side of the panel bed.
   2. Granular materials with particle characteristics different from sand (e.g., ion-exchange resin, activated carbon, etc.) should be used in the panel bed.
   3. The solenoid valve opening time should be included as a variable.
   4. The transducer signals might be transmitted to a digital computer such as the PDP-11 available at the Chemical Engineering Department at VPI & SU. This would provide the easiest method for analysis of the pressure drop data.

REFERENCES

1. Lee, K.C., I. Rodon, M.S. Wu, R. Pfeffer, A.M. Squires: "The Panel Bed Filter", final report to Electric Power Research Institute from The City College Clean Fuels Institute, EPRI Research Project 257-2, May, 1977.

2. Rodon, I.: Filtration of Dust at 150°C by Panel Bed Filter with Puffback, Ph.D. Thesis, The City University of New York, (January, 1978).

3. Squires, A.M.: Treating Liquid and Granular Materials in Panel Bed, U.S. Pat. 4,000,066 (Dec. 28, 1976).

4. Lambe, W.T. and R.V. Whitman: "Soil Mechanics," p. 262, John Wiley and Sons, Inc. New York, N.Y., 1969.

5. McCabe, W.L. and J.C. Smith: "Unit Operations of Chemical Engineering," p. 139, McGraw-Hill Book Co., Inc. New York, N.Y., 1976.

6. Bird, R.B., W.E. Stewart, E.N. Lightfoot: "Transport Phenomena," Ch. 1, John Wiley and Sons, Inc. New York, N.Y., 1960.

7. Muskat, M.: "The Flow of Homogeneous Fluids through Porous Media," Ch. 3, J.W. Edwards, Inc. Ann Arbor, Mich., 1946.

8. D'arcy, H.: "Les fontaines publiques de la ville de Dijon," (1856).

9. Muskat, M.: p. 73.

10. Reference 6, p. 59.

11. Reynolds, O.: Papers on Mechanical and Physical Subjects, Cambridge University Press, 1900.

12. op. cit.

13. Ward, J.C.: Turbulent Flow in Porous Media, J. of Hydraulics Division. Proceedings of A.S.C.E., 90, HY5, p. 1 (1964).

14. Leva, M.: "Fluidization," McGraw-Hill Book Co., Inc. New York, N.Y., 1959.

15. Reference 14, p. 49.

16. Terzaghi, K.: "Theoretical Soil Mechanics," Ch. 9, John Wiley and Sons, Inc., 1943.

REFERENCES - continued.

17. Lambe, W.T., and R.V. Whitman: "Soil Mechanics," p. 141, John Wiley and Sons, Inc. New York, N.Y., 1969.

18. Reference 17, p. 18.

19. Coulomb, C.A.: "Essai sur une Application des Regles des Maximis et Minimis a quelques Problemes de Stratique Relatifs a l'Architecture", Mem. acad. roy. pres. divers savants, 1, Paris, (1776).

20. Lambe, W.T., and R.V. Whitman: "Soil Mechanics," p. 241, John Wiley and Sons, Inc., New York, N.Y., 1969.

21. Ibid.

22. Reference 16, p. 25.

23. Ibid., p. 235.

24. Reference 17, p. 264.

25. Whitman, R.V. and K.A. Healy: "Shear Strength of Sands During Rapid Loadings," Trans. A.S.C.E., 128, p. 1553, (1963).

26. Lee, K.: "Filtration of Redispersed Power Station Fly Ash by a Panel Bed Filter with Puffback", Ph.D. Thesis, The City University of New York, (1975).

27. Ibid.

28. Ergun, S.: Chem. Eng. Prog., 48, p. 89, (1959).

29. Spells: Trans. Inst. Chem. Engrs., 33, p. 79-84, (1955).

30. Worster and Denny: Proc. Inst. Mech. Engrs., London, 169, p. 563-586, (1955).

31. Howard: Trans. Am. Soc. Civil Engrs., 104, p. 1334-1380, (1939).

32. Hughmark: Ind. Eng. Chem., 53, p. 389, (1961).

33. O'Brien, M.P. and R.G. Folsom: "The Transportation of Sand in Pipelines", Col. Univ. Pub. in Eng., 3, 7, (1937).

APPENDIX A

MATERIALS AND EQUIPMENT

All letters in this section refer to Figure 14.

Solenoid Valve. Solenoid valve J, 3.18 mm orifice diameter, 115 volts, 21 watts, model number 16C89C8-5. Manufactured by the Valcor Engineering Corp., Kenilworth, N.J. Used to admit the air from the air reservoir into the clean side of the pulseback filter.

Solenoid Valve. Solenoid Valve J, 6.15 mm orifice diameter, 115 volts, 10 watts, valve number V5-D6960, maximum pressure 50 psi. Manufactured by the Skinner Electric Valve Division, New Britain, Connecticut. Used to admit the air from the air reservoir into the clean side of the pulseback filter.

Pressure Gauge. Pressure gauge O, 0-60 psi. Manufactured by the Ashcraft Instrument Co. Used to monitor the air reservoir pressure.

Bleed Valve. Valve P, 1/4" diameter, 150 S.W.P., 300 W.O.G., Fig. 590. Manufactured by the Milwaukee Valve Co. Used to adjust the line pressure leading to the air reservoir.

Air Regulator. Air Regulator Q, 1/4" diameter fittings, 0-100 psi. Manufactured by the Matheson Instrument Co. Used to set the line pressure leading to the air reservoir.

Solenoid Valve. Solenoid Valve N, 1/8" fittings, 3/32" orifice diameter, 115 volts, 16.7 watts, max. pressure 1000 psi, catalogue number 82644, serial number 15158 S. Manufactured by the Automatic Switch Co., Florham Park, N.J. Used to admit air to the air reservoir.

Electrical Switch. Electrical Switch M, double pole, single throw. Manufactured by the Micro Switch Co., Freeport, Ill. Used to simultaneously operate the solenoid valves upstream and downstream of the air reservoir.

Rubber Stoppers. Two rubber stoppers of unknown origin with small diameter holes bored in the centers. Used to seal ports H and I to prevent sand and water surge from these ports but allow air to pass in and out of the filter case.

Plastic Tubing. Plastic tubing, of unknown origin, 1/4" diameter. Used to transmit air to the air reservoir. Also, used as a sight tube to monitor the filter case water level.

APPENDIX A - continued.

Plastic Funnel. Plastic funnel of unknown origin. Used to fill the sand and support into the filter case.

Balance. Balance R, capacity 2160 grams, model 700, serial number 23634. Manufactured by the Ohaus Scale Corporation, Florham Park, N.J. Used to weight wet and dry sand samples.

Oscilloscope. Oscilloscope A, type 564 storage oscilloscope, serial number 004973. Manufactured by Teletronix, Inc., Portland, Oregon. Used to display and store the pressure drop signal from the electronic subtractor.

Transducer Coupler. Amplifier B & C, model 549A, filter 545B14, piezotran type. Manufactured by the Sandstrand Data Control Corp., Richmond, Wash. Used to transmit the signal from the transducer element to the electronic subtractor.

Transducer Element. Transducer F & G, model 206, range 0-80 psi, 110 mv/psi sensitivity, Kistler type. Manufactured by the Sandstrand Data Control Corp., Richmond, Wash. Used to measure the pressure on the clean and dirty side of the panel bed.

Bed Saddles. Support media, 3/8" ceramic bed saddles of unknown origin. Used to support the panel of sand.

Sand. 20-30 mesh quartz sand. Supplied by the American Graded Sand Co., Paterson, N.J. Used to form the panel bed.

Sand. 8-14 mesh quartz sand. Supplied by the American Graded Sand Co., Paterson, N.J. Used to form the panel bed.

Valve. Valve E, 1" diameter. 150 S.W.P., 300 W.O.G. Manufactured by the Milwaukee Valve Co. Used to drain the filter case.

Camera. 35-mm SLR camera with 50 mm lens. Manufactured by the Canon Optical Co. Used to photograph the oscilloscope screen.

Terminal Strip Block. Terminal block of unknown origin. Used to interconnect the solenoid valves with the electrical switch.

Air Reservoir. Reservoir K, made of plexiglass, 103 cm. cm volume. Manufactured by the Chemical Engineering Shop at the City University of New York. Used to supply air to the panel bed filter.

Air Reservoir. Reservoir K, made of aluminum, 51.4 cu. cm volume. Manufactured by the Chemical Engineering Shop at VPI & SU. Used to supply air to the panel bed filter.

APPENDIX A - continued.

Electronic Subtractor. Manufactured by the Chemical Engineering Staff at VPI & SU. Used to electronically subtract the clean side transducer signal from the dirty side transducer signal.

Rust-Oleum Primer. Used to prime the louver columns prior to painting.

Rust-Oleum Paint. Used to paint the louver columns to inhibit metal degradation.

Gasket Paper. 1/64" gasket paper. Manufactured by the McCord Co. Used to form gaskets for the filter case joints.

Caulk Compound. Silicone caulk compound. Manufactured by the Dow-Corning Co. Used to seal the filter case joints and the transparent window.

Gasket Compound. Permatex gasket compound. Used to seal the filter case joints.

Crack Filler. Plastic filler for aluminum. Manufactured by the Duro Co. Used to fill cracks at the filter case joints.

Epoxy Cement. Epoxy cement. Manufactured by the Elmers Co. Used to seal cracks at the filter case joints.

APPENDIX B

TRANSDUCER SPECIFICATIONS

Model 206 High Sensitivity Pressure Transducer

Specifications

PERFORMANCE

Pressure Range	80 psi
Resolution	0.0008 psi rms
Sensitivity, (units supplied with cal. certif.)	+ 100 mV/psi (80 to 120 mV/psi)
Linearity, zero based best straight line	± 1% F.S.
Resonant Frequency, nom.	130 kHz
Rise Time, 10 to 90%	3 μ sec.
Low Frequency Time Constant at R.T., min.	10 sec.
Temperature Sensitivity Shift	-0.03%°F

ENVIRONMENTAL

Vibration Sensitivity, max.	0.005 psi/g
Shock, 1 ms pulse width	1000 g
Vibration Limit, 5-2000 Hz	500 g
Temperature Range	-65 to +250°F
Pressure Limit	500 psi

ELECTRICAL

Output Voltage F.S., nom.	8V
Output Current	2 mA
Output Impedance	100 ohms
Bias, nom.	11 VDC
Low Frequency Response, -5% point	0.05 Hz
High Frequency Response, +5% point	20 kHz

MECHANICAL

Weight	22 grams
Case Material	Stainless Steel
Case Design	Hermetically Sealed
Mounting Torque	8 ft.lbs.

APPENDIX B - continued.

Specifications

POWER SUPPLY

Constant Current Source, nom.	4 mA
Source Impedance	250 k Ω
No Load Source Voltage	20 to 30 VDC
Supply Ripple, max.	25 mV rms

APPENDIX B - continued.

TRANSDUCER COUPLER SPECIFICATIONS (cont'd)

	Units	549A/ 549A3	549B Same unless otherwise specified.	549C
Output				
Full Scale Signal				
Voltage	V_{pp}	10	-	-
Current (±20%)	mA_{pp}	8	4	8
Impedance (in series with 47 μF)	Ω	≤ 15	-	-
Connector		BNC	-	-
Power				
Voltage (±10%)	Volts	115/230 rms 50-400 Hz	built in batteries NEDA 1604M	+12
Current (±20%)	mA	15 rms	4 DC	160 DC
Connector		3 wire cord	NA	AMP #1-48304-6
Physical				
Weight	grams	440	343	207
Size W x H x D	inches	4.875 x 1.675 x 2.5		
Environmental				
Temperature				
Operating		0 to +50° C		
Storage		-20 to +65° C		
Humidity		20 to 90%		
Vibration		10 g peak, 5 to 500 Hz		
Shock		60 g, 10 millisec. pulse width		

APPENDIX B - continued.

TRANSDUCER COUPLER SPECIFICATIONS

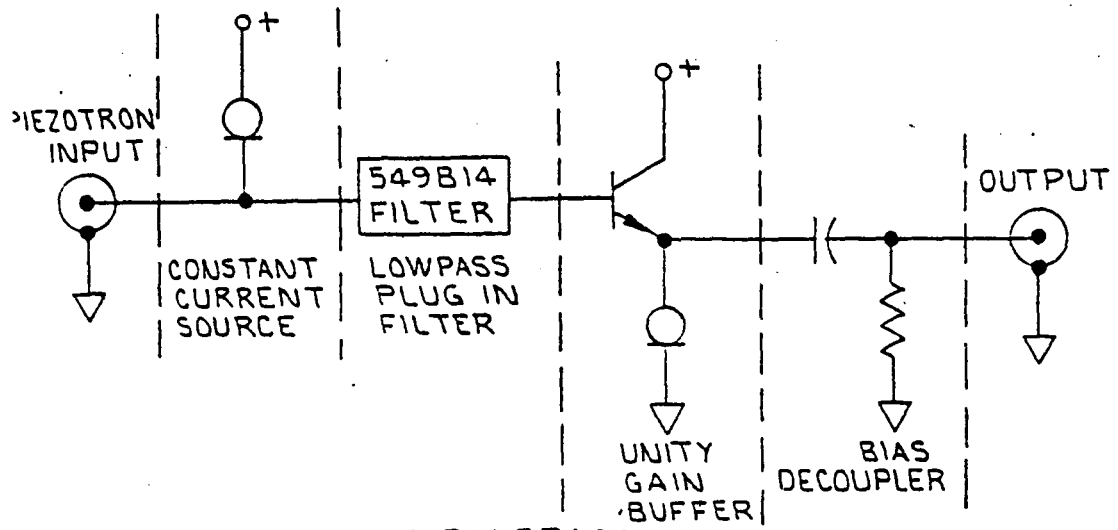

BASIC DIAGRAM
(POWER SUPPLY NOT SHOWN)

SPECIFICATIONS:

	Units	549A / 549A3	549B Same unless otherwise indicated	549C
Piezotron Input				
Current	mA	3.9 ± 0.5	3.9 ± 0.5	2 ± 0.2
Full Scale Signal	V_{pp}	10	-	-
Noise	μV_{pp}	150	20	300
Impedance	KΩ	>200	>350	>200
Connector		BNC	-	-
Transfer Characteristics				
Gain		1.00	-	-
Frequency response (note 1)				
5%	Hz	0.07 to 300K	-	-

APPENDIX C

Electronic Subtractor Circuit

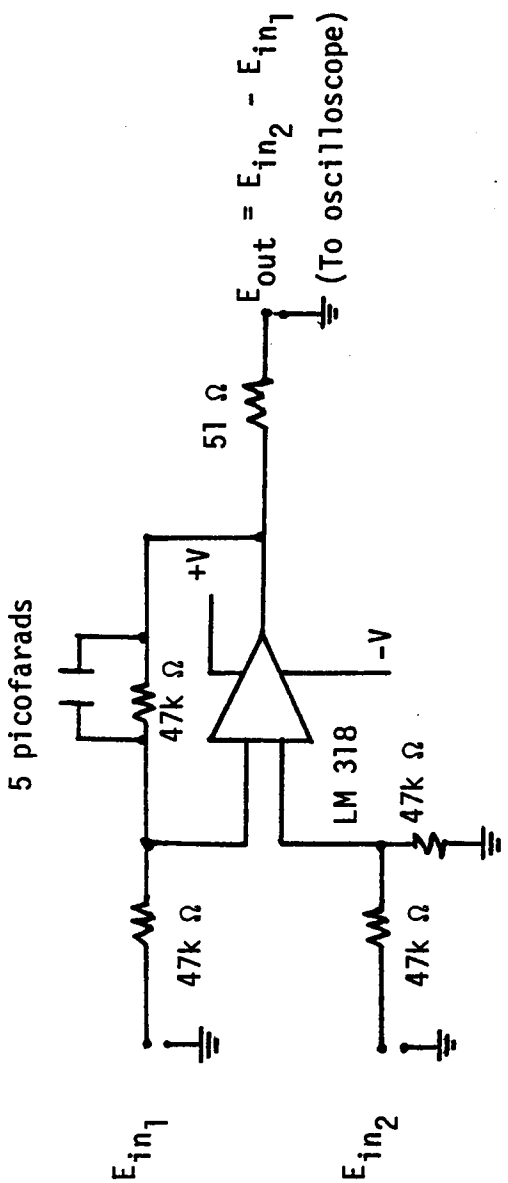

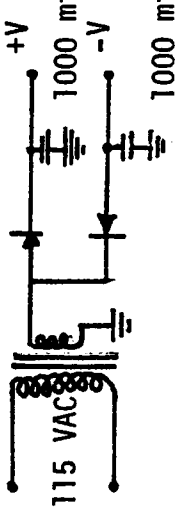

Figure 42. Electronic Subtractor Circuit and Power Supply.

APPENDIX D

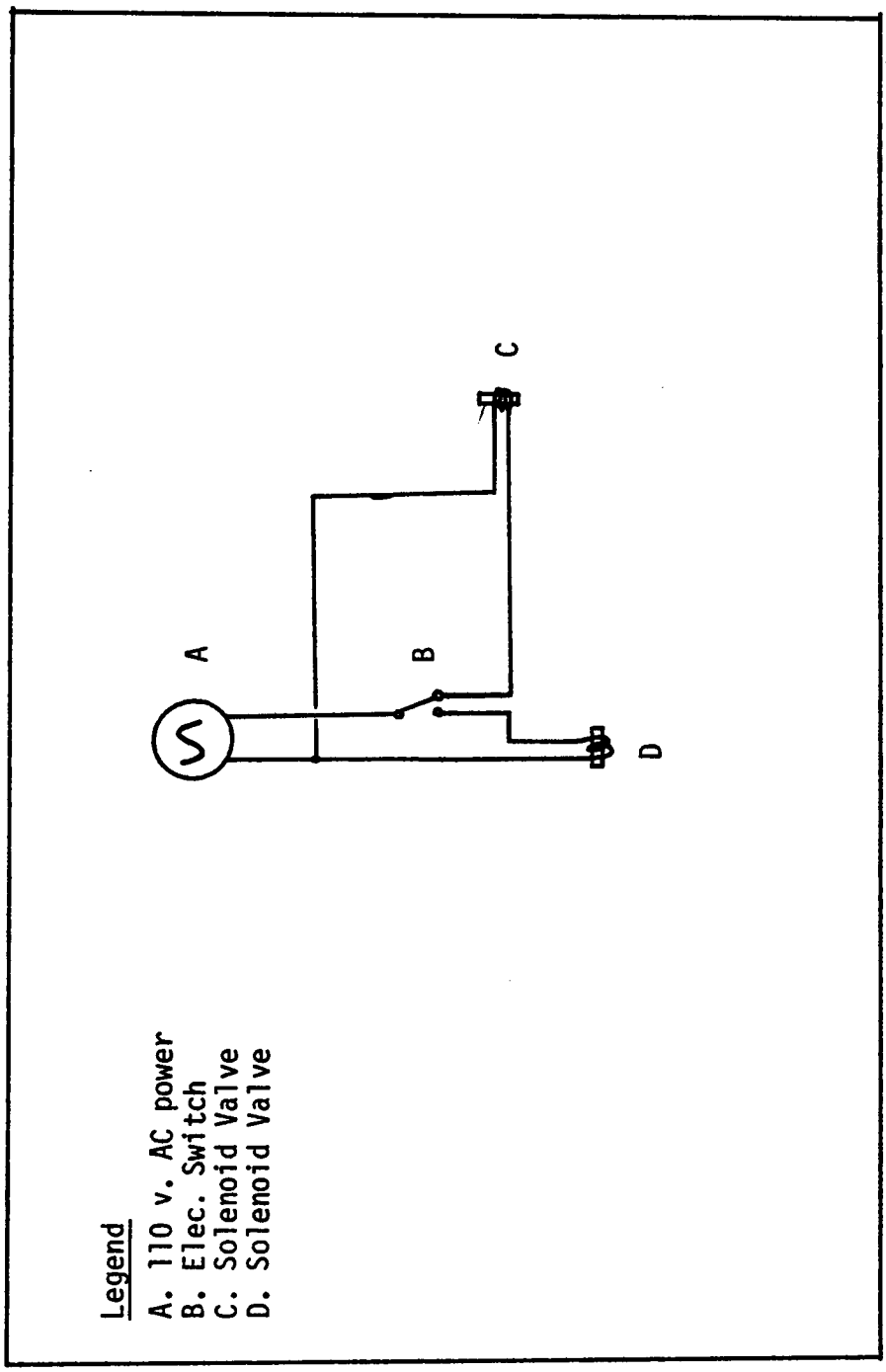

Figure 43. Diagram showing electrical circuit operating the solenoid valves.

APPENDIX E

MODEL OF ΔP-VS-TIME

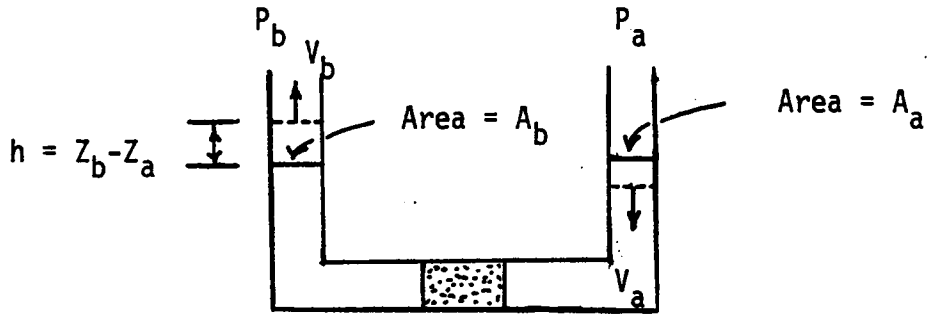

$$V_b = h/t \qquad V_B = V_B\left(\frac{A_b}{A_B}\right) \qquad V_A = V_b\left(\frac{A_a}{A_b}\right)$$

Write the Bernoulli equation from p. 76 of McCabe & Smith:

$$\frac{P_a}{\rho} + \frac{GZ_a}{G_c} + \frac{\overline{V}_a 2}{2G_c} = \frac{P_b}{\rho} + \frac{GZ_b}{G_c} + \frac{\overline{V}_b 2}{2G_c} + lw$$

Regroup:

$$\frac{(P_a - P_b)}{\rho} + \frac{G(Z_a - Z_b)}{G_c} + \frac{\left(\frac{A_a}{A_b}\right)^2 V_b 2}{2G_c} = \frac{V_b 2}{2G_c} + lw$$

$$\frac{(P_a - P_b)}{\rho} + \left(\frac{G}{G_c}\right)(-h) + \left[\left(\frac{A_a}{A_b}\right)^2 - 1\right]V_b 2 = lw$$

$$\left(\frac{P_a - P_b}{\rho}\right) + \frac{G}{G_c}(-h) + \left[\left(\frac{A_a}{A_b}\right)^2 - 1\right] (\partial h/\partial t)^2 = lw$$

Note: Neglect any lost work except for that due to the packed bed.

APPENDIX E - continued.

From p. 147-148, McCabe & Smith:

$$-\Delta P = \frac{L(1-\varepsilon)S_p}{G_c V_p} \left[\frac{k_1 \mu V_B (1-\varepsilon)S_p}{\varepsilon V_p} + k_2 V_B^2\right]$$

To convert this ΔP expression to lost work, divide by ρ:

$$\frac{-\Delta P}{\rho} = \frac{L(1-\varepsilon)S_p}{\rho G_c V_p} \left[\frac{k_1 \mu V_B (1-\varepsilon)S_p}{\varepsilon V_p} + k_2 \rho V_B^2\right]$$

This can now be rewritten and substituted into the previous eq.:

$$\frac{(P_a - P_b)}{\rho} + \frac{G(-h)}{G_c} + \frac{\left[\left(\frac{A_a}{A_b}\right)^2 - 1\right]}{2G_c} (\partial h/\partial t)^2 =$$

$$\frac{L(1-\varepsilon)S_p}{\rho G_c V_p} \left[\frac{k_1 \mu (1-\varepsilon)S_p (\partial h/\partial t)}{\varepsilon V_p} + k_2 (\partial h/\partial t)^2\right]$$

Let, $C_1 = \frac{G}{G_c}$ $\quad C_2 = \frac{\left[\left(\frac{A_a}{A_b}\right)^2 - 1\right]}{2G_c}$ $\quad C_3 = \frac{L(1-\varepsilon)S_p}{\rho G_c V_p}$

$$C_4 = \frac{k_1 \mu (1-\varepsilon)S_p}{\varepsilon V_p} \qquad C_5 = k_2 \rho$$

Rewrite:

$$\frac{(P_a - P_b)}{\rho} + C_1(-h) + C_2(\partial h/\partial t)^2 = C_3 C_4 (\partial h/\partial t) + C_3 C_5 (\partial h/\partial t)^2$$

APPENDIX E - continued.

Given a form for $(P_a - P_b)$ as a function of time and values for the parameters C_7, C_8, and C_6, it is thought that a solution could be obtained.

$$\frac{(P_a - P_b)}{\rho} + C_1(-h) + [C_2 - C_3C_5](\partial h/\partial t)^2 - C_3C_4(\partial h/\partial t)$$

Let,

$$C_6 = -C_1 \qquad C_7 = [C_2 - C_3C_5] \qquad C_8 = -C_3C_4$$

Finally,

$$C_7(\partial h/\partial t)^2 + C_8(\partial h/\partial t) + C_6h = \left(\frac{P_a - P_b}{\rho}\right)$$

APPENDIX F

During his work with puffback cleaning using air, Lee developed a correlation for his puffback data. In this Appendix, Lee's correlation was used to treat the pulseback data from this investigation.

Lee's correlation involves the following three types of plots:

1. Peak Pressure Drop is plotted against Sand Spill as shown in Figures 44 through 51. These plots determine the minimum pressure drop required to cause sand spill. This value is obtained from the intersection of the linear data with the abscissa. Lee found that this minimum pressure drop was a constant for a particular particle size of sand.
2. Time during which the ΔP exceeds the minimum ΔP required for sand spill (active time) is plotted against the sand spill in Figures 52 through 59. Lee found that for puffback, the sand spill was a linear function of the active time and passed through the origin.
3. Peak Pressure Drop is plotted versus the total duration time of the initial ΔP peak in Figures 60 through 67. Lee found that these plots yielded straight lines which passed through the origin.

TABLE IX. Minimum Pressure Drop for Sand Spill Determined by Least Squares Regression for Figures 44 through 51.

Pulseback Code	Minimum Pressure Drop cm of Water
A-1-S	40.1
A-2-S	24.5
A-1-B	7.6
A-2-B	28.0
C-1-S	12.7
C-2-S	6.0
C-1-B	32.4
C-2-B	5.5

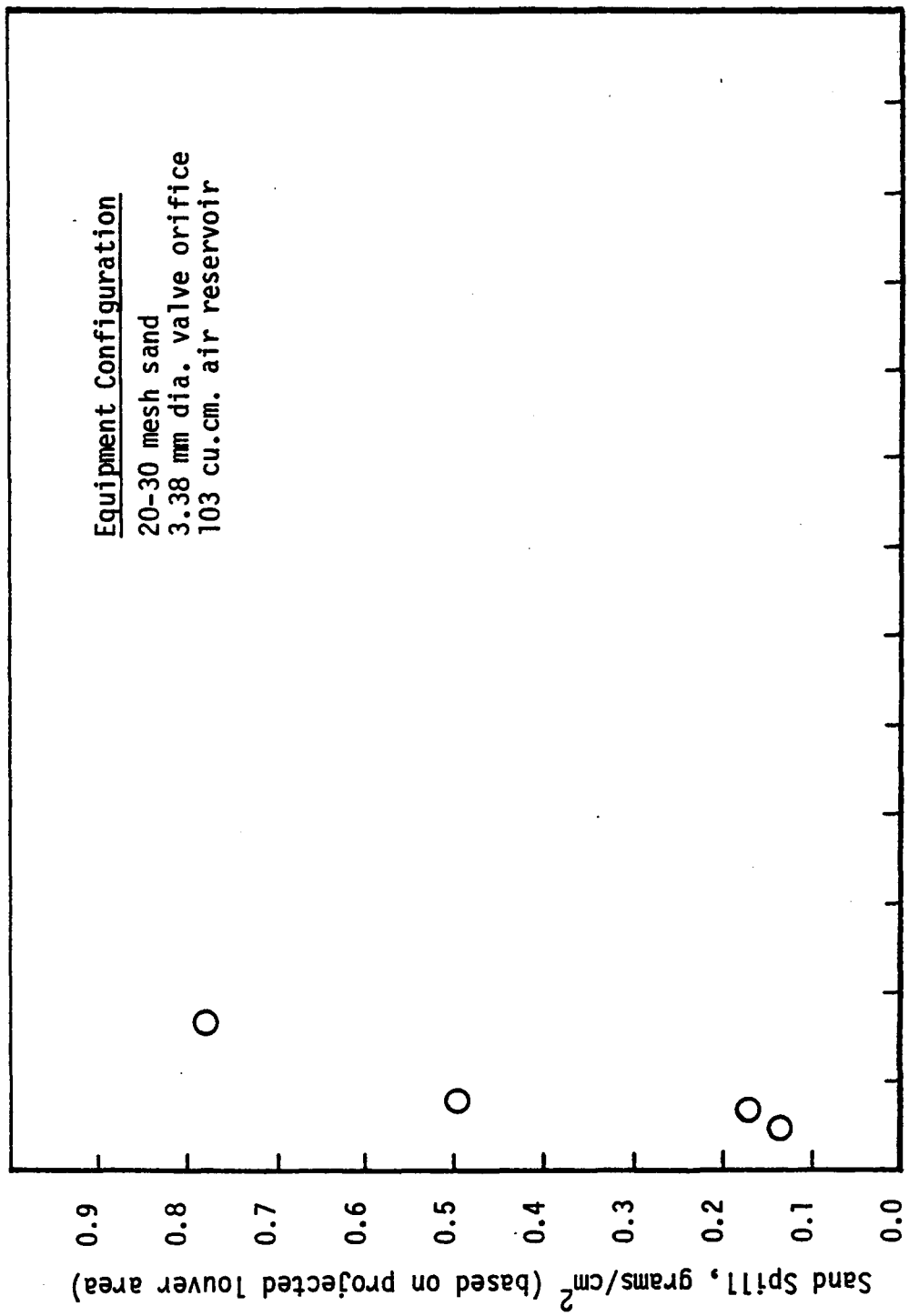

Figure 44. Peak Pressure Drop-versus-Sand Spill.

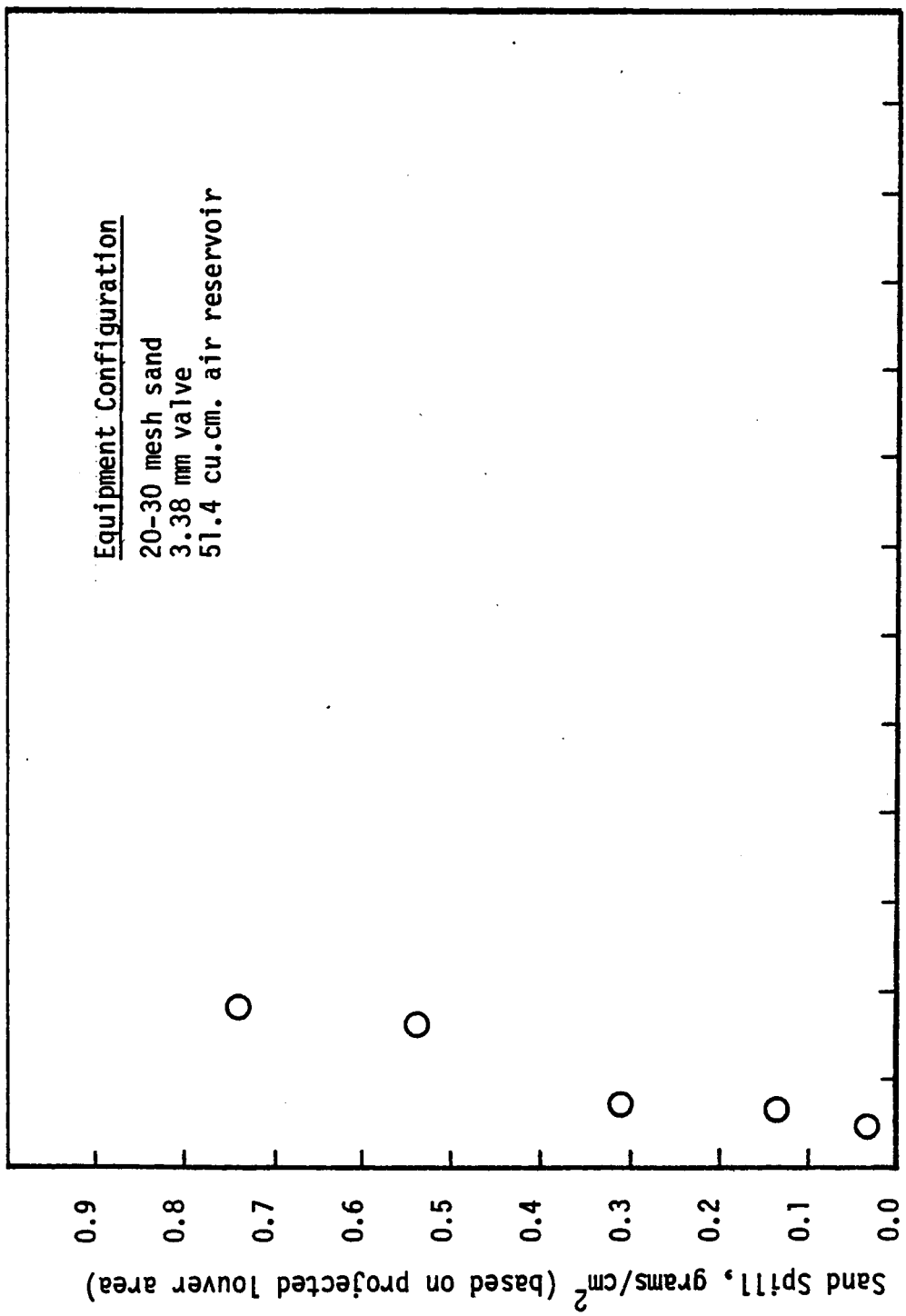

Figure 45. Peak Pressure Drop-versus-Sand Spill.

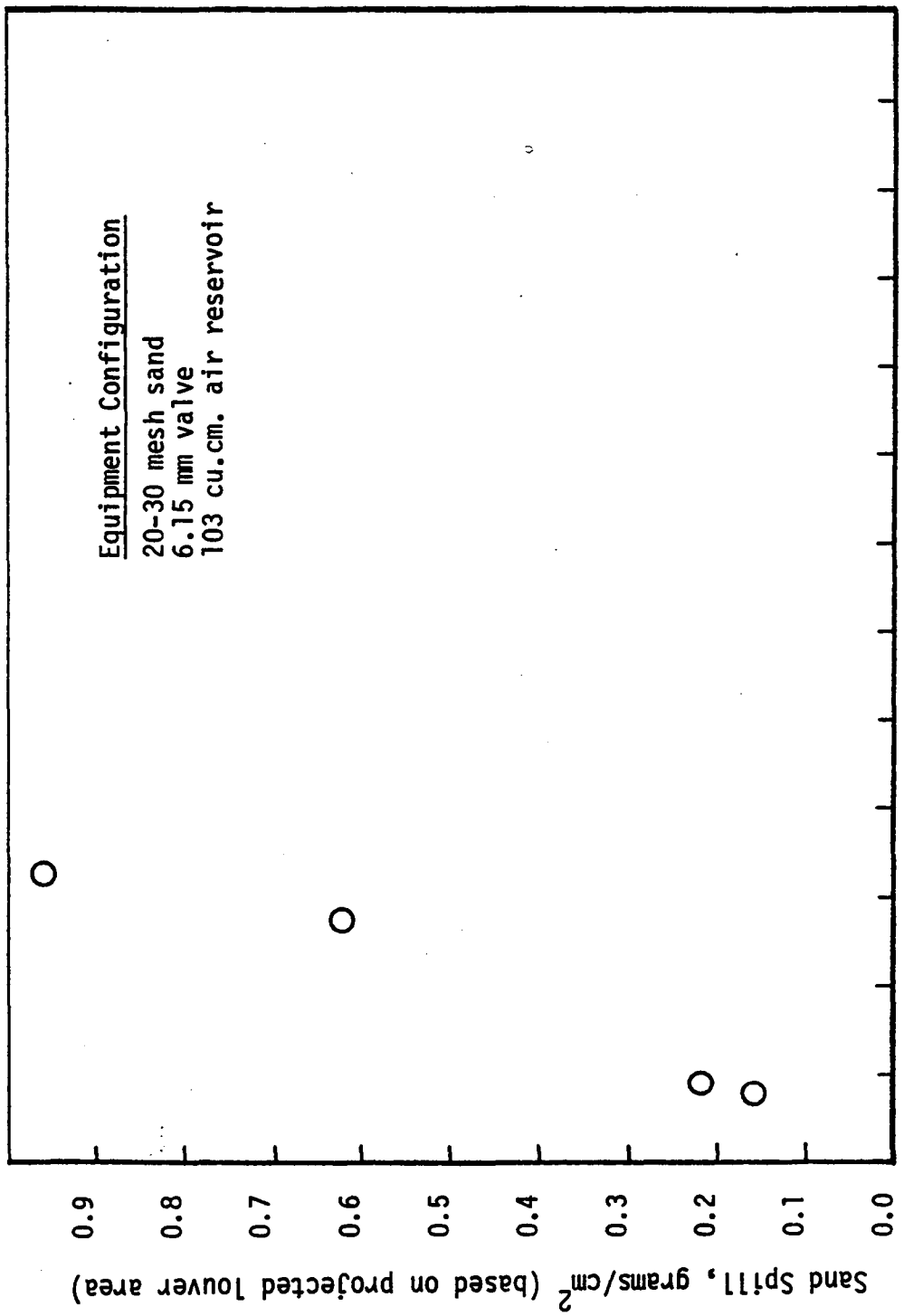

Figure 46. Peak Pressure Drop-versus-Sand Spill.

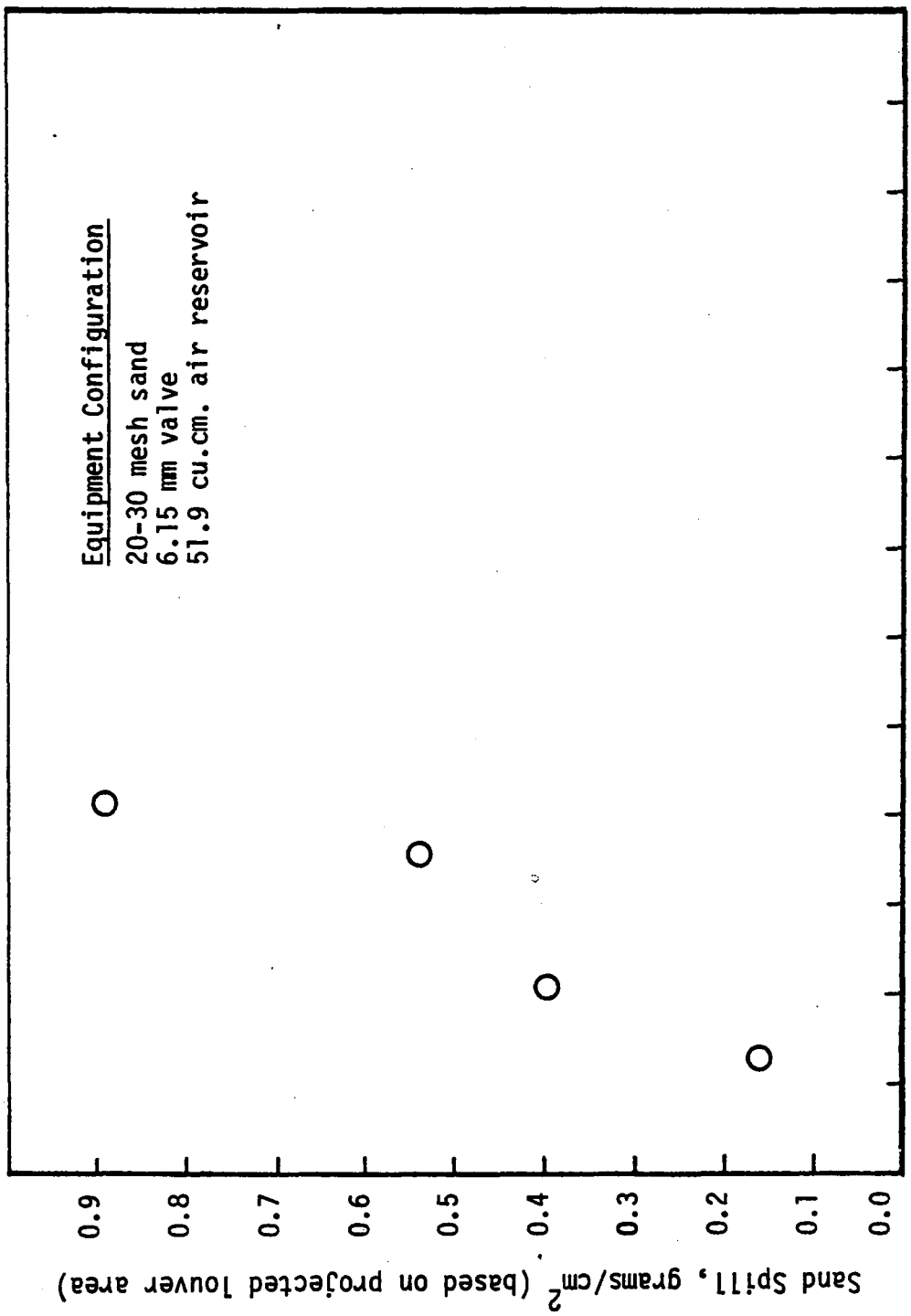

Figure 47. Peak Pressure Drop-versus-Sand Spill.

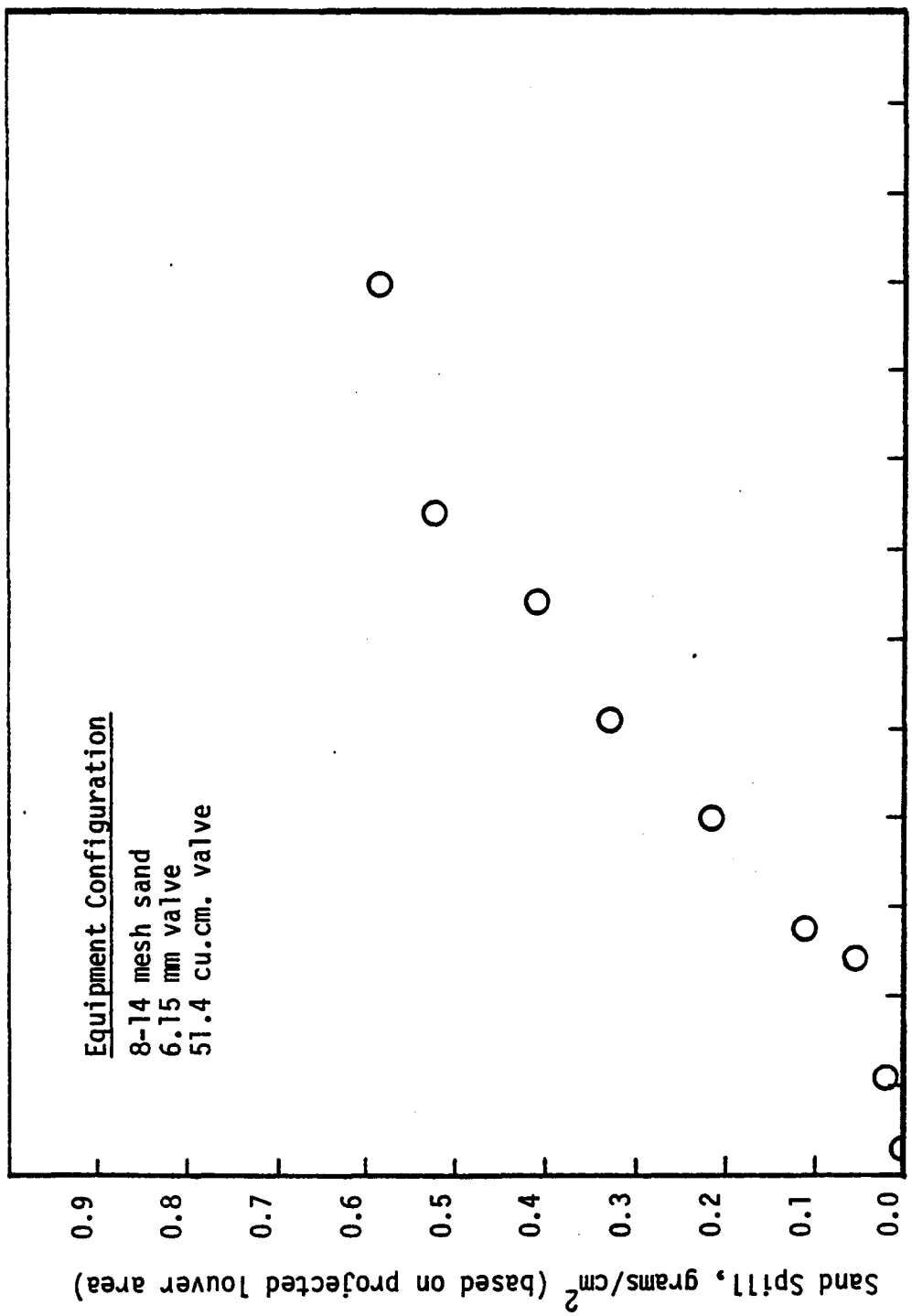

Figure 48. Peak Pressure Drop-versus-Sand Spill.

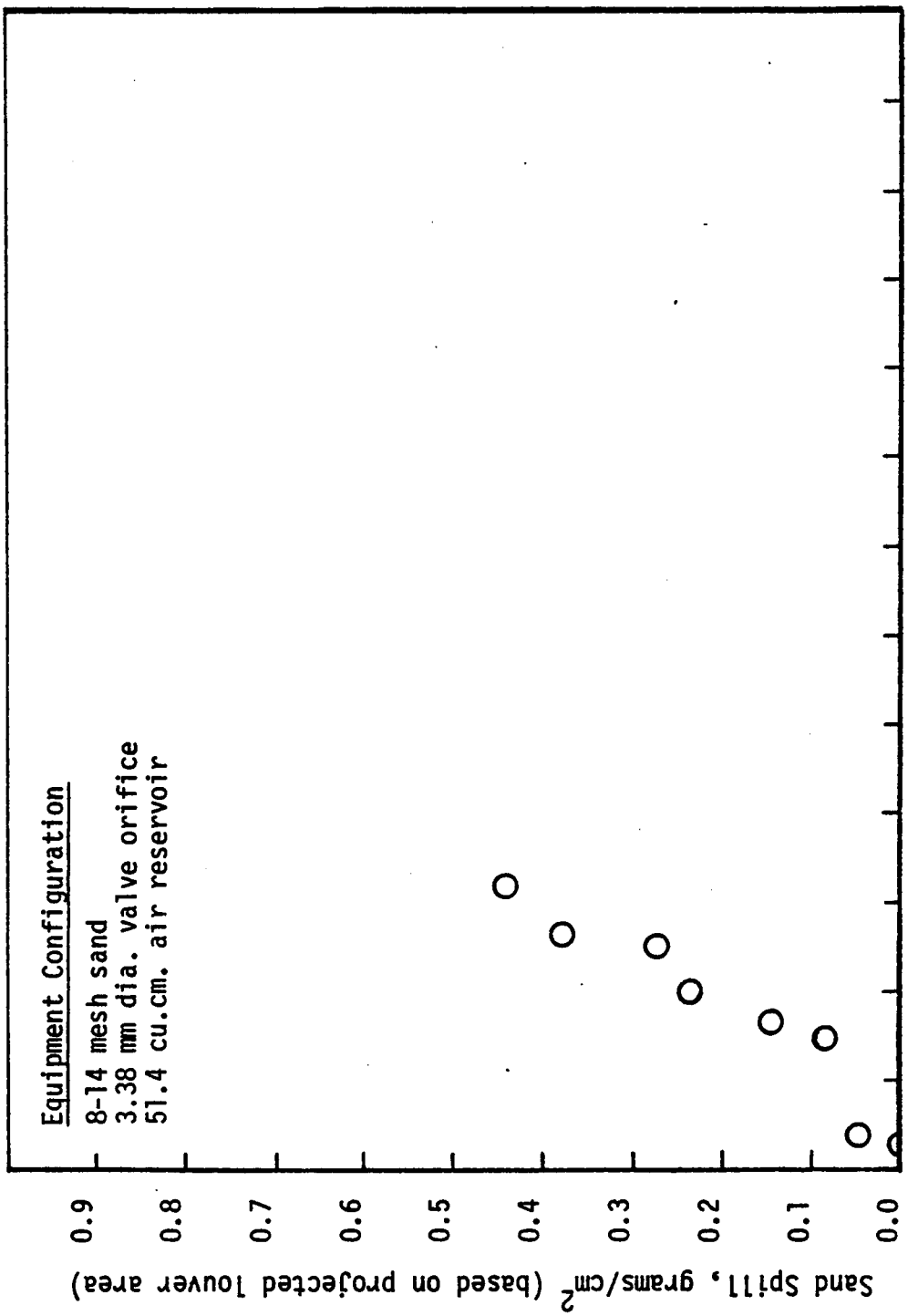

Figure 49. Peak Pressure Drop-versus-Sand Spill.

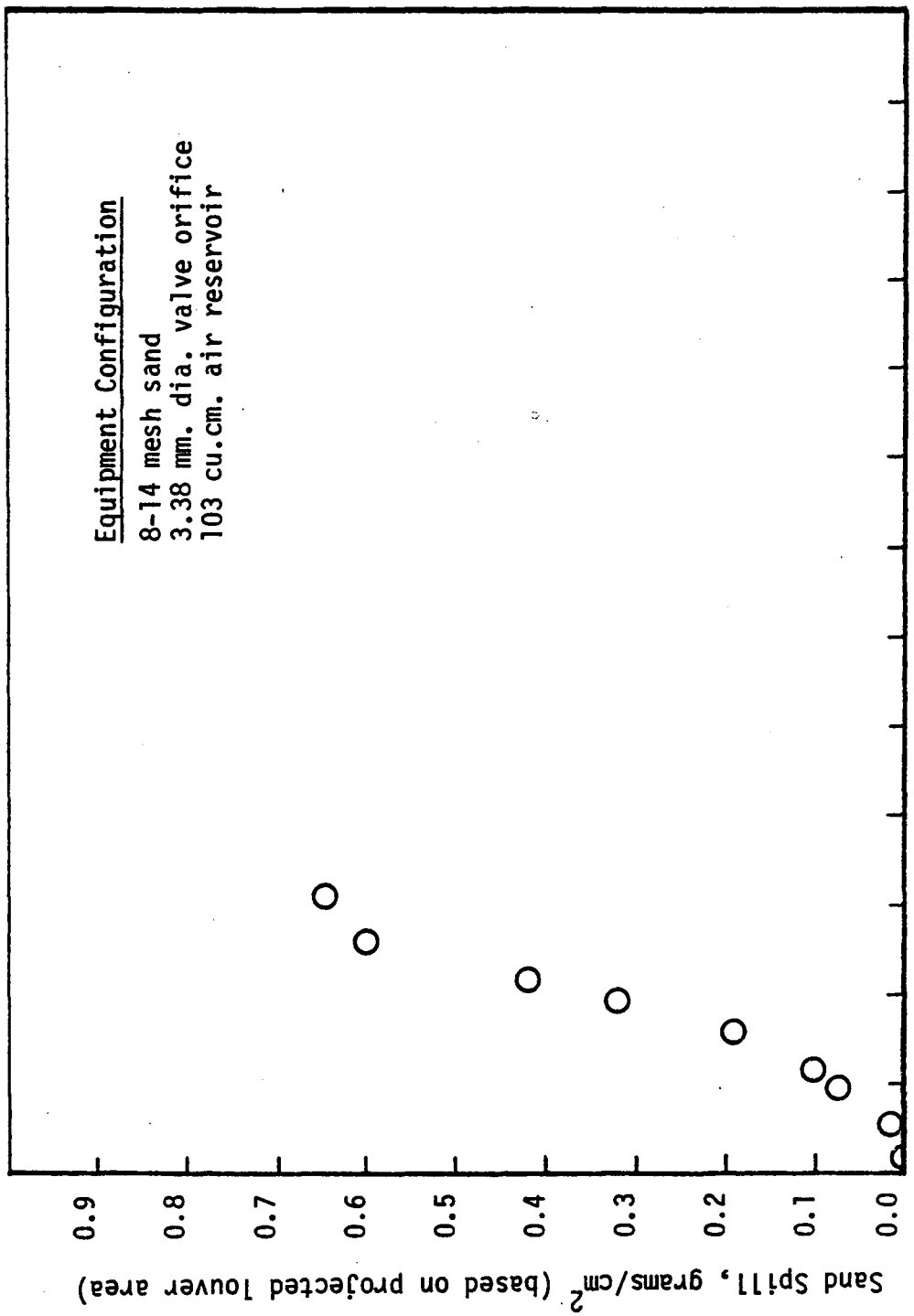

Figure 50. Peak Pressure Drop-versus-Sand Spill

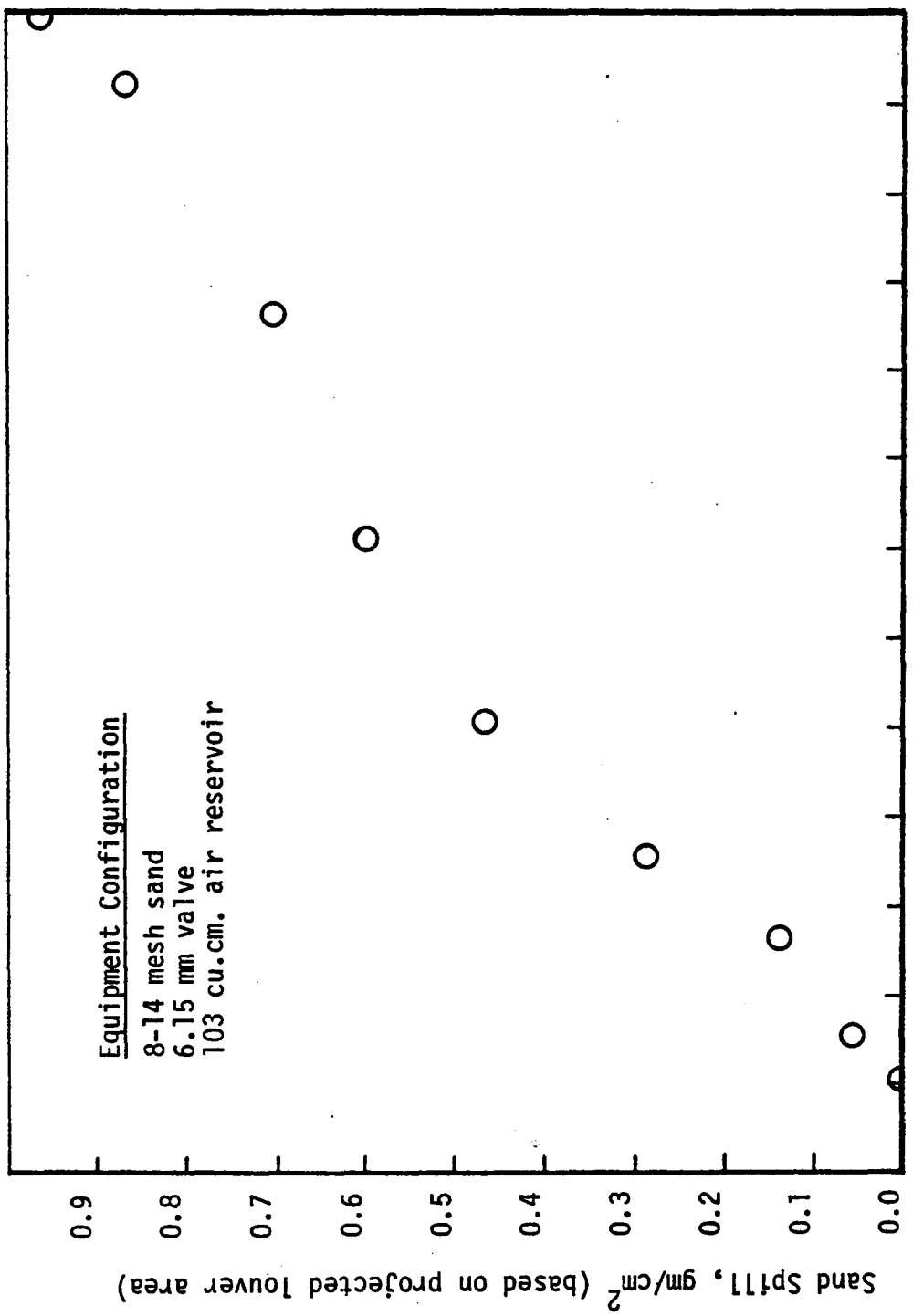

Figure 51. Peak pressure drop-vs-Sand Spill

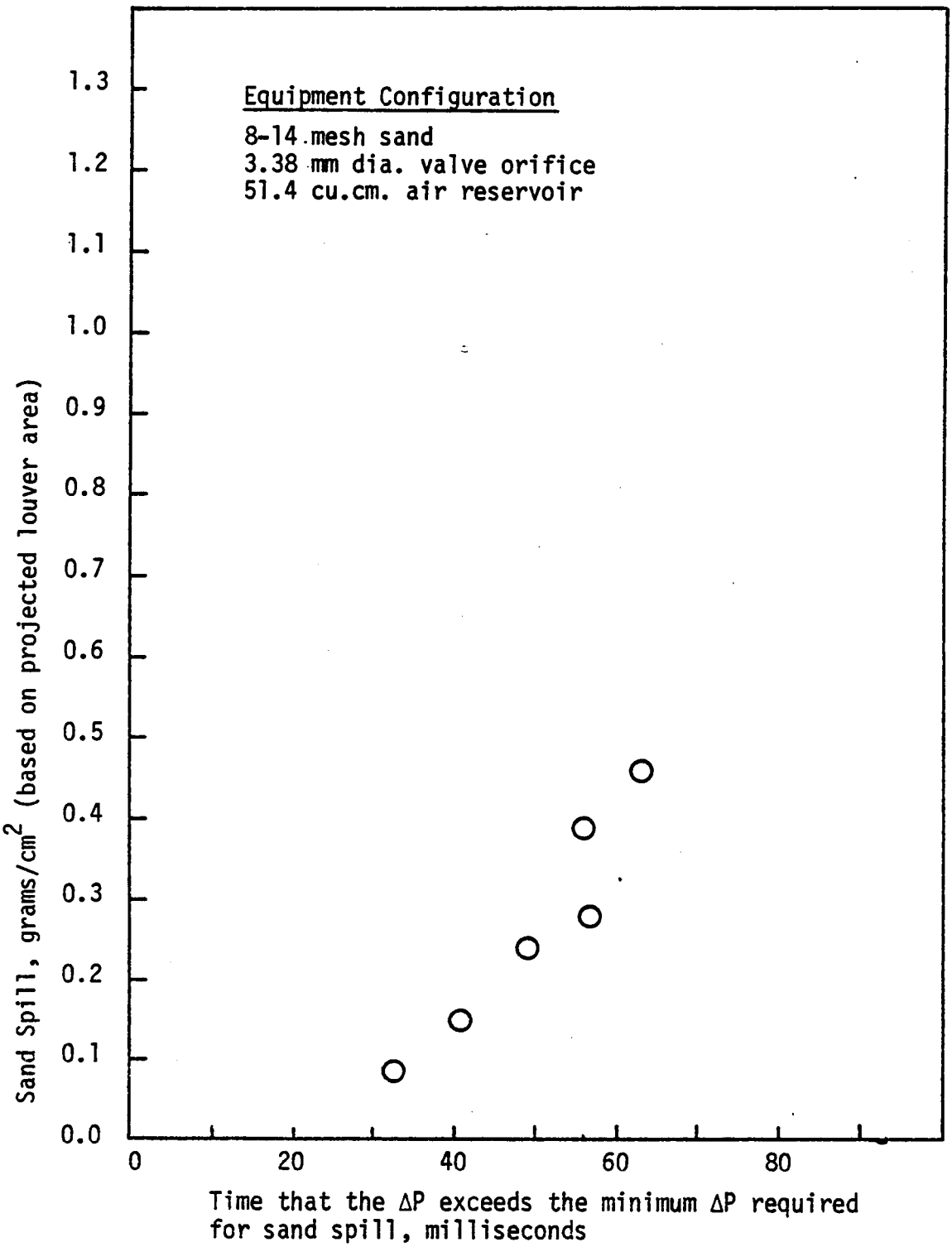

Figure 52. Active time-versus-Sand Spill.

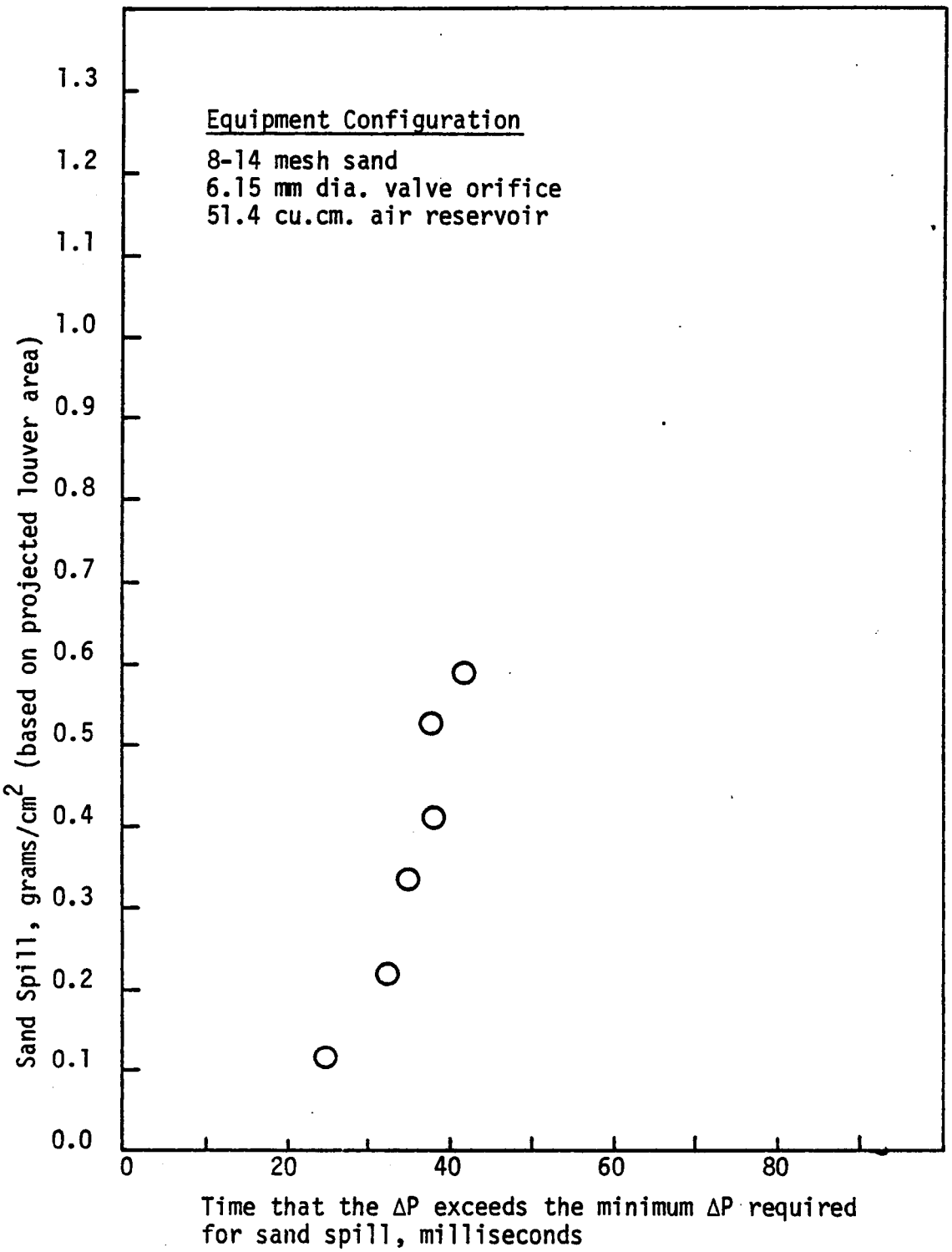

Figure 53. Active time-versus-Sand Spill.

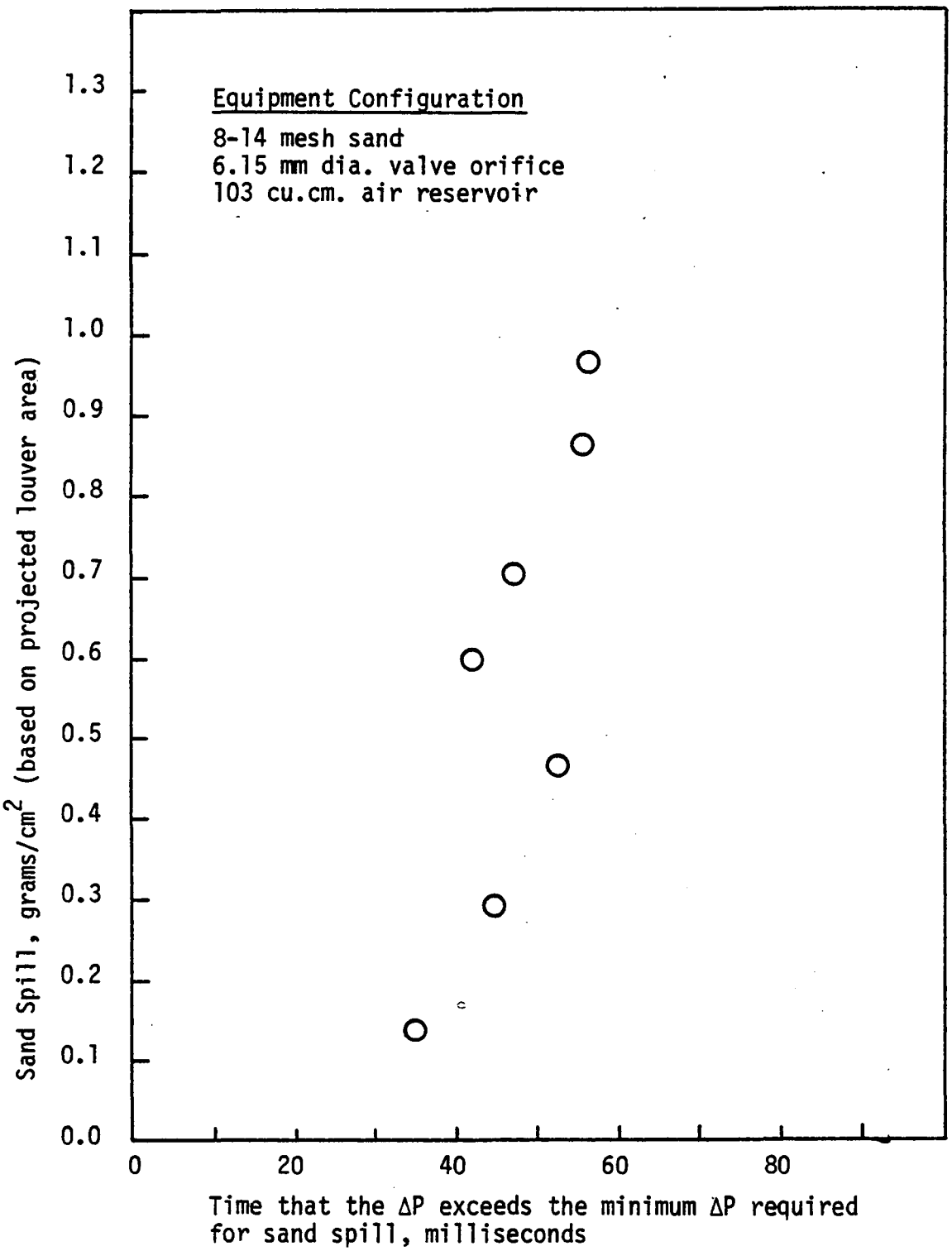

Figure 54. Active time-versus Sand Spill.

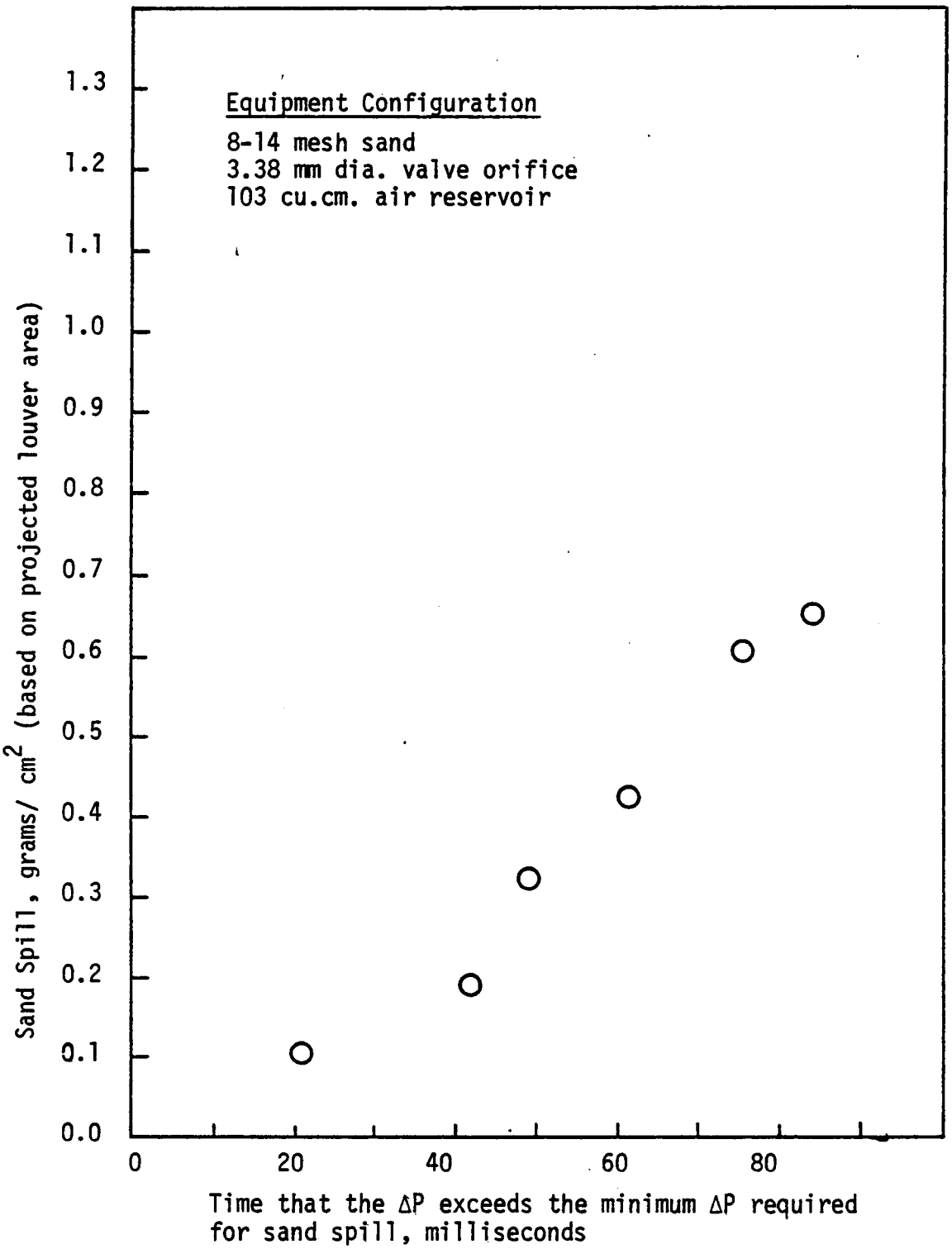

Figure 55. Active time-versus-Sand Spill.

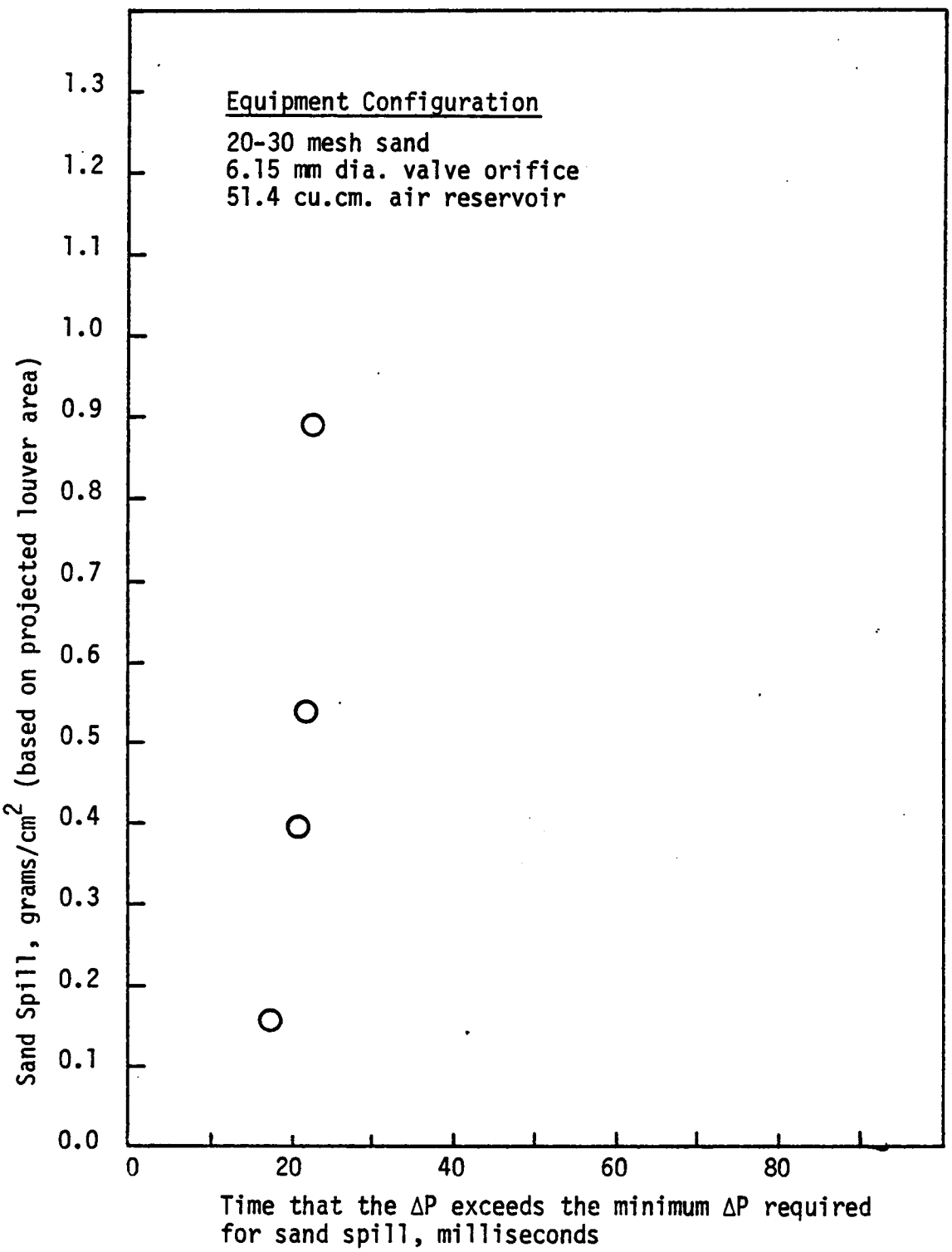

Figure 56. Active time-versus-Sand Spill.

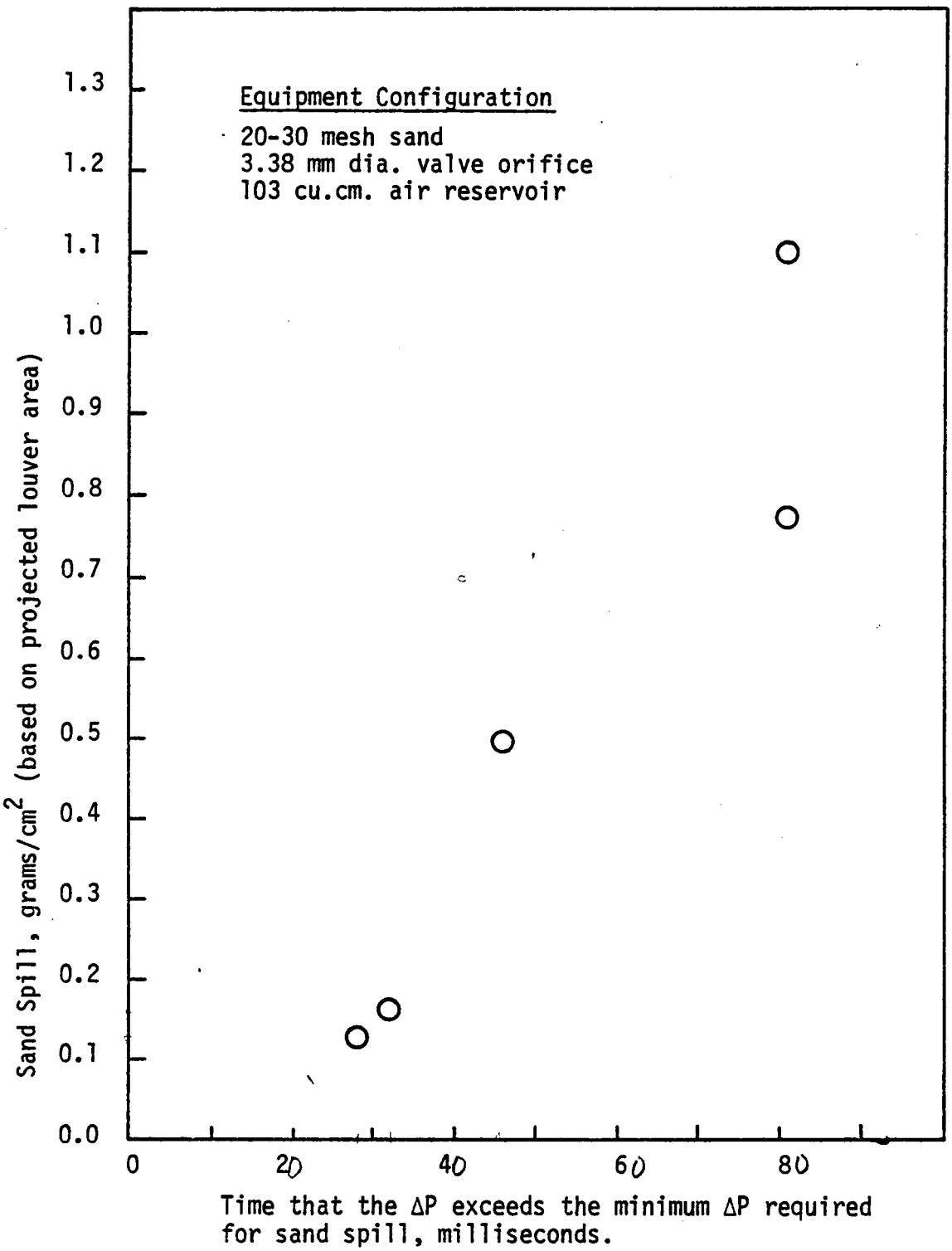

Figure 57. Active time-versus-Sand Spill.

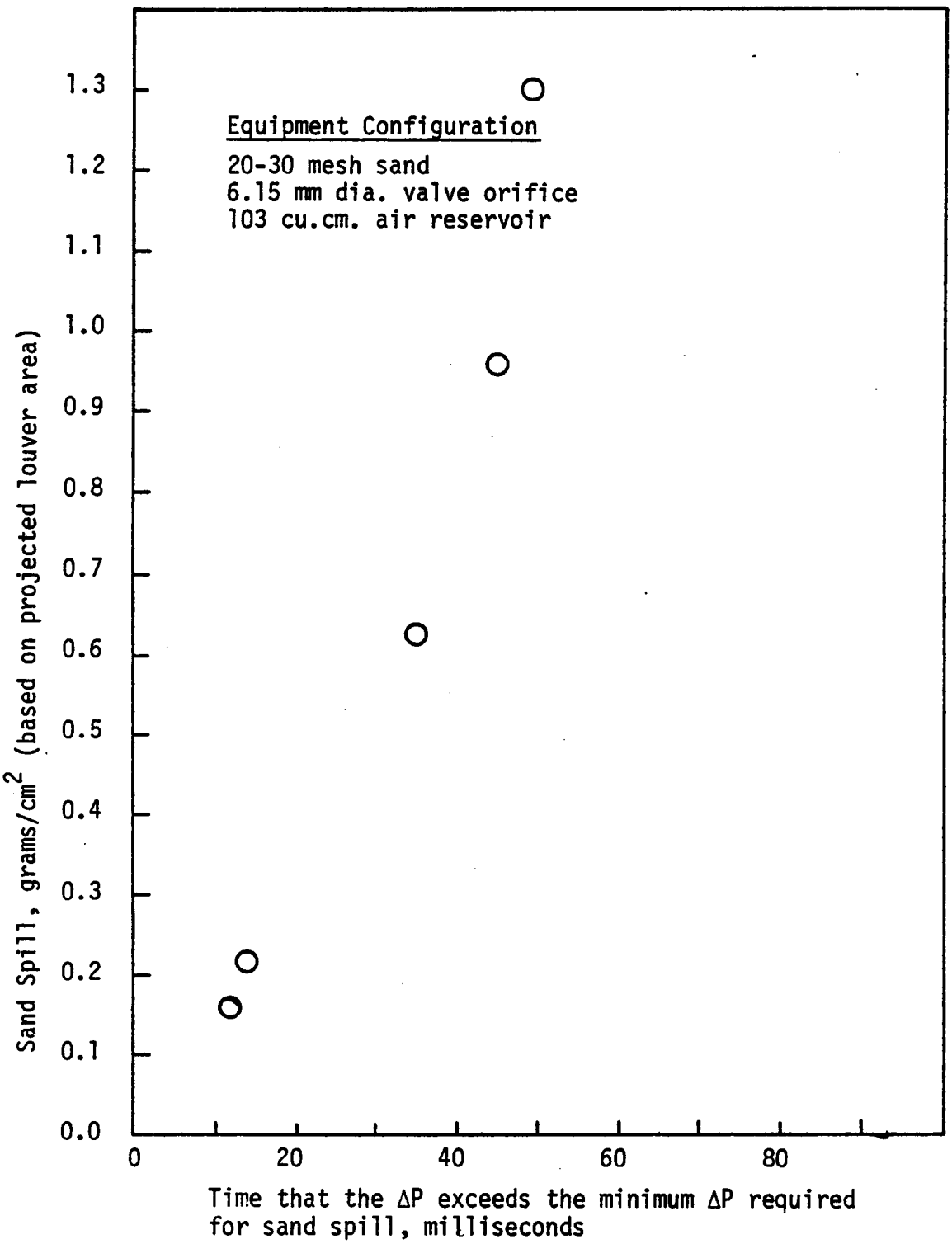

Figure 58. Active time-versus-Sand Spill.

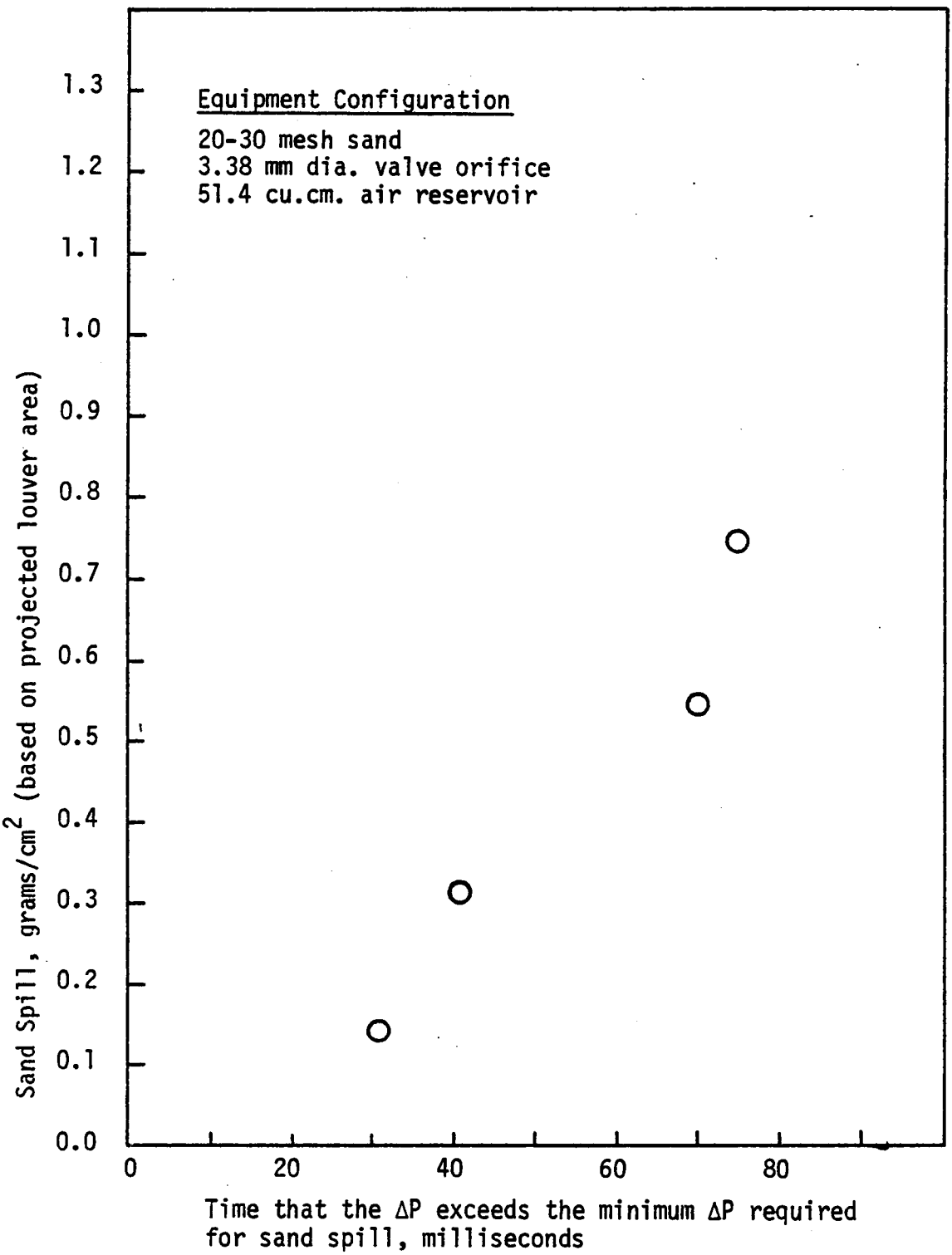

Figure 59. Active time-versus-Sand Spill.

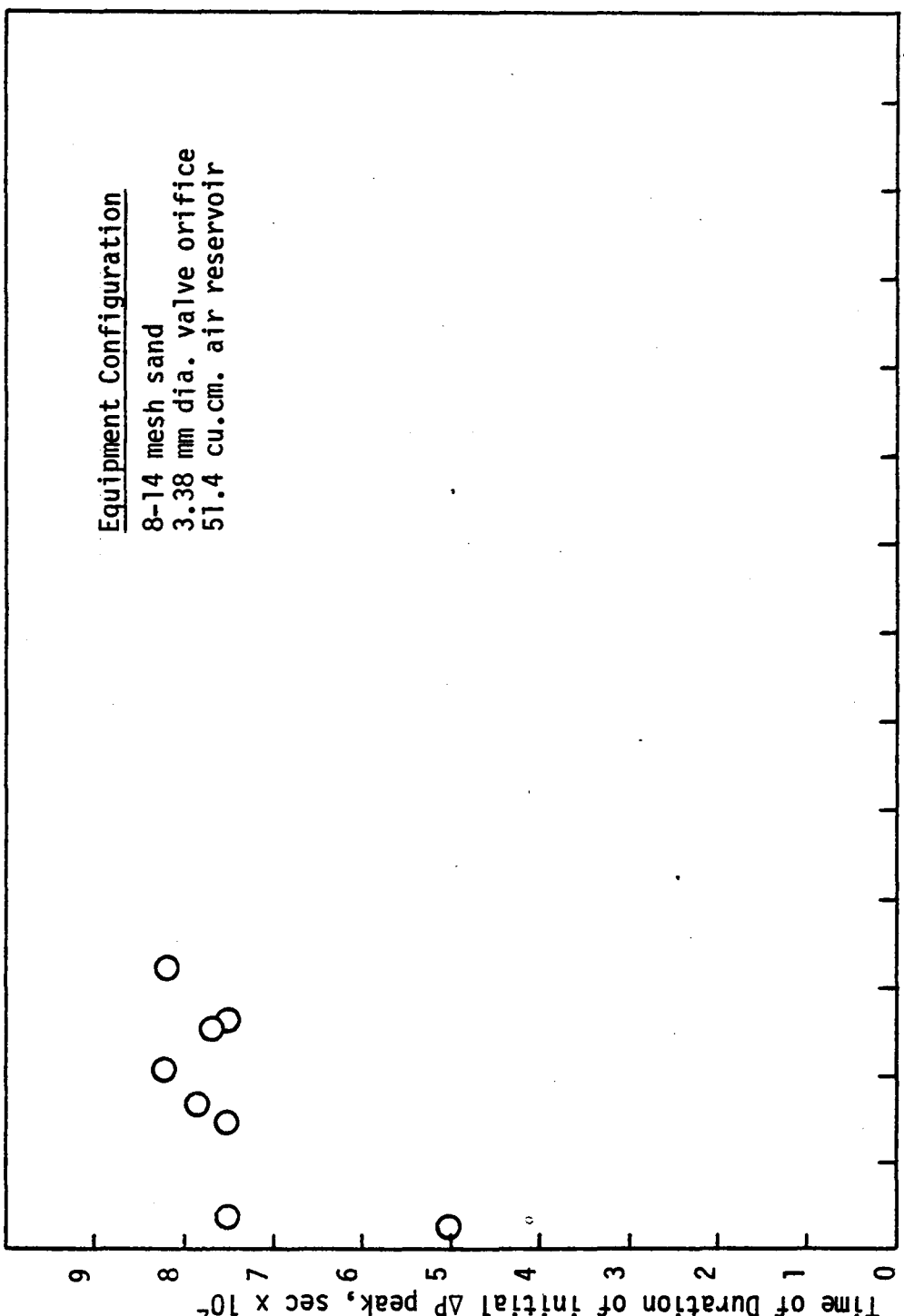

Figure 60. Duration time-versus-Peak Pressure Drop.

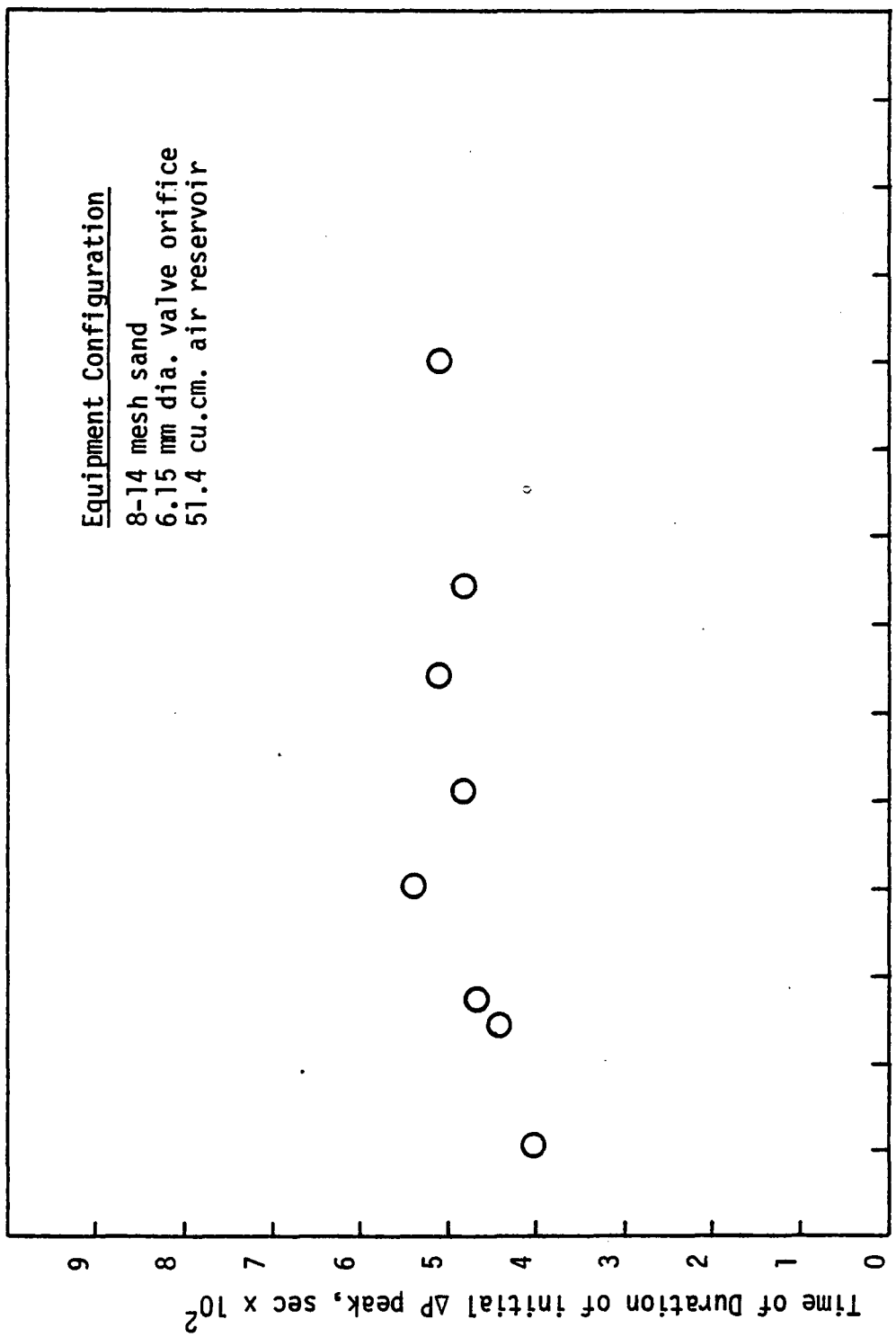

Figure 61. Duration time-versus-Peak Pressure Drop.

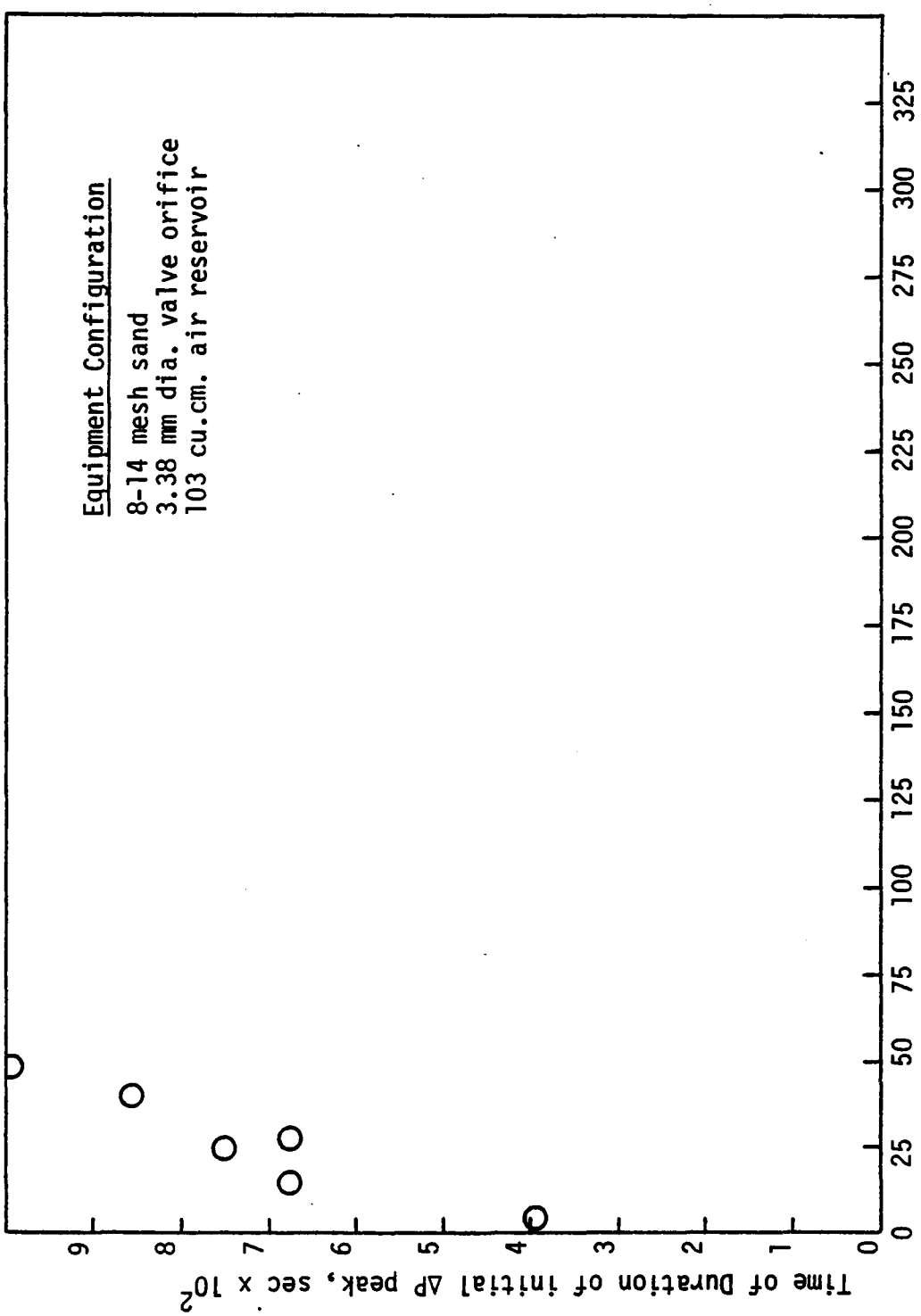

Figure 62. Duration time-versus-Peak Pressure Drop.

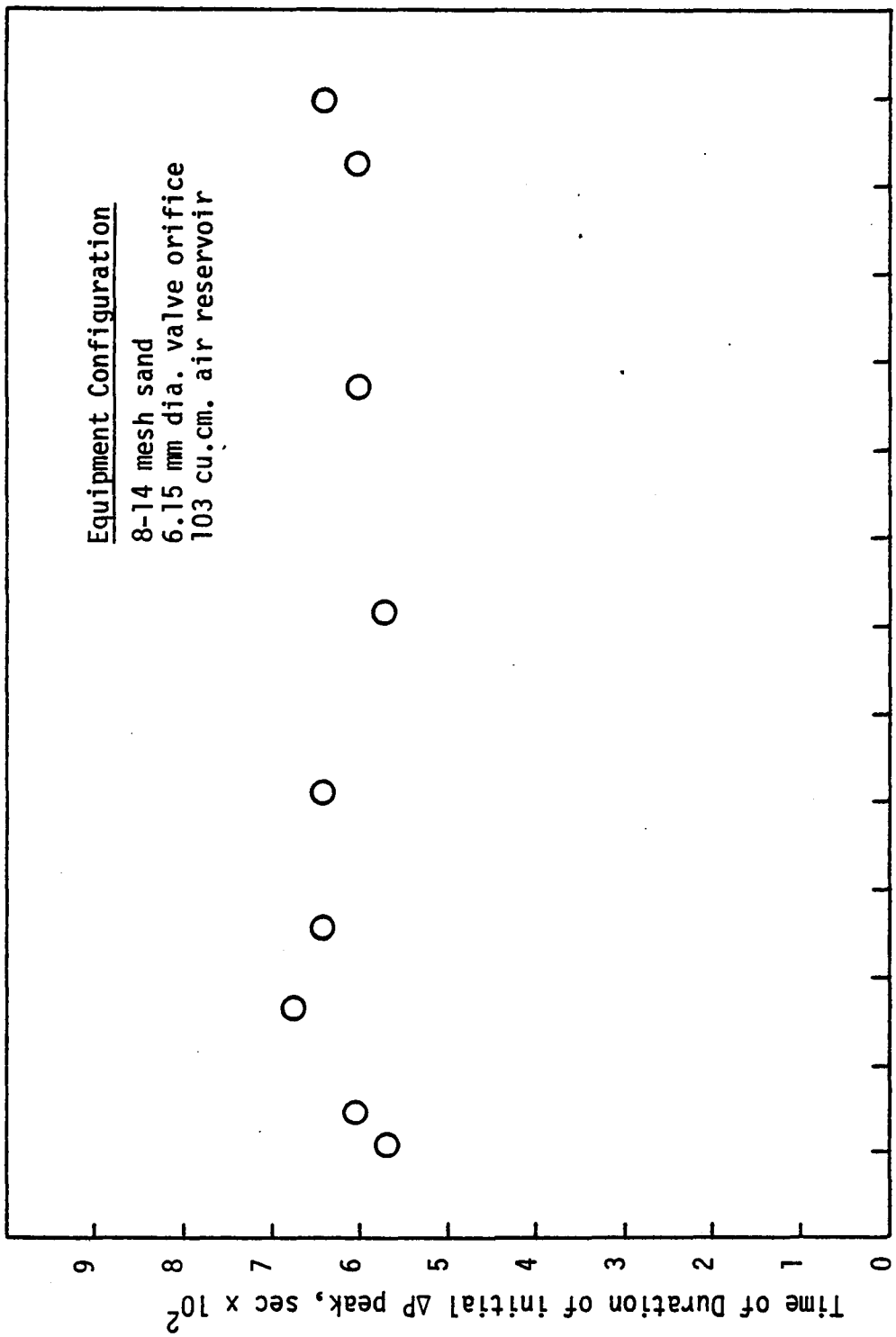

Figure 63. Duration time-versus-Peak Pressure Drop.

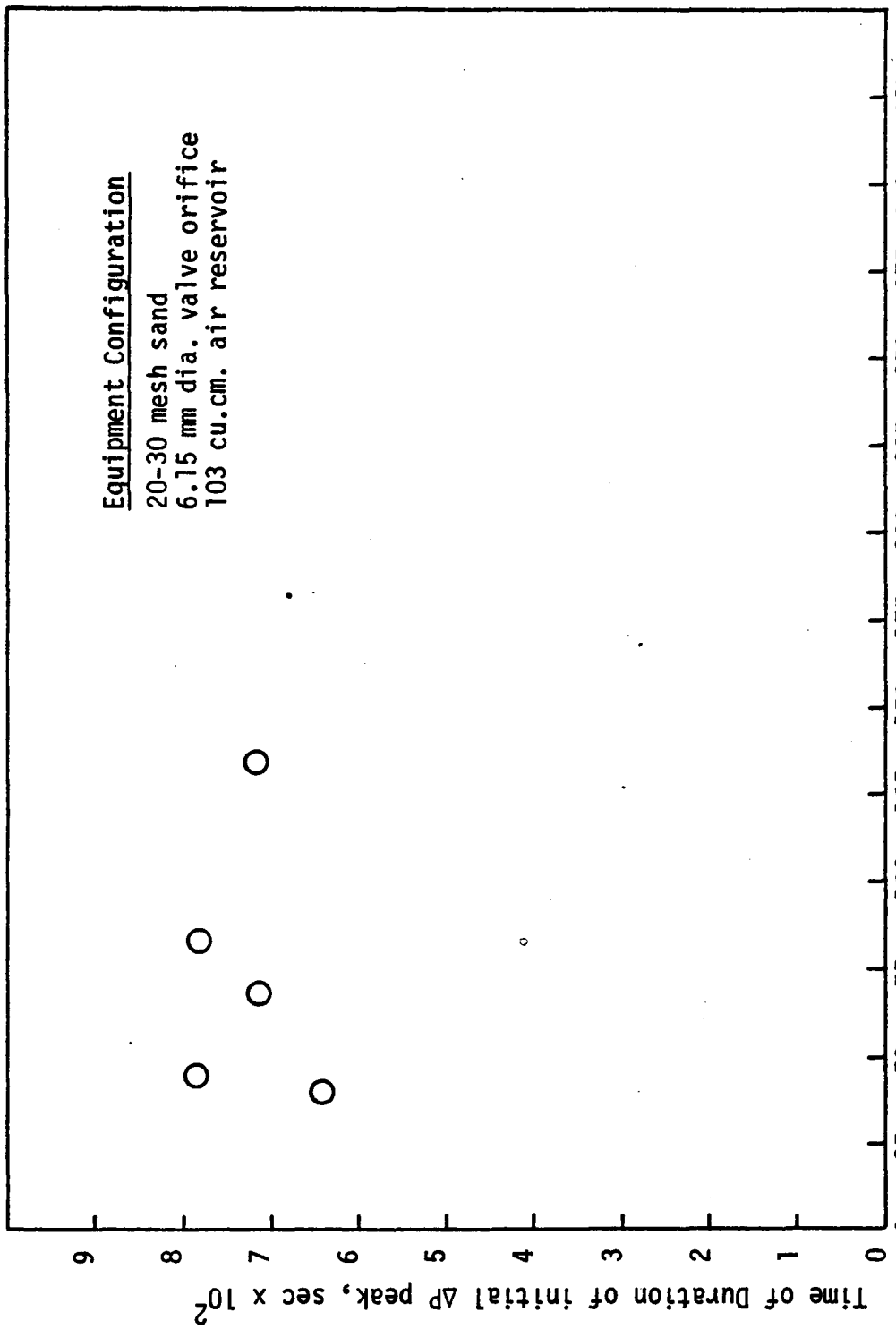

Figure 64. Duration time-versus-Peak Pressure Drop.

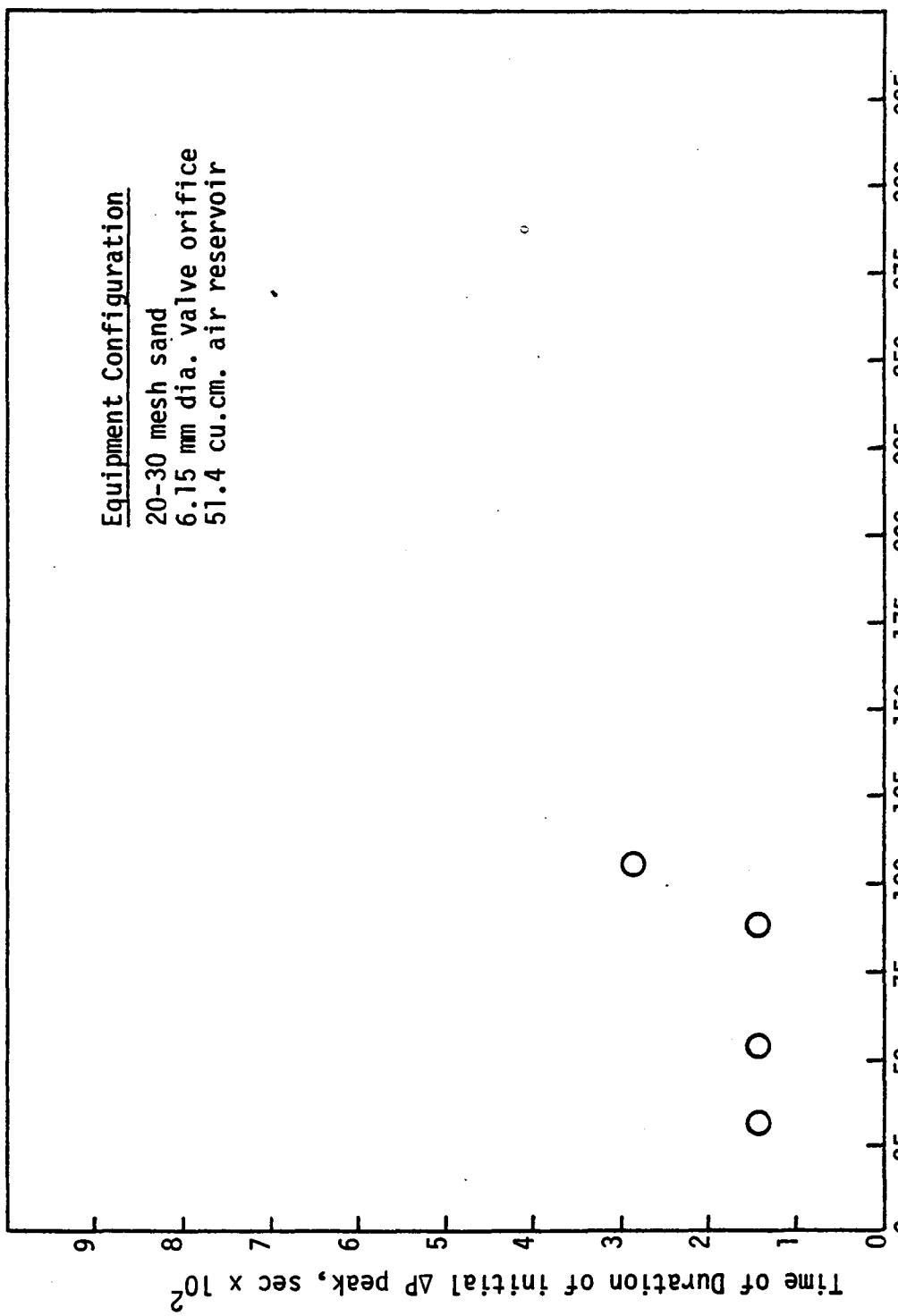

Figure 65. Duration time-versus-Peak Pressure Drop.

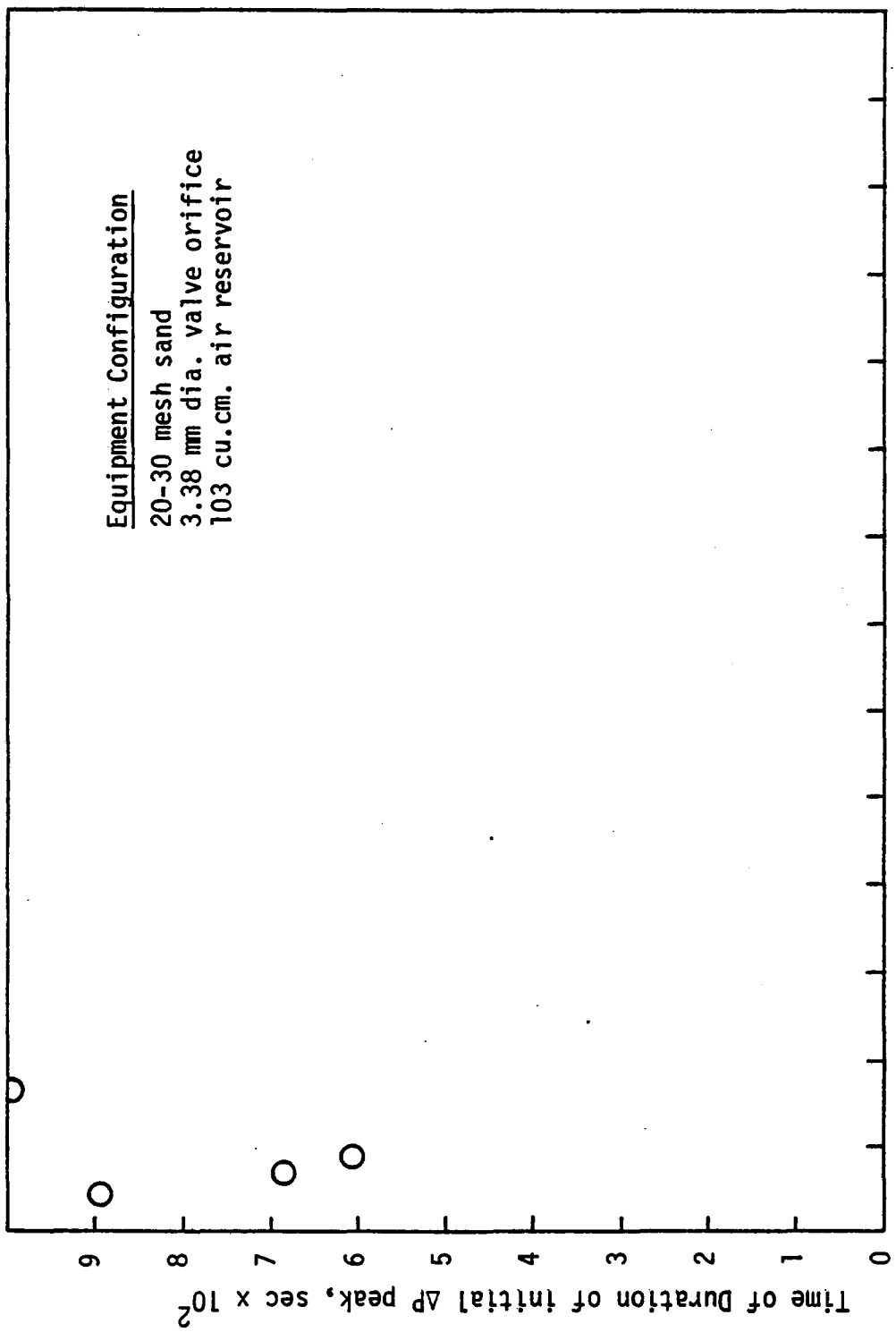

Figure 66. Duration time-versus-Peak Pressure Drop.

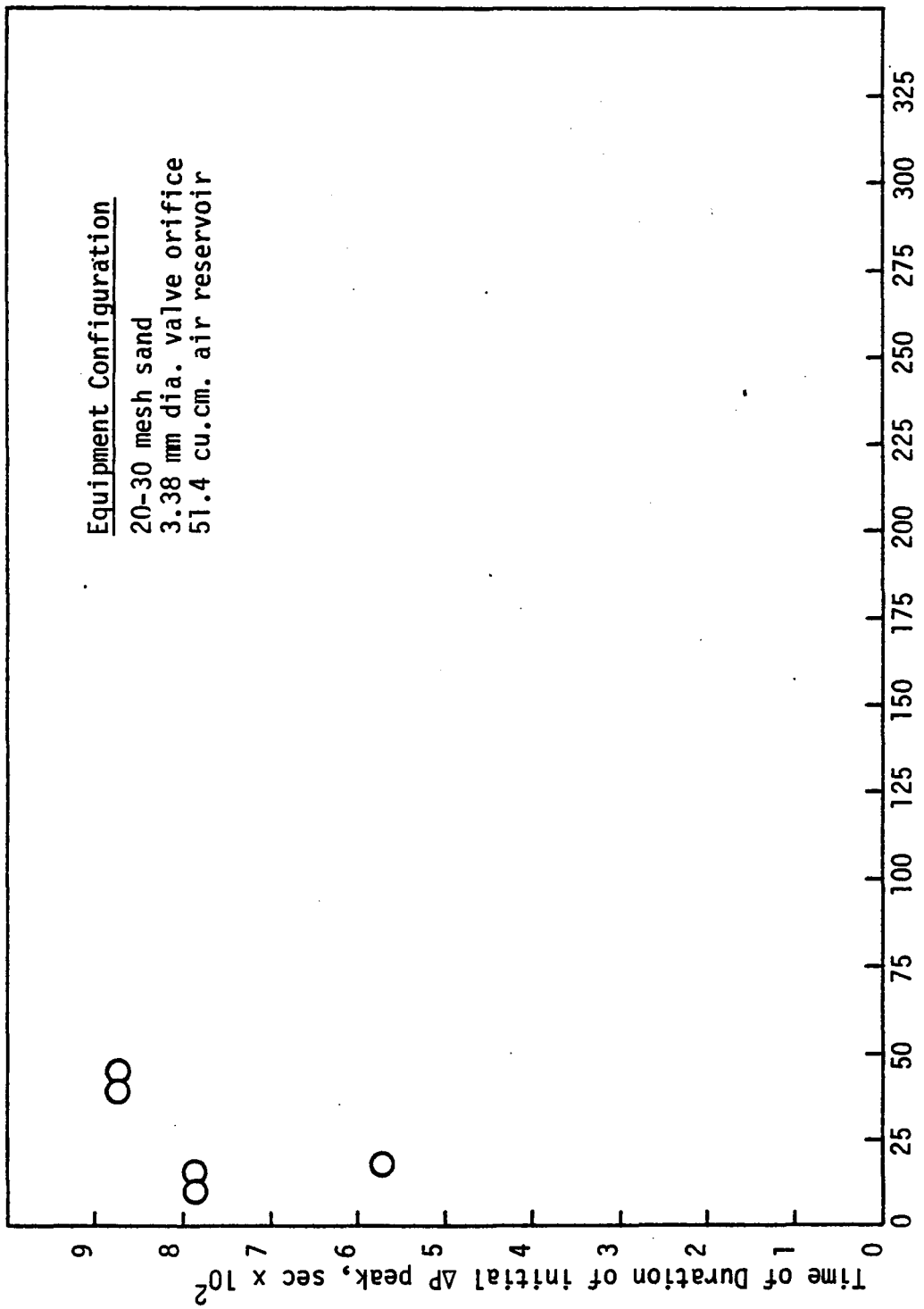

Figure 67. Duration time-versus-Peak Pressure Drop.

The vita has been removed from the scanned document

PULSEBACK CLEANING OF PANEL BED FILTER FOR TREATING A LIQUID

by

David Roberts Whitmire

(ABSTRACT)

A pulseback technique for cleaning and renewing a panel bed contractor suitable for chemical or physical treatment of liquid and granular material was investigated.

Free surfaces of quartz sand for the entry of water were provided by vertical support louvers. A pulseback technique was used to rid the liquid entry surface of the sand.

The pulseback consisted of a reverse transient flow of liquid across the panel bed of sand. The time of duration of the pulseback was a maximum of 100 milliseconds. The amount of sand removed from the panel bed was found to be related to the pressure drop across the panel bed and the duration time of the pulseback.

A description of the pulseback equipment, the pulseback data, and the correlation of the pulseback date are included.